Methods for the development of a DNA based nanoelectronics

Dissertation

zur Erlangung des akademischen Grades

Doktor der Naturwissenschaften

(Doctor rerum naturalium)

vorgelegt von

Dipl.-Phys. Ralf Seidel

geboren am 04.12.1973 in Pirna

eingereicht an der Fakultät Mathematik und Naturwissenschaften
der Technischen Universität Dresden
2003

1. Gutachter: Prof. Dr. Jonathon Howard

2. Gutachter: Prof. Dr. rer. nat. habil. Wolfgang Pompe

3. Gutachter: Prof. Dr. rer. nat. habil. Günter von Kiedrowski

Eingereicht am: 13.06.2003

Verteidigt am: 14.01.2004

Kurzreferat

Die einzigartigen Selbstassemblierungseigenschaften von DNA und ihre Fähigkeit, mit einer Vielzahl von chemischen Verbindungen und biomolekularen Strukturen Verknüpfungen einzugehen, machen DNA zu einem interessanten Baustoff für die Herstellung von künstlichen Nanostrukturen. In dieser Arbeit werden verschiedene Methoden für eine DNA-basierte Selbstassemblierung von elektrischen Nanoschaltkreisen entwickelt. Dabei werden vier grundlegende, für den Assemblierungsprozess notwendig erscheinende Schritte untersucht: (i) Die Herstellung von mehrfach verzweigten DNA-Molekülen basierend auf einem Bausteinprinzip. (ii) Das ortspezifische Anbringen von Nanoobjekten (Goldkolloiden) am Zentrum von DNA-Verzweigungen. (iii) Die Integration von DNA in Goldmikrostrukturen, speziell das Spannen von einzelnen DNA-Molekülen zwischen zwei Elektroden. Dazu wurde eine zuverlässige Methode zur spezifischen Funktionalisierung der Goldelektroden mittels Aminoethanthiol entwickelt, die eine DNA-Anbindung ohne zusätzliche Funktionalisierung des Moleküles erlaubt. (iv) Die Metallisierung von DNA. Hierfür wurde eine Prozedur gefunden, die es ermöglicht, Ketten von 5 nm großen Clustern entlang der DNA herzustellen. Sorgfältige Untersuchungen ergaben, dass diese Art der Metallabscheidung hochspezifisch auf dem Biomolekül aber nicht in der umgebenden Lösung stattfindet.

Abstract

The exceptional self-assembly properties of DNA as well as its ability to interact with different kinds of chemical compounds and biological structures make this biomolecule to an interesting object for the fabrication of artificial nanostructures. In this work several methods for a DNA-based self-assembly of electronic nanocircuitry are explored. For this, four basic steps, which turned out to be essential within a circuit assembly process, are addressed: (i) The formation of multi-branched DNA junctions by a simple building-block procedure. (ii) The site-specific attachment of nanoobjects (gold colloids) at the center of DNA junctions. (iii) The integration of DNA into microstructured gold electrode arrays, in particular the stretching of single DNA molecules between two electrodes. For this a simple, but reliable methods for the functionalization of gold electrodes by using aminoethanethiol was developed, which enables end-specific attachment of the DNA but does not require DNA modification. (iv) The metallization of DNA. A synthesis procedure was developed, which results in the formation of continuous chains of 5 nm platinum clusters along the DNA. The metal deposition process turned out to take place exclusively at the DNA while background metallization is completely suppressed.

Contents

Introduction **1**

1 DNA as a template **5**
1.1 DNA - structure, recognition and assembly 6
1.2 DNA-Technology 11
1.3 DNA based nanostructure assembly 15
1.3.1 Fabrication of complex DNA networks 15
1.3.2 Anchoring DNA to surfaces 18
1.3.3 Metallization of DNA templates 25

2 Artificial DNA junctions **27**
2.1 Construction of a 3-armed DNA junction 27
2.1.1 Design of the linker element 28
2.1.2 Design of the elongation 30
2.1.3 Junction ligation 31
2.2 Multi-branched DNA molecules 33
2.2.1 Building-block principle 33
2.2.2 Ligation of n-armed linkers and junctions 34
2.3 Attachment of colloids to the junction center 38

3 Integration of DNA into microstructures **43**
3.1 Experimental setup 43
3.1.1 Functionalization of gold electrodes and DNA ends 43
3.1.2 Flow cell and fluorescence microscopy 48
3.2 *In-situ* manipulation of single DNA molecules 52
3.2.1 Stretching of DNA between microstructures 52
3.2.2 Determination of stretching forces 61

4 Platinum cluster chains along DNA **69**
4.1 Binding of $PtCl_4^{2-}$ complexes at DNA 70
4.1.1 UV/VIS spectroscopy 71

4.1.2 Gel electrophoreses . . . 77
4.1.3 SFM studies . . . 78
4.1.4 Conclusions about the binding of $PtCl_4^{2-}$ to DNA . . . 80
4.2 Cluster formation without DNA . . . 81
4.3 Cluster formation in the presence of DNA . . . 83
4.3.1 Cluster formation with native DNA . . . 84
4.3.2 Cluster chain formation at activated DNA . . . 86
4.3.3 DNA sequence specificity of the cluster nucleation . . . 90
4.3.4 Discussion of the nucleation mechanism at DNA . . . 92
4.3.5 Influence of control parameters . . . 95
4.4 Formation of continuous wires . . . 101

Summary **105**

Appendix **109**
A.1 Calculations . . . 109
A.1.1 Calculation of the chain line . . . 109
A.1.2 Equilibrium concentrations and kinetics for the hydrolysis of $PtCl_4^{2-}$ . . . 110
A.1.3 Mie theory applied to platinum clusters . . . 111
A.2 Experimental methods . . . 113
A.2.1 Formation of multi-branched DNA junctions . . . 113
A.2.2 Integration of DNA into microstructures . . . 115
A.2.3 Preparation of cluster chains along DNA . . . 116
A.2.4 Preparation of SFM samples . . . 117
A.2.5 Gold enhancement . . . 117

Publications **119**

Bibliography **121**

Acknowledgements **131**

Introduction

Scientifically, the last century was dominated by the large discoveries made in physics and is therefore often called as the "century of physics". Among the experimental as well as theoretical findings are the theory of relativity, the quantum theory, the discovery of the nuclear fission and the invention of laser and transistor, which had not only impact to the scientific and technological world, but also changed the everybody's life tremendously.

For the new, just started century, which began with the decipherment of the human genome [1, 2], an equally great leap forward in knowledge and application is expected to come from biology. For example, a great hope is that with increasing understanding of the processes in living nature, diseases like cancer, Alzheimer and Parkinson can be cured one day. Probably, many of the today's expectations will be disappointed, like it was the case for antibiotics, which did not wipe out the infectious diseases. However, it is right to say that biology will induce large changes on our life in the present century.

The rapid development in molecular biology became not at least possible by the application of technologies coming from the world of physics, like microelectronics and microsystems techniques. Without high-performance computation and DNA-chip technology the sequencing of complete vertebral genomes and the automated screening of genes would not be possible at all. There is a high technological impact of microelectronics and related techniques onto biology. However, today the impact in the opposite direction from biology onto the mentioned techniques is still low and has only recently attracted considerable scientific interest.

What could biology do for the microfabrication techniques? As the name already says, microfabrication techniques rely on the formation of structures in the micrometer or sub-micrometer range, which posses desired electrical, mechanical, physical or chemical properties. The structuring is usually done with light or electron beam lithography, which requires a considerable high effort in equipment, materials and energy. The result are highly complex microchips, which are staggered in different levels and the accuracy of their fabrication is very impressive, if one thinks for example on computer processors of the current generation.

However, the chip architectures are rather coarse in comparison to the structures

of enzymes and proteins found in even the simplest living object. In order to not get misunderstood, the sophisticated microfabrication techniques applied in chip industry are high technology and at the moment there is no alternative method, which can compete with them. But with the proceeding miniaturization, the lithography techniques reach more and more limitations. A decrease in structure size will be only achieved with a tremendous increase in effort. According to Moore's law [3], the transistor density on a chip doubles every 18 month and this law is even said to last for at least another decade. This means, that the structure size of future computer chips will soon be in the range of a few nanometers.

The structure size of the subunits which form larger biological architectures is already in the nanometer range. For example, DNA has a diameter of 2 nm. The whole living nature consists of structures, which building blocks are in exactly the size range, which is desired in future nanofabrication. In contrast to the lithographical methods, where from a large block of material the more elaborate structure is carved out, the formation of biological structures is based on the two fundamental principles of molecular recognition and self-assembly. Biomolecules can attach to each other at highly specific binding sites. Thus, building blocks are formed, which can aggregate with further molecules and assemble from small subunits into well-defined larger superstructures. The availability of a large quantity of different binding sites enables the flexibility and diversity of biological structures.

Recently, this building block concept found in living nature served as inspiration for several attempts to fabricate nanostructured objects with the help of biomolecules. Thus, completely artificial constructs, which were only composed of biomolecules, could be fabricated [4, 5, 6]. Furthermore, a lot of work was also done in a biomolecule mediated assembly of inorganic, in particular metallic or semiconducting, objects. The biomolecules serve during the formation process either as linker elements between the inorganic phase [7, 8] or are used as a template, i.e. as a support, which promotes the selective deposition of inorganic material. The latter method adopts the formation of biological structures, which mainly consist of inorganic material, as they are present for example in bone and the shell of mussels. Different nanometer-sized objects could be fabricated this way, like tubes by metallization of microtubules and tobacco mosaic viruses [9, 10, 11, 12], periodic 2-D assemblies of clusters on S-layers [13, 14] and wires by metallization of DNA [15, 16, 17, 18, 19, 20, 21, 22]. This work shows, that by application of biomolecules and biological principles, biology can have a considerable impact on nanofabrication technologies.

In this framework, also the present work is settled. It explores possibilities, how self-assembly of biomolecules, in particular DNA, can be used to build up electronic circuitry as an alternative method for structure fabrication in future nanoelectronics. The investigations are focused on DNA, because of its exceptional properties like a favorable diameter of only 2 nm and a practically unlimited length, the mechan-

ical [23], thermal, chemical stability, the ability to bind a large number of organic and inorganic molecules [24]. Above all the increasing technological know-how has enabled in the last years the assembly of DNA into complex architectures [4, 5, 6].

To build up circuitry with DNA, the biomolecule has to fulfill different tasks. An electronic circuit is, from a rather simplified point of view, an array of devices, which are connected to each other by a network of wires. Furthermore, a circuit has an interface to the "outer world", where data input and output is realized. Related to a circuit assembly, which is fully accomplished with DNA it means: (i) DNA has to be assembled into network structures. (ii) Functional elements have to be site-specifically be attached. (iii) To establish an interface, the DNA network has to be electrically integrated in a larger electrode structure. (iv) As DNA has poor conductive properties (discussed later in the text), conductivity has to be injected to the DNA assembly.

The intention of this work is to explore these four steps using the *self-assembly* properties of DNA. This means, each part of the assembly process has to be controlled by the functionality of the DNA itself or a functionality, which is additional induced to the molecule. Within this background several particular problems are formulated, which will be addressed here: (i) A basic element of networks are junctions. A procedure for the self-assembly of DNA junctions must allow exact control over the their morphology, e.g. the number of branches. Here, the formation of multi-branched DNA junctions is investigated, where the morphology of a particular junction is controlled by recognition between several smaller DNA building blocks. (ii) Site-specific deposition of devices to a DNA template, by the means of self-assembly, requires recognition between device and biomolecule. It is shown that gold colloids can be attached at the branching point of DNA junctions by functionalization of the biomolecular template at this place. (iii) Integration of DNA into an electrode structure means site-specific attachment of DNA molecules at a given microstructure. A possible solution for this task is to functionalize DNA ends and a substrate in a way that DNA is binding exclusively to predefined pads on the surface. For this, several functionalizations are tested and characterized. (iv) To a DNA template structure, conductivity can be induced by site-specific deposition of metal along the molecule. The metallization process must be highly specific, i.e. metal deposition should only take place at the DNA. A method is investigated, where metal growth at the DNA is controlled by the DNA bases leading to exclusive metallization of the DNA template.

These topics set also the general outline of the present work. The first chapter deals with a description of the properties of DNA and the applied biomolecular methods. Furthermore, a brief review about previous work in the field of nanostructure formation by the use of DNA is given. Subsequently, the investigations done in the framework of this thesis are described. In chapter 2 the formation of multi-branched

DNA molecules by using a simple kit procedure is demonstrated. Beside that, it is shown, how small colloids can be attached specifically at the branching point of the junctions. The integration of DNA molecules into microelectrode structures is investigated in chapter 3. In chapter 4 the metallization of DNA, in particular the growth of cluster chains along the molecule, is studied. The results are briefly summarized in the last chapter and a conclusion about the suitability of DNA for the construction of future electronic circuits is given. A detailed description of the performed experiments is listed in the appendix.

1 DNA as a template

The intention of this work is to use DNA as a template for the construction of future circuitry. As it was already pointed out, on the way to that aim, the DNA has to fulfill different tasks, which are network assembly, site-specific attachment of functional elements, integration into an electrode structure and DNA metallization. All these steps have to be incorporated into one fabrication scheme. A general outlook for that is drawn schematically in Figure 1.1. As a first step the assembly of DNA into networks is proposed (a). Subsequently this DNA network has to be integrated into a contact array (b) and functional functional elements have to be positioned (c). The last step should be the DNA metallization (d), because after this process the DNA looses its biological functionality and steps like the network assembly could not be done anymore.

For a successful assembly of a DNA based circuit in the future, it is essential that all these steps will be very precisely guided and controlled by the DNA molecule itself. Therefore, the understanding the DNA structure and its related properties is a crucial point for establishing methods which enable all the steps of the construction scheme. As a consequence in the following sections the structure of DNA as well as methods for manipulating DNA will be explained. Subsequently, an overview is given about existing methods for the assembly DNA networks, for the binding of DNA to surfaces and for the metallization of DNA.

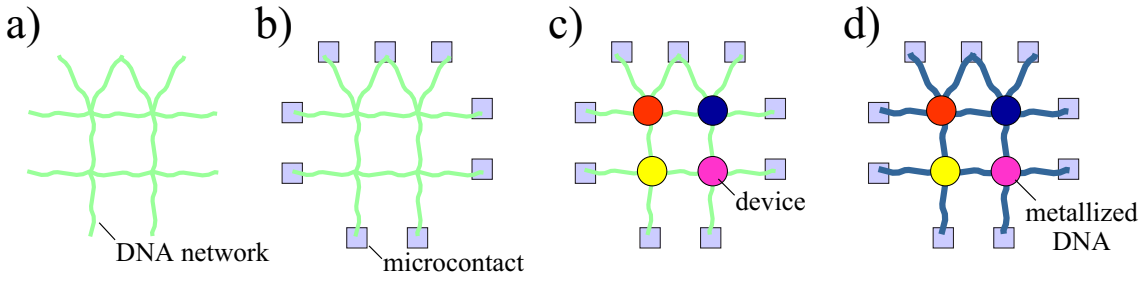

Figure 1.1: Possible construction scheme for a DNA-based circuit: a) DNA template assembly. b) Integration of the template into an electrode array. c) Positioning of functional elements. d) Deposition of metal or semiconductor material on the DNA template.

1.1 DNA - structure, recognition and assembly

Today everyone knows that DNA forms a double helix and is the carrier of the genetic code. However, a bit more than 50 years ago this for today basic knowledge was completely unknown and the majority of scientists at this time believed that the genes are located in the proteins found in the chromosomes [25]. With the discovery of the structure of B-DNA by Watson and Crick [26] in 1953 and the subsequent elucidation steps in the synthesis of DNA, RNA, and proteins the corner stone for modern molecular biology was laid. The development of DNA sequencing by Sanger [27] and of the polymerase-chain reaction (PCR) by Mullis [28] were the foundations for the rapid and large scale application of gene technology. From this time biology and biochemistry have been revolutionized. Although now in many fields processes in living nature become increasingly understood there are still more open questions than answers. A key role for the understanding plays the knowledge about the interaction of DNA sequence, structure and function.

DNA is linear polymer composed by a sequence of four different monomers the so-called nucleotides. Part of each nucleotide is one of the four DNA bases adenine, guanine, cytosine and thymine (Fig. 1.2).

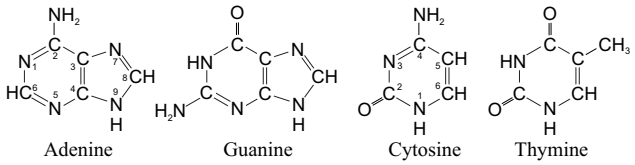

Figure 1.2: The four bases of DNA are the purines adenine(A) and guanine(G) as well as the pyrimidines cytosine(C) and thymine(T).

Each base is bound to a pentose forming together the nucleoside. The pentose in DNA is the 2-deoxyribose where the OH group at the 2'-site is missing in comparison to ribose which is part of RNA (Fig. 1.3). Coupling a phosphate to the 5'-site of the pentose leads finally to the nucleotide.

A linear DNA strand is formed by polymerization of the nucleotides via phosphate and deoxyribose, which form the DNA backbone (Fig. 1.4). Note that a DNA

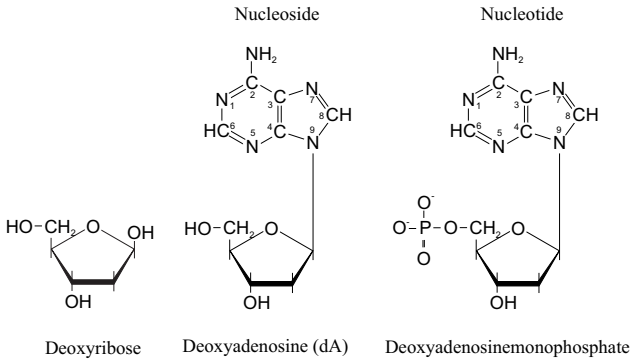

Figure 1.3: The pentose found in DNA is deoxyribose. Pentose and DNA base form a nucleoside. Together with a phosphate on the 5'-carbon of the pentose, it is called nucleotide.

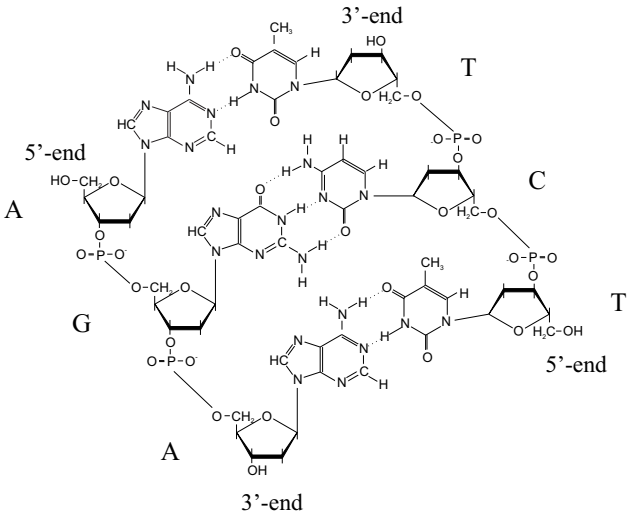

Figure 1.4: Base pairing of the DNA double helix. In DNA the nucleotides are linked via phosphate and pentose to a linear strand. The base pairing of guanine with cytosine as well as of adenine and thymine via three or two hydrogen bonds, respectively, enables the formation of the double stranded helix.

strand has an end-to-end chemical orientation: the *5'-end* has a free hydroxyl or phosphate group on the 5'-carbon of its terminal sugar; the *3'-end* has a free hydroxyl group on the 3'-carbon of its terminal sugar. The phosphate group is at neutral pH negatively charged, which leads to a charging of the DNA backbone of $1\,e^-$ per nucleotide.

Native DNA, which structure was found by Watson and Crick, consists of two associated polynucleotide strands that form the well-known double helix. The orientation of the two strands is antiparallel; that is, their 5'→3' directions are opposite. The strands are held in precise register by a regular base-pairing between the two strands: G is paired with C through three hydrogen bonds; A is paired with T through two hydrogen bonds (Fig. 1.4). The base pairing is caused by size, shape and chemical composition of the bases. Furthermore adjacent DNA bases are stacked on top of one another in parallel planes. The large number of base pairs leads to the high stability of the helix structure.

The helix can, in principle, be right-handed or left-handed. The native form of the helix structure, however, is right-handed and called B-DNA (Fig. 1.5).

In nature, during the processes of DNA replication and the copying of RNA from DNA, it is essential that the two helix strands are separated one from each other at least temporarily or locally. This strand separation can also be induced under experimental conditions, for instance by heating a solution containing DNA. The induced thermal energy is large enough to break the hydrogen bonds. On the opposite, cooling a solution containing complementary DNA single strands leads to reassociation and formation of the helix structure, which is called *hybridization*. This means, the process of strand separation, also described as *denaturation* or *"melting"*, is reversible, which can be, e.g., monitored by UV-VIS spectroscopy.

DNA shows an absorption maximum at 260 nm wavelength, which is caused by electronic excitations of the DNA bases. The transition dipoles associated with

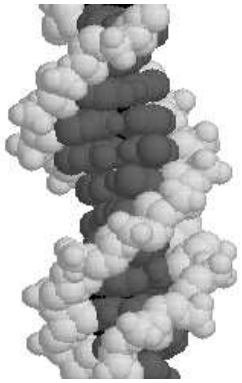

Chirality	righthanded
Base pairs per turn	10
Angle between two bases	36°
Distance between base pairs	0.33-0.34 nm
Angle between helix axis and base planes	90°

Figure 1.5: Structure image and morphological data of B-DNA

the electronic transitions of the bases are located in the planes of the aromatic rings. The parallel stacking of the DNA bases in the double helix enables dipole coupling between adjacent bases, thus lowering the effective dipole moment. Therefore, the absorption for the ordered helix structure is decreased in comparison to single stranded DNA (Fig. 1.6a), where base stacking is completely lacking. This effect is called hypochromism. UV/VIS measurements show that for double stranded DNA the absorption at 260 nm (A_{260}) corresponds to 1 at a DNA concentration of 50 μg/ml whereas only 40 μg/ml of single stranded DNA are required to yield the same value [29]. Thus measuring A_{260} provides not only a useful method to determine DNA concentration down to 0.5 μg/ml, but it also allows monitoring of DNA melting and hybridization transitions (Fig. 1.6b). The DNA melting temperature T_m is defined as the temperature at which half of the bases in a double stranded DNA sample have denatured.

As a GC base pair (bp) has one hydrogen bond more than an AT base pair, the energy required to separate guanine from cytosine is higher than the energy to separate adenine from thymine. Therefore, the temperature, required for the separation of two DNA strands is a function of the GC content. The negatively charge of the DNA backbone leads to a repulsion of the two DNA single strands, which lowers the melting temperature. Thus, the salt concentration of the solution is another parameter, which influences T_m, as the repulsion can be partly compensated due to screening with cations.

For DNA larger than 100 bp the melting temperature can be estimated by using the equation of Baldino *et al.* [30]:

$$T_m = 81.5°\mathrm{C} + 16.6°\mathrm{C} \cdot \lg c_{Na^+} + 0,41 \cdot \%GC - 675/L, \tag{1.1}$$

where c_{Na^+} denotes the concentration of monovalent cations, $\%GC$ the fraction of guanine-cytosine bases pairs and L the DNA length in base pairs.

For shorter oligonucleotides, T_m can be derived by using the two thermodynamic equations: $\Delta G = \Delta H + T \cdot \Delta S$ and $K = \exp(-\Delta G/(R \cdot T_m)) = c_{ds}/(c_{ss1} \cdot c_{ss2}) =$

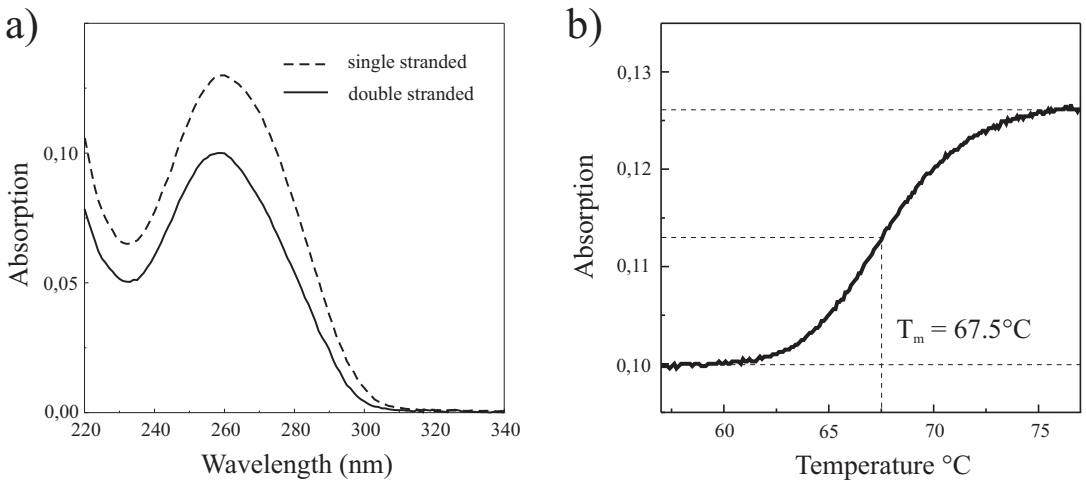

Figure 1.6: a) Absorption spectra of a single and double stranded DNA at a concentration of 5 μg/ml. b) Thermal denaturation of salmon sperm DNA at a concentration of 5 μg/ml in a solution containing 10 mM Na_2SO_4. T_m denotes the melting temperature, derived from the graph.

$1/(c_T/4)$ for the equilibrium constant K at melting temperature T_m, where the concentration of duplex strands c_{ds} equals the concentrations of both single strands, c_{ss1} and c_{ss2}, which correspond to a quarter of the total strand concentration c_T. Replacing ΔG in the equations leads to:

$$T_m = \frac{\Delta H}{\Delta S + R \ln(c_T/4)} - 273.15°\text{C}. \tag{1.2}$$

The change in enthalpy ΔH and in entropy ΔS can be calculated for short oligonucleotides using the nearest neighbor method of Breslauer *et al.* [31]. For example, ΔH of the oligomer ATGCTT is the ΔH for AT + ΔH for TG + ΔH for GC + ΔH for CT + ΔH for TT. In the same manner is also the value for ΔS obtained.

As explained before, two complementary single DNA strands can be reassociated by hybridization. An underlying fundamental principle of this process is *molecular recognition*, which is a basis of the processes in living nature. A part of the sequence of the first strand has to find - to "recognize" - a complementary sequence on the second strand, thus forming a nucleation center for the further association process. This means, recognition is essential for the self-assembly of the DNA helix structure (Fig. 1.7a). However, this principle can not only be used to combine two single strands. A common technique in molecular cloning to "glue" site-specifically two double stranded DNA fragments together, which posses short single stranded overhangs with complementary sequences - the so-called *sticky ends* (Fig. 1.7b).

Furthermore recognition is the driving force for all kind of interaction between

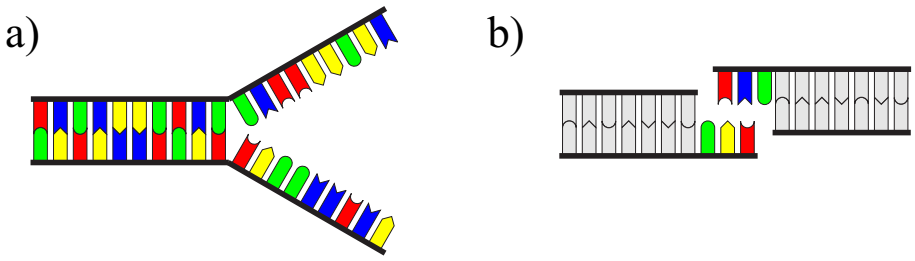

Figure 1.7: Recognition of complementary DNA sequences a) of two DNA single strands b) of two double stranded DNA fragments via cohesive sticky ends.

DNA and proteins as well as between proteins and proteins. It is not only used to mediate the assembly of structures but also to enable different functions. There exist lots of enzymes binding DNA at specific sequences and manipulating it, for instance restriction enzymes which can cleave DNA or topoisomerases which release torsional stress in a DNA double strand. Other enzymes regulate cell functions like the Tet repressor (Fig. 1.8a), which blocks the transcription of genes by binding to DNA in dependency on the tetracycline content.

Examples for protein-protein recognition are antibodies which specifically bind to receptors of viruses or bacteria, blocking this way their function. In the later described experiments, the protein streptavidin and the coenzyme biotin were used. Streptavidin carries four affinity sites for biotin (Fig. 1.8b) and is therefore often used as a linker between two biotinylated objects. Furthermore, it provides one of the strongest noncovalent interactions in nature [32].

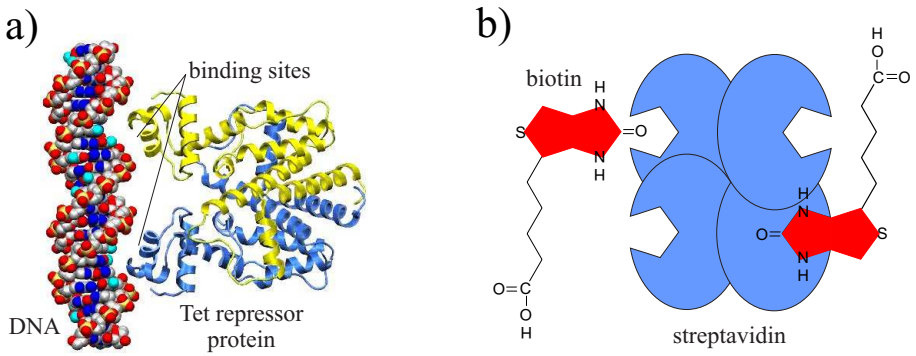

Figure 1.8: Recognition of a) DNA and protein b) the protein streptavidin with the coenzyme biotin.

The highly specific recognition among biomolecules is the driving force for their *self-assembly*. Small building blocks can bind at well defined positions and form stepwise a larger and larger structure with a specific shape and function. The

name self-assembly is derived from the fact, that the assembly process occurs in the absence of any manipulation tool and requires only thermodynamic movement followed by the binding of the biomolecules.

1.2 DNA-Technology

As shown in the previous section, the structure of DNA enables various possibilities for its self-assembly as well as its manipulation. In the following, different molecular-biological techniques, which were used in this work to fabricate artificial DNA structures, are briefly described.

The construction of DNA templates requires the synthesis of appropriate DNA fragments possessing the required length, sequences and so on. Beside molecular biological methods for DNA preparation, advances in synthetic chemistry permit now the chemical synthesis of single stranded DNA. Any sequence can be obtained this way. However, as the yield of the method drops dramatically for oligomers longer than 100 bp, chemical synthesis is restricted to this length. As there is an increasing demand for such short oligonucleotides due to applications in DNA chip technology as well as in PCR, nowadays synthesis is done by an increasing number of companies. Therefore oligomers with the desired sequence can be inexpensively purchased within a few days.

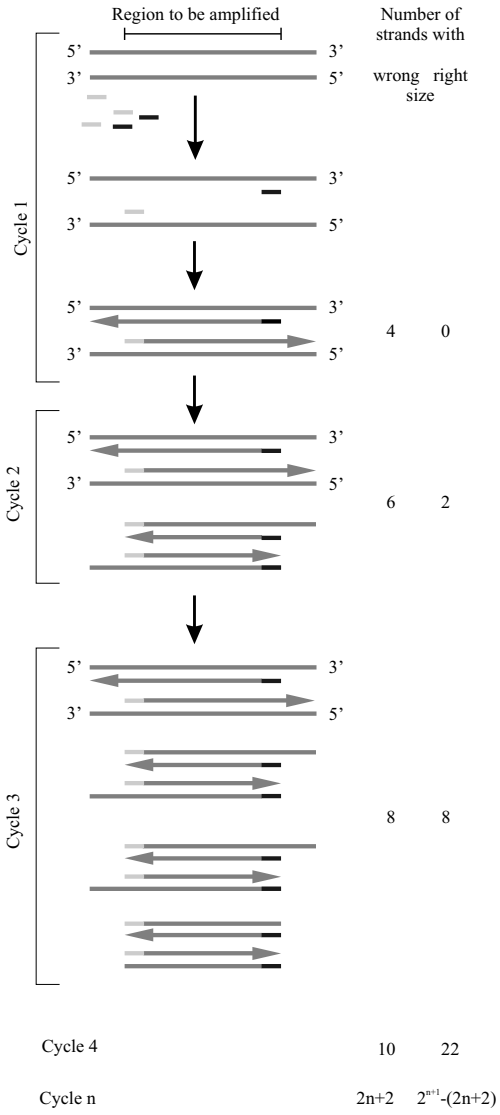

Figure 1.9: Schematical representation of the polymerase chain reaction.

In the past, DNA fragments longer than 100 bp were usually obtained by amplification in microorganisms like viruses, bacteria or yeast. The accuracy of this method is very high, however one needs a circular template and the preparation is time consuming. The invention of the *polymerase chain reaction* (PCR) in 1987 [28] provided a much easier way to amplify a large number of fragments from a small number of targets *in vitro*, opening this way new fields of ap-

plication. Like in living organisms an enzyme called polymerase is used to replicate the DNA. For this, at least partial denaturation of the double helix is required. *In vivo* this is done by the cooperation of many enzymes. PCR, however, separates the strands by heating the DNA solution to 95°C . The crucial point for the invention of the method was to get a polymerase which could survive such temperatures, but finally one found the appropriate enzyme in a thermophylic bacteria called *Thermus aquaticus* which is living in hot springs. The polymerase extracted from this organism is called *Taq* polymerase. This enzyme, however, can not just copy single stranded DNA, but needs as a starting point a short double stranded region, which is then further elongated from its 3' end. Therefore, for running a PCR, one has to add short oligomers, so-called primers, in large excess to the reaction mix. They hybridize to the single-stranded DNA and specify the region of the template DNA which will be copied. This means, choosing the right forward and backward primers, a gene or other part of interest can be specifically amplified. Suitable primers have to fulfill certain rules. For example, they should hybridize to a unique position at the template DNA, should not form dimers with themselves and both forward and backward primer, should have similar melting temperatures. Primer design can be easily done using commercial software, which checks all the criteria[1].

A scheme of DNA amplification by PCR is depicted in Figure 1.9. One adds polymerase, primers, template DNA and nucleotides (dNTPs)[2] to a suitable reaction buffer and heats the solution up to 95°C in order to obtain single-stranded DNA. Then the temperature is lowered to 50-60 °C to allow primer hybridization. At the end of the cycle the primers are elongated by the *Taq* polymerase at 72 °C and the next cycle starts again with DNA denaturation. After the first cycle one ends with two new strands which are longer than the designed fragments (Fig. 1.9). However, in the second cycle the transcription of these strands yields the desired DNA. The number of these "right" fragments increases now exponentially as it is doubled every step, whereas the number of "wrong" fragments is incremented only by two at each cycle. Finally, after about 25 cycles the yield is dominated by the desired fragment.

Beside tailoring suitable DNA fragments, one has also to find ways to link these strands in order to obtain the artificial DNA structures one needs. As already shown in the previous section a common technique, coming from molecular cloning, is to use complementary single stranded overhangs, the so-called sticky ends. These overhangs can be easily prepared by using *restriction enzymes*. These type of enzymes recognize a specific 4- to 8-bp region, called *restriction site*, and then cleave both DNA strands at this site. Restriction enzymes have been purified from several hundred species of bacteria, allowing DNA molecules to be cut, also called *digested*, at a large number of different sequences. Many restriction sites like the

[1]Here the free software Generunner 3.05 from Hastings Software Inc. was used.

[2]dNTP stands for nucleotide triphosphate, i.e. nucleotides carrying three phosphates.

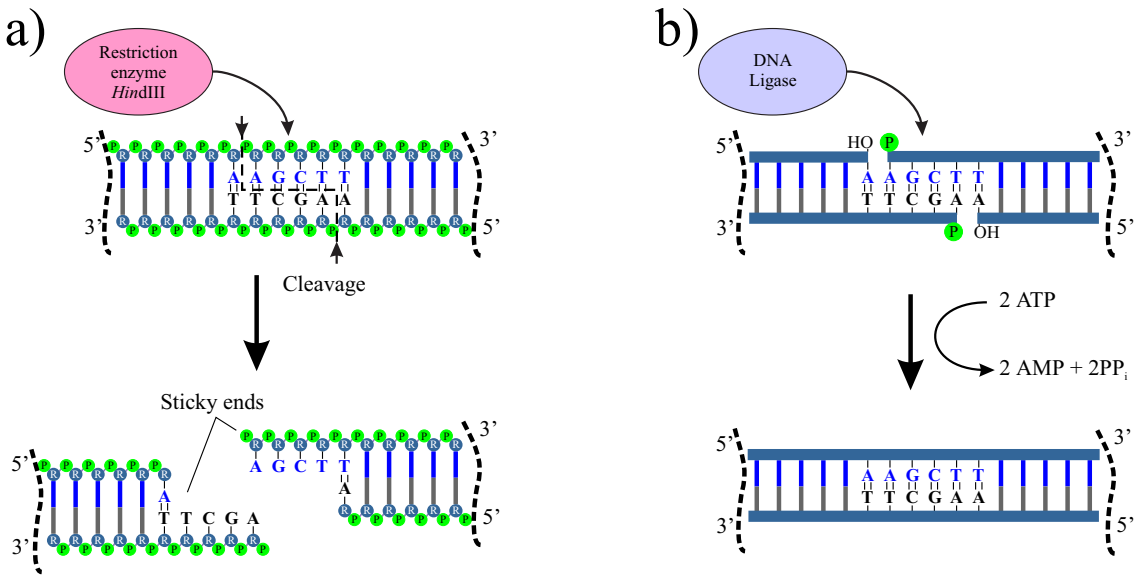

Figure 1.10: a) Recognition and cleavage of DNA by *Hin*dIII restriction endonuclease. b) Ligation of DNA fragments carrying complementary sticky ends.

*Hin*dIII site, shown in Figure 1.10a, are short inverted repeat sequences. That is, the restriction-site sequence is the same on each DNA strand when read in the 5' → 3' direction. Furthermore, *Hin*dIII makes staggered cuts in the two DNA strands. This results in the formation of two 4 bp long 5'-overhangs, which posses the same self-complementary sequence. The length of the overhang depends on the particular restriction enzyme. Each length, from 0 bp (so-called *blunt ends*) up to more than 10 bp is possible.

The reverse process to DNA cleavage is *ligation* mediated by an enzyme called *ligase*, which can catalyze the formation of a covalent linkage between the 3'-hydroxyl end of one restriction-fragment strand and the 5'-phosphate end of another restriction-fragment strand during the time that the sticky ends are transiently base-paired (Fig. 1.10b). This enzyme reaction for covalent coupling DNA fragments, carrying complementary sticky ends, is necessary as, for example, the melting temperature of two hybridized 4 bp overhangs like in Figure 1.10b is only about 12 °C . This means, the connection is not stable at room temperature. Thus, adding DNA ligase and ATP to a solution containing fragments with sticky ends leads to covalent coupling of the DNA strands.

5'-overhangs can be modified using an enzyme called Large fragment of polymerase I or *Klenow polymerase*. It fills in 5'-overhangs using dNTPs creating this way blunt ends. This reaction can be very useful. For example, if biotinylated bases are added to the reaction, one can easily prepare DNA which is functionalized with

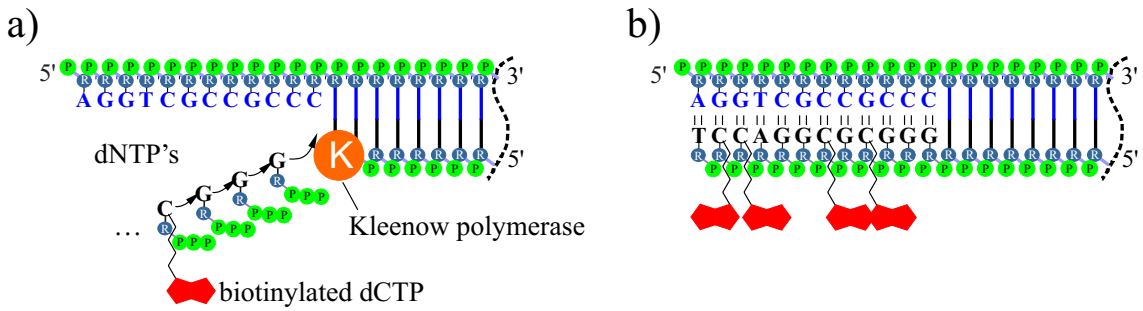

Figure 1.11: Biotinylation of an DNA end using Polymerase I, Kleenow fragment and biotinylated bases. The 5'-overhang is filled by the enzyme with dNTP's. The dCTP is linked to a biotin molecule over a carbohydrate spacer.

biotin at its ends (Fig. 1.11). If during the fill-in step not all dNTPs are added one can partially fill the 5'-overhang. Thus, the self-complementarity of restriction fragment ends can be broken. For instance, if one uses only dATP to fill-in the 4 bp long 5'-overhang left by the *Hin*dIII restriction enzyme (Fig. 1.10a), one ends up with a 3 bp overhang which is not self-complementary anymore.

Once the desired DNA structures are fabricated, they have to be analyzed and separated from the reaction mix. A powerful and in molecular biology widely spread method for doing this is *gel electrophoresis*, which separates DNA fragments according to their size. As already previously mentioned, DNA is highly charged near

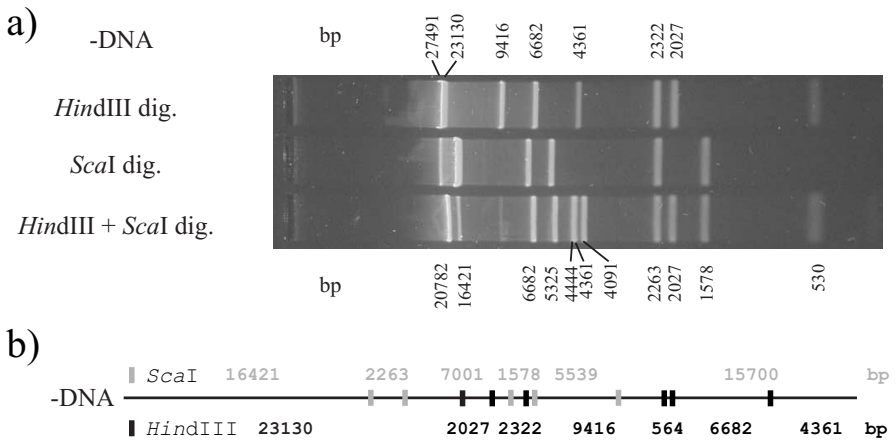

Figure 1.12: a) Fluorescently stained gel of λ-DNA digested with *Hin*dIII, *Sca*I and using both restriction enzymes at the same time. b) Map of the *Hin*dIII and *Sca*I restriction sites of λ-DNA. The significant band patterns can be used to assign the molecular weights of the separated fragments, which can be obtained, if the DNA sequence and the sequence of the restriction site are known.

neutral pH because the phosphate group in each nucleotide contributes one negative charge. Therefore, in an electric field DNA moves towards the positive electrode. This is used by electrophoresis. DNA is brought into a gel matrix, which consists of long, tangled chains of polymers which are separated by interconnecting channels or pores. Applying an electric field causes DNA movement at a rate inversely proportional to the log of the length of the fragments, which are separated this way from each other forming bands according to their molecular size. The DNA can be stained by a fluorescence dye and the bands are visualized using an UV lamp (Fig. 1.12). The length of unknown DNA fragments can be easily interpolated from DNA with known fragment size, the so-called *molecular weight standard*, which is run in the same gel. Common standards are restriction fragments of a DNA with known sequence. Typical materials used for casting gels are agarose or polyacrylamide.

1.3 DNA based nanostructure assembly

The use of DNA for the fabrication of nanostructures is at the moment an rapidly increasing field of research, within different directions have to be distinguished:

- The fabrication of artificial networks consisting of native DNA.
- The integration of DNA onto solid state surfaces.
- The formation of metal and semiconductor nanoparticle assemblies along DNA.

Work, which has been previously done in these three fields, is briefly reviewed in the following.

1.3.1 Fabrication of complex DNA networks

In the early 80s Nadrian C. Seeman introduced in a pioneering theoretical work the concept of *DNA nanotechnology* [33]. The idea behind that, is to use the exceptional self-assembly properties of DNA to build up complex artificial DNA structures. In the following years different structures[3] could be synthesized like a cube [4], a truncated octahedron [5] and 2-D DNA crystals [6,34]. Furthermore nanomechanical devices [35] as well as logical computation [36] could be established. These supramolecular structures are assembled from small rigid building blocks, which are simple DNA junctions or double and triple crossover molecules, comprising several DNA junctions (Fig. 1.13). Short synthetic oligomers are used to hybridize the DNA building blocks. Their specific coupling, which induces self-assembly, is accomplished by sticky end directed ligation.

[3] An image gallery can be found at Seeman's hompage http://seemanlab4.chem.nyu.edu

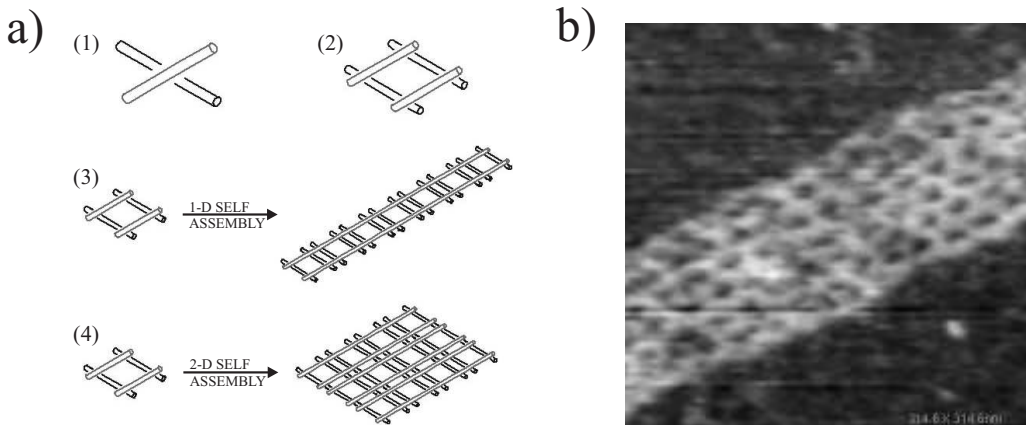

Figure 1.13: Two-dimensional DNA Holliday junction array taken from Ref. 34. a) Construction scheme of the array starting from a 4-armed (Holliday) junction (1) to a parallelogram with four of these junctions (2) and ending with 1-D (3) and 2-D DNA lattices (4). b) AFM image of the assembled 2-D lattice.

DNA junctions are important structures in nature, too. For example a 3-armed junction is forming the DNA replicational fork. During DNA recombination, where homologous sequences of two double stranded DNA strands are exchanged, a 4-armed junction, the so-called Holliday junction, is generated. Figure 1.14 shows a schematic view, how these junctions are formed using DNA single strands. However, junctions in nature are dynamic structures and are able to migrate along the strands, as they naturally consist of homologous sequences [37]. Because of that, it is impossible to synthesize these junctions *in vitro* by hybridization. In order to get stable, that is immobile, junctions the sequence design has to be made in a way, that homologous sequences at the branching point are avoided to prevent migration. Furthermore, all kind of dimers between the single oligomers should be restricted to few paired bases. To find an optimized sequence for the junction Seeman introduced the concept of *critons* [33]. Every single strand is considered to be composed of overlapping segments of a given criton length N_c. For example, a 10 bp long strand can be composed of 7 critons with a length of 4. The complementary sequence to a criton is called anti-criton. For a given value of N_c, 4^{N_c} critons are available. If in all strands, forming the DNA junction, every criton is unique, there will be no undesired base pairing with a length $\geq N_c$. Beside the discrimination of unwanted base pairing, migration of the junction as well as hairpins[4], have to be avoided. For fulfilling these requirements, the following four rules turned out to be sufficient [33]:

(1) Every criton in the individual strands forming the junction must be unique throughout all strands.

[4]Loops formed by base pairing within one single strand

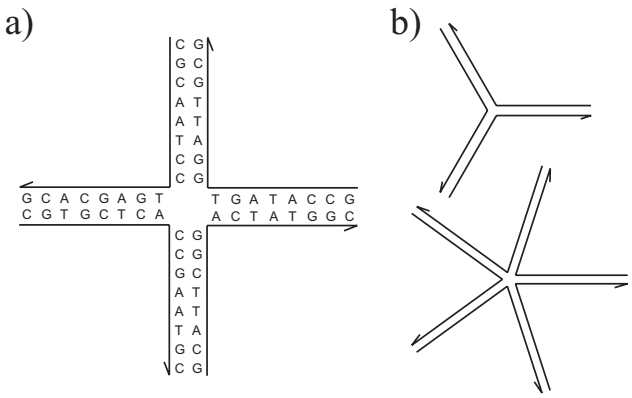

Figure 1.14: a) Sequence of an immobile 4-armed DNA junction taken from Ref. 33. b) Schematic view of a 3-armed and a 5-armed DNA junction. The 3'-ends of the single strands are indicated by half-arrowheads in both images.

(2) The anti-criton to any criton which spans the bend in a strand must not be present in any strand.

(3) Self-complementary critons are not permitted if N_c is an odd number, this injunction holds for all critons of size $(N_c + 1)$.

(4) The same base pair can only abut the junction twice. If it is present twice, those two occurrences must be on adjacent arms.

The last rule assures the immobility of the junction, whereas the first three rules are necessary as well as sufficient to enable pairing specificity for a pairing length of $\geq N_c$. Figure 1.14a shows a 4-armed junction, which fulfills these rules for a minimum $N_c = 4$. This junction was successfully synthesized [38]. Furthermore the existence of 3-armed, 5-armed and 6-armed junctions (Fig. 1.14b) could be demonstrated. However, junctions with more than four arms required 16 bp long arms to be stabile [39].

An alternative route to synthesize DNA junctions was chosen by the group of Günter von Kiedrowski, who used a chemical trisfunctional linker to couple three oligonucleotides at their 3'-ends [40]. Self-assembly of these branched molecules led to supramolecules called "nano-acetylene", consisting of two trisoligonucleotidyls, and "nano-cyclobutadiene" consisting of three trisoligonucleotidyls in analogy to the chemical compounds. The advantage of these molecules is that their assembly is based just on self-assembly without using ligation like in the work of Seeman. This way even a self-replication of the junctions could be realized by "chemical copying of their connectivity" [41].

Biotin streptavidin provides also an excellent possibility to link different DNA molecules. The DNA ends can be easily modified with biotin, just by using commercial biotinylated primers within a PCR process. Via a streptavidin bridge different strands can be coupled, and, as streptavidin has four binding sites for biotin, random networks could be obtained [42]. Denaturation of these structures and rapid cooling on ice led to the formation of supramolecular streptavidin-DNA rings [43].

1.3.2 Anchoring DNA to surfaces

Elasticity of polymers

The double helix structure of DNA can be assumed as stiff and rigid on a length scale of a few base pairs. Longer molecules are flexible. Without any external forces they adopt the energetically and entropically most favorable state and form coils in solution. The use of DNA for building up nanostructures, however, requires a well-defined morphology of the DNA molecules. There are no problems for structures with small lengths of the branches, as the are not very flexible. By contrast, longer molecules, as they are used for the integration into microstructures, have to be manipulated to avoid random coils, i.e., they have to be stretched. For this process one has to apply forces. In the following, these forces will be described in order to get quantitative values for the stretching of DNA to a certain extension.

Polymers, like DNA, consist of a large number of identical subunits. Applying statistics the molecule can be described as a set of N vectors $\{\overrightarrow{l}\} = \{\overrightarrow{l_1}, \overrightarrow{l_2}, ..., \overrightarrow{l_N}\}$ and the end to end vector $\overrightarrow{r}$ equals the sum of all $\overrightarrow{l_i}$. The scalar magnitude r of $\overrightarrow{r}$ can then be written as [44]:

$$r^2 = \overrightarrow{r} \cdot \overrightarrow{r} = \sum_{i,j} \overrightarrow{l_i} \cdot \overrightarrow{l_j} = \sum_i l_i^2 + \sum_{i \neq j} \overrightarrow{l_i} \cdot \overrightarrow{l_j} = \sum_i l_i^2 + 2 \sum_{0<i<j\leq n} \overrightarrow{l_i} \cdot \overrightarrow{l_j}. \quad (1.3)$$

A further quantity characterizing the configuration of the polymer is the radius of gyration s which is defined as the root-mean-square distance of the groups forming the molecule from their common center of gravity:

$$s^2 = (n+1)^{-1} \sum_0^N s_i^2, \quad (1.4)$$

where s_i is the distance of group i from the center of gravity.

Integrating the energy $E(\{\overrightarrow{l}\})$ over all possible configurations $d\{\overrightarrow{l}\}$, leads to the configuration partition function Z from which the statistical weight $w(\{\overrightarrow{l}\})$ of each configuration can be derived:

$$Z = \int \exp\left(-\frac{E(\{\overrightarrow{l}\})}{kT}\right) d\{\overrightarrow{l}\}, \qquad w(\{\overrightarrow{l}\}) = \exp\left(-\frac{E(\{\overrightarrow{l}\})}{kT}\right) \cdot Z^{-1}. \quad (1.5)$$

In order to obtain the force for a given extension one can calculate the partition function for a particular $\overrightarrow{r}$:

$$Z_r = \int_{\sum_i \overrightarrow{l_i} = \overrightarrow{r}} \exp\left(-\frac{E(\{\overrightarrow{l}\})}{kT}\right) d\{\overrightarrow{l}\}, \quad (1.6)$$

and the free energy of the system equals $E_f = -kT \ln Z_r$. The mean force $\langle \overrightarrow{F} \rangle$ is the derivative of the free Energy by the extension:

$$\langle \overrightarrow{F} \rangle = -\frac{\partial E_f}{\partial \overrightarrow{r}} = kT \frac{\partial \ln Z_f}{\partial \overrightarrow{r}}. \tag{1.7}$$

The most easy model to describe a polymer is the **Freely jointed chain model**. The polymer is treated as a chain of N uncorrelated segments of equal length l, where the orientation of adjacent segments does not influence the energy. Thus $\langle \overrightarrow{l_i} \cdot \overrightarrow{l_j} = 0 \rangle$ for $i \neq j$ and one derives from Equation 1.3:

$$\langle \overrightarrow{r}^2 \rangle = N\, l^2. \tag{1.8}$$

The energy $E(\{\overrightarrow{l}\}) = E = constant$ for all possible configurations $\{\overrightarrow{l}\}$ of the molecule. Introducing spherical coordinates one gets for the partition function:

$$Z = \int \exp(-\frac{E}{kT}) d\{\overrightarrow{l}\} = (4\pi)^N \exp\left(-\frac{E}{kT}\right), \tag{1.9}$$

and the statistical weight for each $\{\overrightarrow{l}\}$ equals $w(\{\overrightarrow{l}\}) = 1/(4\pi)^N$.

In real polymers adjacent bonds are not uncorrelated, but posses distinct fixed bond angles [44]. Within the model of the **Freely rotating chain** the polymer is simplified by N bonds of fixed length joined at fixed bond angles. All bond lengths l and bond angles θ are taken to be equal. Similar to the Freely jointed chain model the energy as well as the incidence of occurrence of each configuration is equal to that of every other. The projection of bond $i+1$ on bond i is $l \cos\theta$. Using this, one obtains

$$\langle \overrightarrow{l_i} \cdot \overrightarrow{l_{i+k}} \rangle = l^2 \cos^k \theta, \tag{1.10}$$

because only the in-plane projections have to be averaged, as the mean value for the transverse projections is always zero. In analogy to equation 1.8 the mean square end to end distance results to

$$\langle \overrightarrow{r}^2 \rangle = N\, l^2 + 2l^2 \sum_{i<j} \cos^{j-i} \theta. \tag{1.11}$$

In the limit of large N one can transform this equation to

$$\langle \overrightarrow{r}^2 \rangle = N\, l^2 \frac{1+\cos\theta}{1-\cos\theta} =: N\, l^2\, \alpha. \tag{1.12}$$

Thus, fixed bond angles increase the extension of the polymer, due to the increased stiffness of the polymer. A quantity characterizing this stiffness is the *persistence*

length a [45], defined as the average sum of the projections of all bonds $j \geq i$ on bond i in an indefinitely long chain

$$a := \lim_{N\to\infty} l \sum_{i}^{N} \cos^j \theta := \frac{l}{1 - cos\,\theta}. \tag{1.13}$$

In contrast to the now introduced two models, DNA is better described as a flexible continuous rod instead of constructed from discrete units. In 1949 Kratky and Porod introduced the **Worm-like chain (WLC) model** to describe this type of semiflexible molecules [45], which can be derived from the freely rotating chain by increasing the number of segments, while keeping the *contour length* L as well as the persistence length a constant[5]. As a consequence the bond angle θ vanishes, and in the limit $N \to \infty$ and $l \to \infty$ one derives from Equation 1.12

$$\langle \overrightarrow{r}^2 \rangle = 2\,a\,L. \tag{1.14}$$

From this one sees easily that DNA molecules are strongly coiled. With persistence lengths, found in the literature, one can calculated the average end-to end-distance (Fig. 1.15a). For example, the 16 μm long λ-DNA, which is also used in the following experiments, has under the applied conditions an average end-to-end distance of only 1.3μm. The persistence length dependents very much on the ionic strength of the solution (Fig. 1.15 Inset). As under low salt concentrations the backbone charge shielding is reduced, the repulsion of the chain segments is increased and the persistence length is raised. However, at monovalent cation concentrations of larger 10 mM, as they are typically used in experiments, a value of 53 nm is a good approximation [46]. Single stranded DNA is much more flexible and has persistence lengths of smaller than 10 nm [48].

Within the WLC model also the force, required to hold the DNA in a fixed extension, can be derived. However, there is no exact solution for this problem. Therefore, often an interpolation equation is used, which gives a reasonable approximation for extensions x smaller than the contour length L [46]:

$$F = \frac{k_B T}{a}\left[\frac{1}{4}\left(1 - \frac{x}{L}\right)^{-2} - \frac{1}{4} + \frac{x}{L}\right], \tag{1.15}$$

where k_B denotes the Boltzmann constant and T the absolute temperature. This equation describes just the entropic elasticity of the WLC, arising from the reduced entropy of the stretched chain. It assumes that the DNA is inextensible. Within this restriction, it is in good agreement with experimental force measurements of non-overstretched DNA (Fig. 1.15b). From the the force-extension curve one can now

[5] $L := \sum |\ \overrightarrow{l_i}\ | = N\,l$

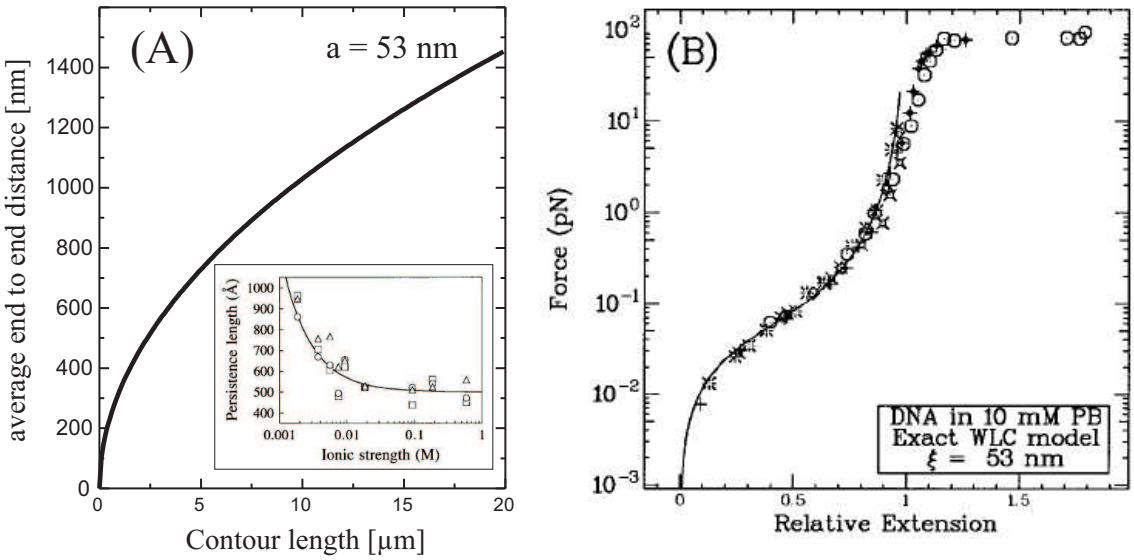

Figure 1.15: a) Mean square end-to-end distance of DNA as a function of the molecule length for a persistence length of $a = 53\,\text{nm}$. Inset) Dependence of the persistence length on the monovalent ionic strength taken from Ref. 46. b)Force-versus-extension curve for 16 μm long λ-DNA taken from Ref. 47. For extensions below the contour length the curve is well described by the worm-like chain model (continuous curve).

obtain numbers for the anchoring forces necessary to attached DNA to a surface and to stretch it there. In the further experiments mainly λ-DNA is used, which has a length of 48502 bp corresponding to 16.17 μm. To stretch this DNA to 8 μm, which corresponds to half of the contour length almost 0.1 pN are necessary. 1 pN is required to stretch it to 14 μm, whereas with 10 pN one increases the length to just 15.4 μm. From experimental investigations it is known [23,49], that it is also possible to overstretch DNA beyond the contour length, which is reached at about 35 pN. At about 70 pN a transition plateau is reached, where the DNA is cooperatively stretched to the so-called S-DNA conformation which is about 1.7 times longer than B-DNA (Fig. 1.15b).

In conclusion, to keep a stretched, straight DNA molecule with the end attached to a surface, one needs anchors, which at least last a few pN. In the following, different methods for the attachment of DNA to surfaces will be considered with respect to this aspect.

Methods for anchoring DNA to surfaces

For the fabrication of DNA-based circuits, the site specific attachment of DNA to a patterned surface, in particular electrode structures, is necessary for the following reasons: i) The establishment of an electrical connection of the structure to the

surrounding chip structure. ii) The positioning of the DNA using microcontact pads, which can serve as predefined DNA binding sites. In both cases binding only at the DNA ends is desirable. Three different methods for such an end-specific attachment of DNA can be used:

- electrostatic interaction between DNA and a substrate
- covalent binding of a chemical group attached to the DNA end and surface atoms
- binding of a protein attached to the DNA end to its antibody immobilized at the surface.

As DNA is a negatively charged molecule it can be easily immobilized on a positively charged surface using **electrostatic interaction**. However, as not only the DNA extremities but also the midsegment are charged, the attachment is normally not end-specific. Thus, if a DNA coil is approaching the surface it will probably stick to it in this coiled form. Recently, Bensimon *et al.* discovered a method to circumvent this problem [50]. They found that in a certain pH range, which is very much dependent on functional surface groups, DNA binds specifically at its extremities [51]. Using the receding meniscus of a droplet it was possible to stretch and even to overstretch DNA molecules in a very precise way, which was called *molecular combing*. For surfaces covered with ionizable groups , like amines, a possible explanation of this effect is, that at a pH below the pK_a value protonation takes place (i.e. $\text{-NH}_2 \rightarrow \text{-NH}_3^+$). The surface is positively charged, but gets less and less charged for increasing pH. At low pH, i.e. at high charge density, the DNA sticks very strong to the surface and no stretching is observed. At high pH t surface gets neutral. As in a high dielectric medium a charged object near a low dielectric surface is repelled from the surface [51], the DNA does not bind anymore. However, at intermediate pH a crossover between repulsion and adhesion takes places. But, as the DNA ends are higher charged than the midsegment, also the interactions with the surface are different for the ends and for the rest of the molecule. Thus, an end-specific binding can be obtained by balancing exactly the surface charge. The bond of the DNA to the surface is very stable and withstands capillary forces of >160 pN [50]. The molecular combing technique has now also been applied to study enzyme activity on single DNA molecules, like the digestion with restriction enzymes [52] and the transcription of DNA by RNA polymerase [53].

Different methods can be applied to **couple DNA covalently to surfaces**. For example, amino-modified DNA can be bound to an aldehyde-functionalized substrate or DNA carrying $-SH$, so-called thiol, groups at its ends can directly be bound to a clean gold surface. Gold as substrate is very interesting, as it can be easily used to fabricate microstructures, which opens a way to integrate DNA

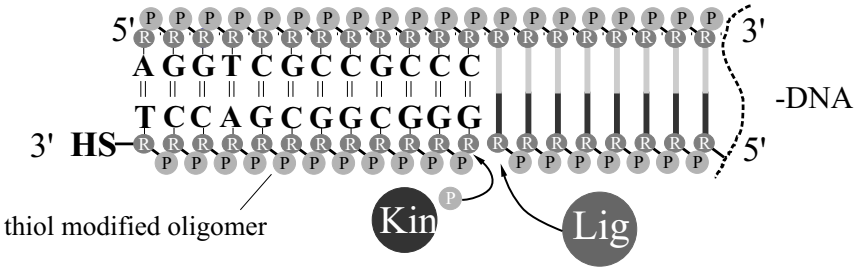

Figure 1.16: Hybridization of a thiol modified oligomer to the sticky end of λ-DNA. The single stranded nick can be closed by phosphorylation of the oligomer before hybridization using T4 kinase (Kin) and ligation after hybridization using T4 ligase (Lig).

site-specifically into electrode arrays. Therefore, in the following the attachment of DNA to gold substrates using thiol groups is described.

The thiol group is binding to gold by releasing hydrogen and establishing a stabile gold-sulfur bridge. Experimental results showed, that the forces necessary to rupture an sulfur-gold anchor are in the range of 1 nN, although one has to keep in mind that these forces depend strongly on the force loading rate, which determines the lifetime of the bond[6] [55].

During chemical oligonucleotide synthesis a thiol group can be easily attached either to the 3'- or the 5'-end. Longer DNA fragments with thiol labelled ends can be synthesized either by PCR using 5'-thiol modified primers or by hybridization of thiol modified oligomers with single stranded overhangs of DNA (Fig. 1.16). As PCR is restricted to amplify fragments of 20-30 kbp maximum length, in particular the latter method is suitable for very long DNA molecules. However, the bond of a hybridized oligomer to the DNA is not very strong. For example, the oligomer which is complementary to the 12 bp long 5'-overhang of λ-DNA has a melting temperature of only 55°C and the rupture force of a decamer, which ranges at high the force loading rates from 40 pN down to a few pN at low loading rates [56]. In order to improve the stability of the bond, it is possible to close the single stranded nick between the 5'-end of the oligomer end the 3'-end of the λ-DNA. For this, before the hybridization a phosphate has to be attached at the OH-terminated 5'-end of the oligomer, which can be done by an enzyme called polynucleotide kinase (Fig. 1.16). After the hybridization process a covalent linkage between the phosphate of the oligomer 5'-end and the hydroxy terminated 3'-end of the λ-DNA can be established using a ligase as it was shown in Section 1.2. Thus, a bond between DNA and gold surfaces can be established, which can last forces in the nN range. If the hybridization is not done in solution, but at the substrate (Fig. 1.17a), a further advantage of this method in comparison to the electrostatic attachment is that a

[6] 1.4 nN at a force loading rate of 10 nN per second [54]

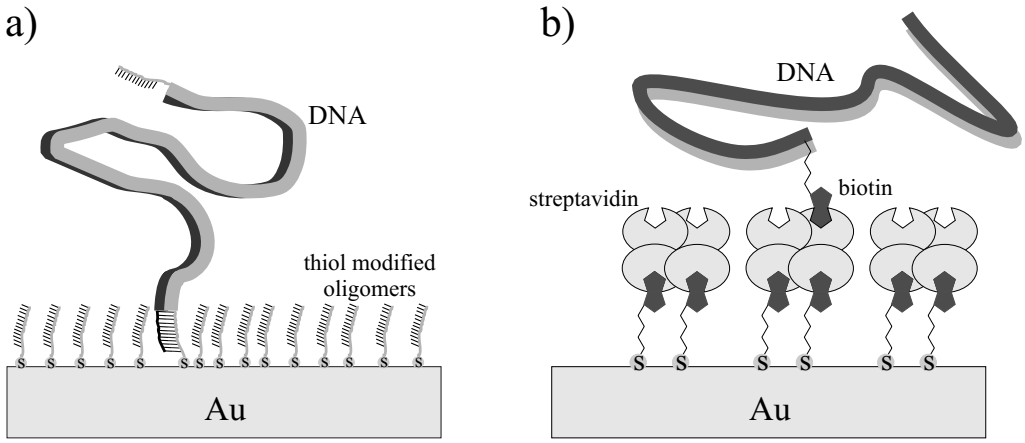

Figure 1.17: a) Attachment of a DNA end to a gold surface by hybridization with an oligomer, which is anchored by a thiol group to the substrate. b) Attachment of a biotinylated DNA end to a substrate covered with streptavidin, which was immobilized by a biotin-thiol linker at the gold surface [57].

single DNA end can be addressed, as the two single ends of λ-DNA do not have the same but complementary sticky ends. Thus, it was possible to stretch a λ-DNA molecule between two electrodes in a very controlled way. Here, one electrode was modified with oligomers complementary to the first end. The other electrode was covered with oligomers complementary to the second end [15].

Non-covalent anchoring of DNA can be achieved using biotin-streptavidin binding (Fig. 1.8), which is one of the strongest noncovalent interactions in nature [32] (Section 1.1). The force between biotin and streptavidin can be as high as 160 pN at high loading rates, but drops to only 20 pN at a loading rate of $1\,\mathrm{pN\,s^{-1}}$ [58]. As already discussed in Section 1.2 several biotin molecules can be easily incorporated into the DNA 5'-overhangs (Fig. 1.11, p. 14). Therefore, the biotin streptavidin linkage provides a suitable method for the attachment of DNA to surfaces. Zimmermann and Cox used it first to anchor λ-DNA molecules to gold microstructures (Fig. 1.17b) and to stretch single molecules with hydrodynamic flow or an electrostatic field [57]. In these experiments, a single biotin molecule turned out to be sufficient to withstand the stretching forces. Klenow polymerase was used to incorporate biotin into the λ-DNA sticky ends. By controlling carefully the nucleotides supplemented to the reaction, it was possible to label one end with a single biotin and the other with a single digoxigenin molecule, which can be bound to its antibody antidigoxigenin. Thus, end-specific labelling was accomplished.

1.3.3 Metallization of DNA templates

In the previous sections it was shown, that DNA is a polymeric molecule, which can be handled, manipulated and which has the ability to self-assemble into complex networks. Furthermore, there are efficient ways to anchor DNA at surfaces, to stretch it between electrodes, i.e. to integrate it into microfabricated contact arrays. The diameter of the molecule of only 2 nm and the large aspect ratio makes it an ideal object for a nanowire, which connects functional elements in future electronic circuits. If DNA would possess the appropriate electrical properties, it could be ready-to-use applied for this purpose. However, investigations of the conductivity of the native molecule suggest an insulating behavior on a length scale of more than 100 nm [15, 59, 60]. In order to establish a certain conductivity of a DNA-based nanowire, a promising approach is to use the DNA as a template and to cover it with materials possessing the desired electrical properties.

When the experimental work for this thesis started, there have been only a view attempts to build metallic and semiconducting nanoparticle assemblies along single DNA molecules [7, 15, 16, 61]. Meanwhile, this field has attracted more and more interest, which is reflected by the increasing number of published works [17, 18, 19, 20, 21, 22, 62, 63]. Within the possibilities to associate DNA and nanoparticles, three different basic principles can be distinguished:

(1) The electrostatic binding of positively charged colloids to the negatively charged DNA [62], which has been shown for CdS clusters.

(2) The specific binding of colloids to DNA via a chemical bond [7, 61, 63]. Either DNA and/or colloids are modified with functional groups, which can be, for example, thiol groups and biotin-streptavidin complexes. Also colloids carrying oligonucleotides can be used to hybridize them to single stranded parts of DNA. Up to now, this method has only been applied to short DNA fragments, where a small number of particles was attached per single DNA strand.

(3) The direct growth of particles at the DNA [15, 16, 17, 18, 19, 20, 21, 22]. This is accomplished by the formation of nucleation sites along the DNA and further metal or semiconductor deposition by chemical reduction of the corresponding salts. As nucleation centers serve catalytically active materials among them silver [15, 17], cadmium [16], palladium [18], platinum [19, 20, 21] and copper [22]. They are formed by allowing the corresponding metal ions to bind to the DNA.

All these basic methods have their advantages and disadvantages. The first method has to deal with the problem of inhomogeneity of the coverage with particles [64]. The resulting colloid chains tend to have larger gaps. Thus, if one tries to close the gaps in order to get a wire by a further deposition of metal, the continuous

regions tend either to be quit short or, if more additional material is deposited, the wire diameters get quit large [65]. Up to now, the second method was only shown for short DNA strands. The mayor problem here will be the specificity of particle deposition versus undesired background binding.

Most promising is the third principle, as the metal ions, which are used to create nucleation centers at the DNA, can bind densely along the DNA, which leads to a homogeneous distribution of nucleation sites. Pioneering work in this filed was done by Coffer *et al.*, who bound Cd^{2+} ions to plasmid DNA and reduced them with H_2S, leading to 5 nm CdS clusters at the circular DNA [16]. Braun *et al.* set the first milestone by synthesizing the first conductive wire on a λ-DNA template, which was previously stretched between two electrodes [15]. Thus, they proofed the principle of integration of DNA into microelectrode structures and subsequent transformation of the electric properties of the DNA bridge by metallization. The resulting silver wire, however, had still a diameter of 100 nm and revealed a non-linear, history-dependent I-V curve. Later on the conductive properties of DNA based wires could be improved by using palladium [66] and gold [17] for the metallization. The obtained I-V curves showed ohmic behavior at room temperature. However, up to now the diameter of these wires could not be pushed below 50 nm. Other attempts to get a thinner metallization did not result in continuous structures [21, 22]. From the miniaturization in microelectronics, future requirements consist of the fabrication of wires with diameters of smaller than 10 nm and demand a highly specific template metallization process on chip. Therefore a work, which still has to be done, is the construction of thinner conductive wires, which is one of the intentions of the present work.

Besides the formation of a plain wire along DNA, the idea to use the information, i.e. the base sequence, of the DNA in order to control the metal deposition, is most challenging. Resulting metal constructs along DNA could thus have gaps on predefined positions, which could act as tunnel barriers. Recent work in this field could indeed accomplish such a sequence-dependent metallization [17]. Keren and coworkers used *Rec*A protein, which is the driving force during DNA recombination, to screen the DNA at specific sequences with the protein. This way silver ions could not bind there and metallization of the DNA took only place at the non-screened parts of the DNA. The sequence-dependent metallization of DNA is a further tool, which broadens very much the range of metal constructs which can be constructed with the help of the carrier of the genetic code.

2 Artificial DNA junctions

For a potential use of DNA in future nanoelectronics the formation of complex DNA networks is essential. A lot of work in this field has been already done by SEEMAN[1]. However, as he uses short and stiff synthetic oligonucleotides, the branch lengths of the building blocks, used for the assembly of large networks, are restricted to a few or a few tens of nanometers (Fig. 1.13, p. 16). At the moment the "state-of-the-art" DNA metallization achieves wires with diameters of several tens of nanometers and cluster assemblies with cluster sizes of about 5 nm (see Section 1.3.3). Metallization of the mentioned DNA networks would result more in a continuous metal film than in a network. Therefore, in order to circumvent these problems, DNA structures with increased branch lengths of more than 100 nm are required. A further advantage of such larger structures is that their dimensions fit better to the distances in microfabricated arrays, which enables the integration of the DNA templates between microelectrodes.

One basic element of DNA networks are junctions. In the following the construction of multi-branched DNA junctions by the use of a simple kit procedure, which is based on a building block principle, will be shown. Furthermore, it is demonstrated that small gold colloids, as representatives of a functional element can be attached to the center of the DNA junction, which is functionalized by only a small change in the synthesis procedure.

2.1 Construction of a 3-armed DNA junction

The simplest junction which exists is a 3-armed junction. The construction scheme, which was used in the following experiments to synthesize such a junction, is depicted in Figure 2.1. In a first step a small DNA linker molecule is formed, which has three coupling sites, i.e. sticky ends, for longer DNA strands, the so-called elongations. These are fabricated in a second step. Finally, linkers and elongations are "glued" together. The linker element carries the structural information. It determines for example whether a 3-armed or a 4-armed molecule is formed (see Section 2.2.1). The structure of the linker is determined by the sequence of the DNA strands which form

[1] A brief review is given in Section 1.3.1

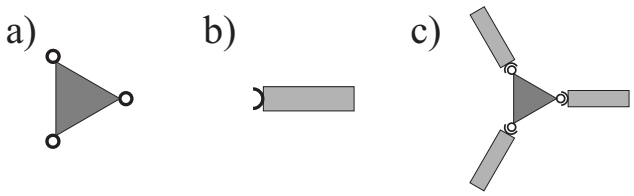

Figure 2.1: Fabrication scheme of a 3-armed DNA junction: a) Synthesis of a small linker element with three affinity sites. b) Synthesis of an elongation c) Coupling of linker and elongation.

the molecule. As only synthetic oligonucleotides allow full sequence flexibility, such DNA strands were used to form the linker. However, the use of these oligomers with their restricted length requires the elongation of the linker arms, i.e. the synthesis of longer straight strands, which are finally coupled to the linker.

2.1.1 Design of the linker element

The linker element is composed of three DNA single strands which are partly complementary to each other (Fig. 2.2). Thus a 3-armed molecule can be formed, which has furthermore at all ends GCT 5'-overhangs, which serve as sticky ends while attaching the elongations. The linker element is synthesized by hybridization of the three oligomers. For our first experiments the sequence *S1* (Fig. 2.2a) was used, which was designed in collaboration with Peter Seibel (University Würzburg). It contains only GC base pairs in the vicinity of the branching point, which could be useful for a sequence-dependent metallization at this place (see Section 4.3.3). The successful formation of the linker can be proven by gel electrophoresis (Fig. 2.3). When only two of the three oligomers, which form the junction, are hybridized to each other, a band pattern due to several dimers can be observed in the gel (lanes *S1* o1+o2, *S1* o2+o3, *S1* o1+o3, in Figure 2.3). The band at around 50 bp is attributed to the expected dimer, whereas the other bands are caused by mispairings. When all the three oligomers are hybridized a new band appears at higher molecular weight than the dimers (lane *S1* o1+o2+o3 in Figure 2.3). Obviously it is the desired 3-armed linker. However, as one can see in the intensity profile still many dimers are formed

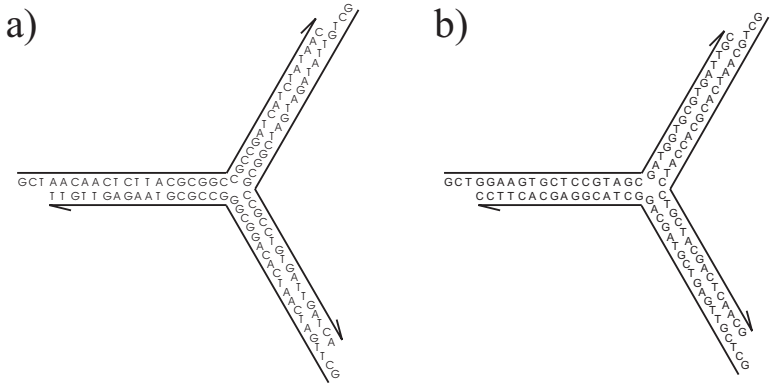

Figure 2.2: Sequences used for the 3-armed linker element. a) Non-optimized sequence *S1*. b) Optimized sequence *S2* taken from Ref. 39. The 3'-ends of the single strands are indicated by half-arrowheads.

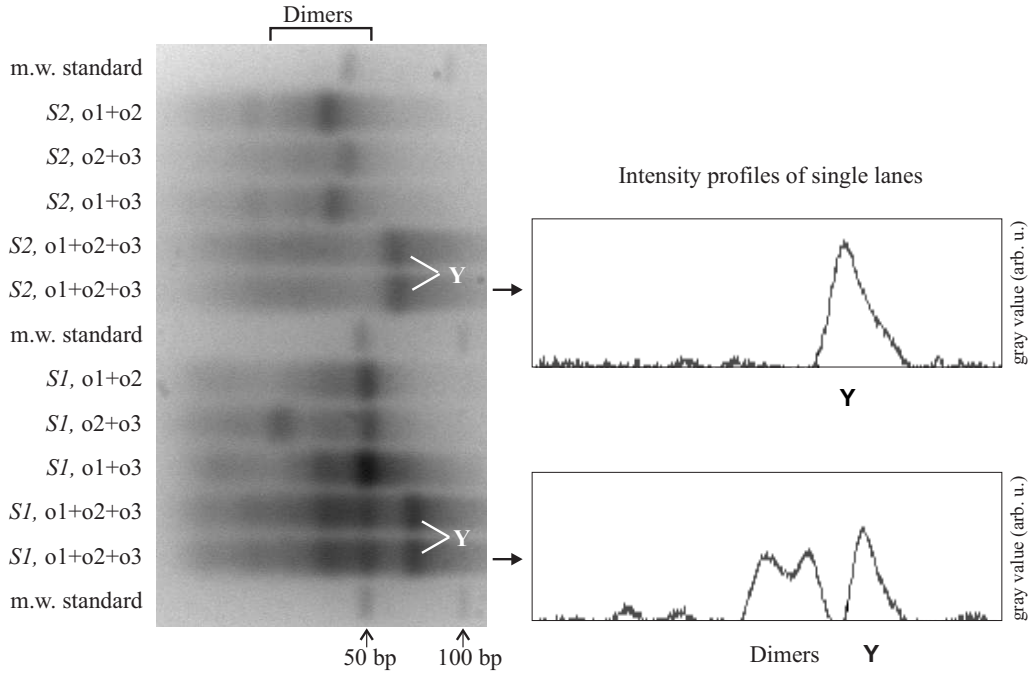

Figure 2.3: Gel electrophoresis of the 3-armed linker.

beside the 3-armed linker. Summarizing the gray scale values of the different bands, which are equivalent to the quantity of the DNA, a yield of the linker *S1* of only 34% is obtained. Analysis of the linker sequence with a home-made software provides a criton length of 8 (The criteria of optimum sequence design are explained in Section 1.3.1). Furthermore, three of the critons are self-complementary and for three critons, which span the bend, the anti-criton is present. Two of these unfavorable critons at the bend are even self-complementary and extend from 5 bases before the bend till 3 bases behind. The difficulties with this sequence arise mainly from the fact, that the bases flanking the branching point consist exclusively of guanine and cytosine, which leads to poor sequence diversity. Thus, undesired base pairings can occur leading to different stabile dimer structures. To avoid these mispairing problems, an optimized sequence [39] with added GCT 5'-overhangs was applied. Its criton length is 7 and there are no self-complementary critons. For only 1 criton at the bend the anti-criton is present and it extends till only 1 base behind the bend. Hybridization of the sequence-optimized oligomers leads to the desired result, i.e. the almost exclusive formation of the 3-armed linker *S2* (Fig. 2.3).

The product yield, however, is not only influenced by the sequence of the oligomeric strands but also by the hybridization conditions like temperature and ionic strength. For optimization, different salt and buffer conditions were tested. The hybridization was made by heating the solution with a stoichiometric amount of the oligomers

to 95°C and subsequent cooling to 4°C . Like in Ref. 40 a fast cooling on ice with a subsequent relaxation step at 4°C as well as a small temperature gradient with -0.1°C min^{-1} were tried. By comparison of the electrophoretic bands in the gel, the best yield could be obtained in a buffer containing Tris-HCl, NaCl and $MgCl_2$ with a slow cooling procedure.

As synthetic oligomers are not phosphorylated at their 5'-ends, phosphate groups were introduced after hybridization using T4 polynucleotide kinase. This step is necessary in order to enable ligation of the elongations to the linker.

2.1.2 Design of the elongation

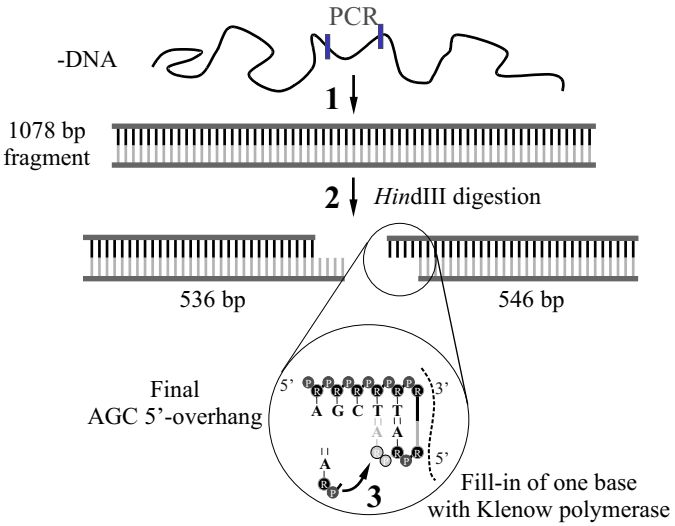

Figure 2.4: Preparation scheme of the elongation. 1) A 1078 bp fragment is amplified by PCR from λ-DNA. 2) *Hin*dIII digestion of the fragment into two almost equally long strands carrying AGCT 5'-overhangs. 3) Fill-in of adenosine leading to the final AGC 5'-overhang.

The design of the elongation should meet two criteria. First, it has to be longer than 100 nm or 300 bp. Second, one end must possess an 5'-overhang complementary to the 5'-overhangs of the linker molecule. In this case the use of synthetic DNA is not longer possible as the length of such strands is restricted to 100 bp. Therefore, PCR was chosen to amplify fragments of an appropriate length. An 5'-overhang can be easily made by using restriction enzymes. However, most enzymes produce self-complementary overhangs, which can not be used as religation among the fragments can occur. Self-complementarity can be easily destroyed be filling in one base with the help of Klenow polymerase. By using these considerations, the elongation synthesis was made in the following way: Two PCR primers[2] were designed, which copy the 24616 till 25693 bp region of λ-DNA. The resulting 1078 bp fragment has a

[2]forward primer: 5'-CAATAAATTCTGACTGTAGCTG, backward primer: 5'-AGTAGTACTGCAAGAGGTTCC

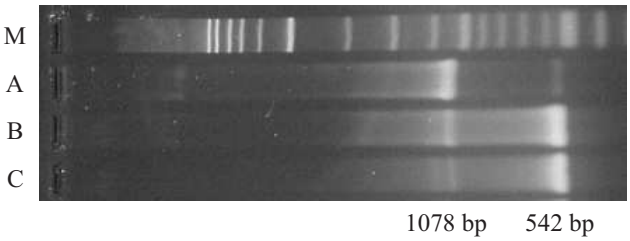

Figure 2.5: Gel electrophoreses of the elongations. M) Molecular weight marker. A) Religated *Hin*dIII fragments. B) Final elongations with modified 5'-overhangs after ligation. C) *Hin*dIII digested 1087 bp fragment.

*Hin*dIII restriction site in about the middle of its length (Fig. 2.4). Thus, by cleavage with *Hin*dIII a 536 bp and a 546 bp fragment with 5'-AGCT overhangs are produced. For breaking the self-complementarity of the overhangs, the fragments are incubated with dATP and Klenow polymerase. This way adenosine is filled-in, but as the solution does not contain dGTP, the reaction stops at this point and 5'-AGC overhangs remain. Furthermore, dTTP is supplied to the reaction mix to prevent extensive degradation of the fragment's blunt ends. The polymerase possesses an 3'→5' exonuclease activity. If no dGTP and dCTP are present the polymerase removes this bases from the 3'-end. Therefore only the blunt end formed by the forward primer is degraded by one guanine whereas the other blunt end remains unchanged.

The final elongation fragments are 536 bp or 546 bp long, which corresponds to about 180 nm. They have one phosphorylated 5'-AGC overhang and a blunt or a one base recessed end, which is not phosphorylated at the 5'-end, because of the non-phosphorylated primers. Thus, fragment religation at the blunt ends but also at the 5'-AGC 5'-overhang is disabled. But, ligation of the 5'-AGC overhang to its complementary GCT overhang at the linker is enabled.

Successful linker preparation is proven by gel electrophoresis. As one can see in Figure 2.5, the 1078 bp fragment can be successful digested into about 542 bp long strands (lane C). As their 5'-overhangs are self-complementary, religation, the reverse process, is possible and one obtains again the 1078 bp fragment (lane A). After the fill-in step of adenine into the overhang religation should be disabled, which is indeed observed in the experiment (lane B). This way one can not exactly prove that the 5'-AGC is obtained, however, it proves, that this end was modified.

2.1.3 Junction ligation

After successful preparation of linker and elongation, they are connected by ligation. For this elongations and linker are mixed in a molar ratio of 3.3 : 1 to have a small excess of elongations and T4 ligase is added. The result is studied with gel electrophoresis. In comparison with lane B in Figure 2.5, where the elongations were ligated without the linker element, a new band appears at about 2000 bp (band 3(Y), Fig. 2.6), which, according to our previous considerations, has to be the 3-armed

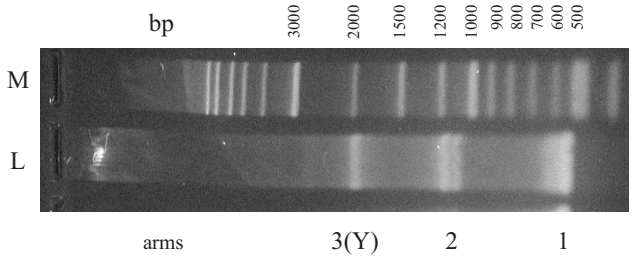

Figure 2.6: Gel electrophoresis of the 3-armed junction. M) Molecular weight marker. L) Ligation of 3-armed linker and elongations.

junction. The non-linear shape of the molecule can already be seen in the gel as the attributed electrophoretic molecular weight is 2000 bp - about four times but not three times larger than a single arm, as one would expect from its real molecular weight. In contrast to the case without linker (lane B, Fig. 2.5), the bands 1 and 2 are both split into two subbands. Measuring the weight difference between the subbands one obtains about 70 bp which corresponds to the size of a single 3-armed linker molecule. The subband with the higher and the subband with the lower molecular weight correspond to elongations with and without coupled tripod, respectively. For band 1 it is clear that it is one elongation with or without linker. According to this, the high molecular weight fragment of band 2 are two elongations coupled via one linker molecule. The lower weight fragment of band 2, however, is originated by incomplete digestion of the 1078 bp PCR fragment.

As it is clearly to be seen in the gel, the yield of the junction is far away from 100%. Different ratios between linkers and elongations as well as longer ligation times were tested in order to shift the balance towards the junctions. However, a better yield could not be accomplished. Therefore, the junctions are purified from the other products by slicing the corresponding band out of the gel and eluting the

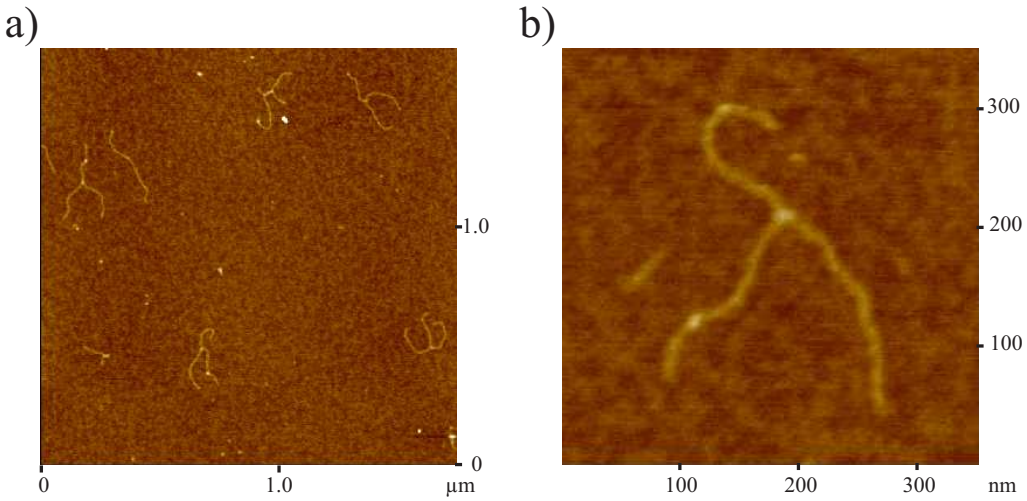

Figure 2.7: SFM images of the 3-armed junction. Height scale is 5 nm.

DNA. This way pure junctions are prepared. In AFM investigations the expected morphology of the junction is finally confirmed (Fig. 2.7). The overview (Fig. 2.7a) shows that lots of the 3-armed junctions can be found on the sample, although some broken molecules are present. Length measurements of the arms of the 3-armed junction provide 185 ± 14 nm in good agreement with the real lengths of 184 nm for a 553 bp and 187 nm for a 563 bp arm[3]. Angle measurements between the arms of the 3-arm junctions show a standard deviation of 14.5° from the average of 120°. Thus, the junctions are quite rigid structures at the branching point, where only low flexibility is allowed.

2.2 Multi-branched DNA molecules

In the previous section the fabrication of a 3-armed DNA junction is described. However, for the formation of complex DNA networks branching points with a higher number of branches are required. One way to solve this task is the hybridization of n semi-complementary oligomers to form a n-arm junction as it is discussed previously (Fig. 1.14, p. 16). In order to design an immobile junction this method is restricted to $n = 8$, according to rule (4) for optimized sequences (Section 1.3.1). A further disadvantage is that non-homologous sequences for n-oligomers have to be designed, which strongly increases complexity of sequence design. To circumvent these difficulties, an alternative construction scheme for a n-armed linker element was proposed, which uses the general sequence design of the 3-armed linker and changes only its sticky ends.

2.2.1 Building-block principle

The idea of such an alternative scheme for the construction of n-armed linker molecules is to use the 3-armed linkers as building blocks. If two of these linkers are connected via one arm a molecule is formed, which has four coupling sites for elongations, i.e. it is a four armed linker. To enable the coupling, exactly one arm of the first linker has to be made sticky to exactly one arm of a second linker molecule. This can be achieved by hybridization of a linker molecule, which has two sticky ends for the elongations (5'-AGC) but one end with a different sequence for which in particular 5'-TAG was taken (Fig. 2.8a). The other linker has again two elongation coupling sites and one end which is sticky to the 5'-TAG end of the first linker, i.e. it must have an 5'-CTA overhang (Fig. 2.8b). This way a 4-armed linker molecule is well-defined assembled. Elongation of the arms leads finally to a 4-armed junction (Fig. 2.8d). This assembly scheme can be further extended to construct linkers with any number n of arms. If one couples to the 4-armed linker

[3] 536 or 546 bp of the elongation plus 17 bp arm length of the linker

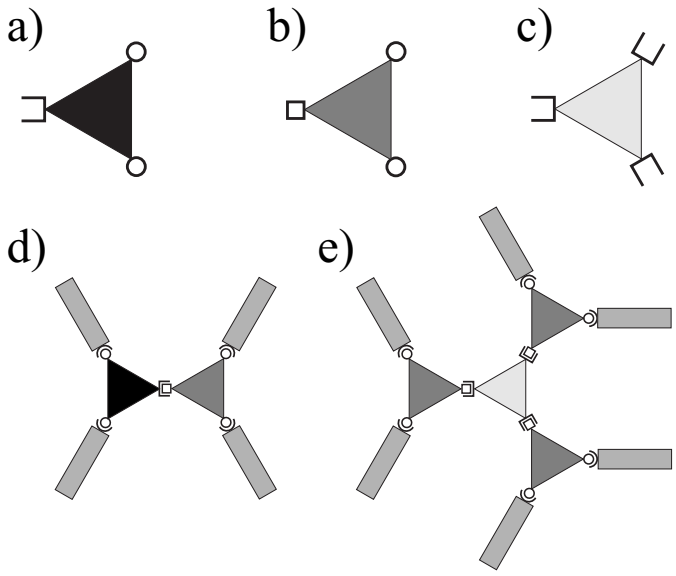

Figure 2.8: Construction scheme of multi-branched junctions. a)-c) Used three-armed linker building blocks. For all of them the sequence $S1$ was taken for the double-stranded regions. Only the sticky ends are different. ○ denotes an 5'-GCT overhang which is complementary to ⊂, which is a 5'-AGC overhang. Accordingly ⊏, which denotes a 5'-TAG end, is sticky to □, a 5'-CTA end. d), e) Design of a 4-armed, 6-armed junction based on 3-armed linkers.

another 3-armed linker, a 5-armed linker is formed. Addition of another 3-armed linker leads to a 6-armed linker, and so on. This means an n-armed linker can be assembled by $(n-2)$ 3-armed linkers. Figure 2.8e shows one possibility how a 6-armed linker can be formed. A new 3-armed linker with three 5'-TAG ends (Fig. 2.8c) is used to couple another three 3-armed junctions possessing two elongation coupling sites.

In the following the three described linkers are denoted as ⟨⊏○○⟩, ⟨□○○⟩ and ⟨⊏⊏⊏⟩ according to the symbols used to represent their sticky ends in Figure 2.8a-c.

2.2.2 Ligation of n-armed linkers and junctions

Indeed the formation of such n-armed junctions can be shown under experimental conditions. Figure 2.9a shows the result of ligating the 3-armed linkers to 4- and 6-armed linkers. For the 4-armed linker element the two 3-armed linkers ⟨⊏○○⟩ and ⟨□○○⟩ are ligated together forming a molecule with about the double molecular weight. As expected, in the gel a second band (band 2) at double molecular weight appears, which is therefore the desired 4-armed linker. Correspondingly, for the 6-armed linker, which is composed of four 3-armed linkers, three ⟨□○○⟩ linkers are ligated with one ⟨⊏⊏⊏⟩ molecule. Indeed, in the gel four bands can be observed, whereas the band with the highest molecular weight (band 4) is the 6-armed linker. As one can see, the yield of the reaction is not very high, as all the other intermediate molecules (single, double, triple 3-armed linkers) are apparent. In order to form a junction with longer arms, the linkers can be used to couple the elongations. For the 4-armed junction four bands are expected to be seen in the gel, which arise from molecules composed of one, two, three and four elongations. This is exactly seen in

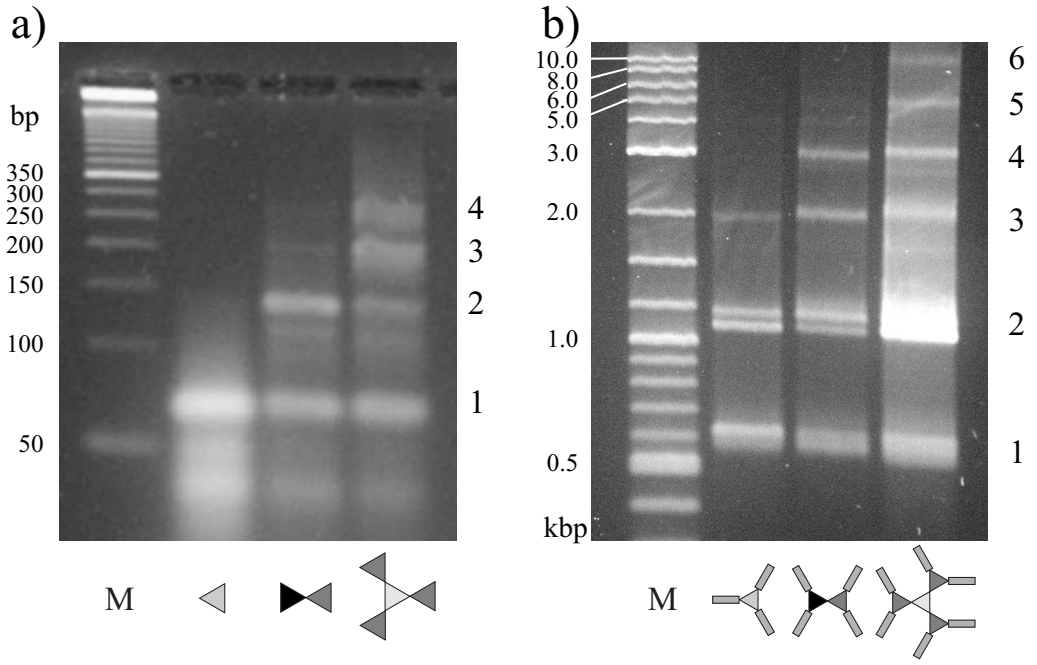

Figure 2.9: a) Gel electrophoresis of the ligation of 4-armed and 6-armed linkers molecules from 3-armed linkers. The lanes are indicated by the schematic drawing of the linker molecules. One triangle symbolizes the 3-armed junction. 2 and 4 connected triangles are the 4- and 6-armed linkers, respectively. The gel bands assign the number of 3-armed linkers, which are coupled together. b) Gel electrophoresis of the ligation of 4-armed and 6-armed junction molecules. The lanes are indicated by the schematic drawing of the junction molecules. The numbers of the gel bands assign the number of junction arms the corresponding molecule. In both images lane M indicates the molecular weight marker.

experiment (Fig. 2.9b). In comparison to the 3-armed junction a new band (band 4) at the high molecular weight side is present, which is attributed to the 4-armed molecule. In analogy the band pattern for the 6-armed junction shows 6 bands. At the high molecular weight side a 5-armed molecule (band 5) and the desired 6-armed junction (band 6) are found. The running behavior of the linkers and junctions in the agarose gel is also interesting. If one compares the real molecular weight (MW) of the molecules with the electrophoretic molecular weight (EMW), which is obtained by comparison of the corresponding band with the molecular weight marker, one finds that the electrophoretic weight of the linkers increases linearly with its real weight, as it is normally expected (Fig. 2.10a). Thus, coupling of two 3-armed linkers results in an EMW which is twice the EMW of one 3-armed linker and so on. Analysis of the slope of the linear curve shows that that the electrophoretic weight increases by a factor of 1.18 in comparison with the real weight. This means the molecular weight of a single 3-armed linkers appears in the gel increased by a factor of 1.18.

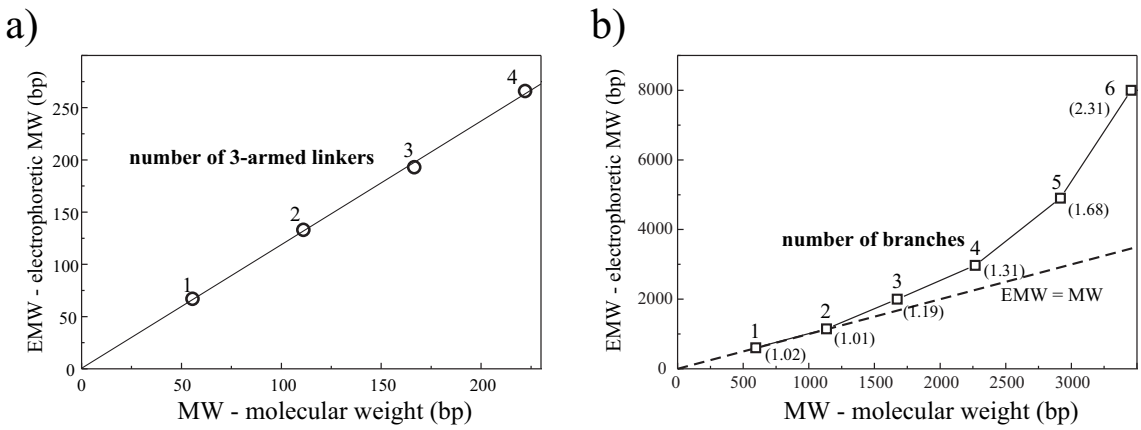

Figure 2.10: a) Gel electrophoretic mobility of the multi-branched linkers which are composed of 3-armed linkers. EMW denotes the molecular weight as it is obtained from the gel by comparison of a band with the molecular weight marker. The slope of the linear fit is 1.18. b) Gel electrophoretic mobility of the multi-branched junctions. The values in brackets show the ratio EMW/MW.

This is approximately the same value which is obtained for the 3-armed junction molecule (Fig. 2.10b), where 1.20 is found. Obviously, the branched structure, which retards the movement in the gel, can be observed in the gel by an increase of about 1.2 in the molecular weight for 3-armed molecules, independent on the arm lengths. For junctions with more than three arms, however, this ratio between EMW and MW is further increasing (Fig. 2.10b). So it seems that for branched DNA molecules the running behavior in the gel is just determined by the number of arms at the branching point. For the linker elements the gel "sees" only three arms at every branching point. By contrast, for the larger junctions the structure of the branching point is not longer detected by the gel and the number of long arms determines the gel mobility.

The prepared junctions are again purified by slicing the corresponding bands out of the gel and eluting the DNA. SFM samples are prepared and the expected structure of the synthesized junctions can by proven by direct visualization. Figure 2.11 shows images of a 4-armed junction as well as of a 6-armed junction. The measured arm lengths correspond within the error limits to the expected ones. For the 4-armed junction even the short 37 bp long arm, which connects the two single tripods can be seen. The measured length is with 15 nm a bit larger than the expected 12.5 nm. This way one can now distinguish the arms which are coupled by the same 3-armed linker. Measurements of the mean angle between adjacent arms connected by the same 3-armed linker provide a value of only 95°. This asymmetry can be explained by assuming a tetragonal instead of a planar structure of the 3-armed linker. The question, which three-dimensional structure 3-armed junctions

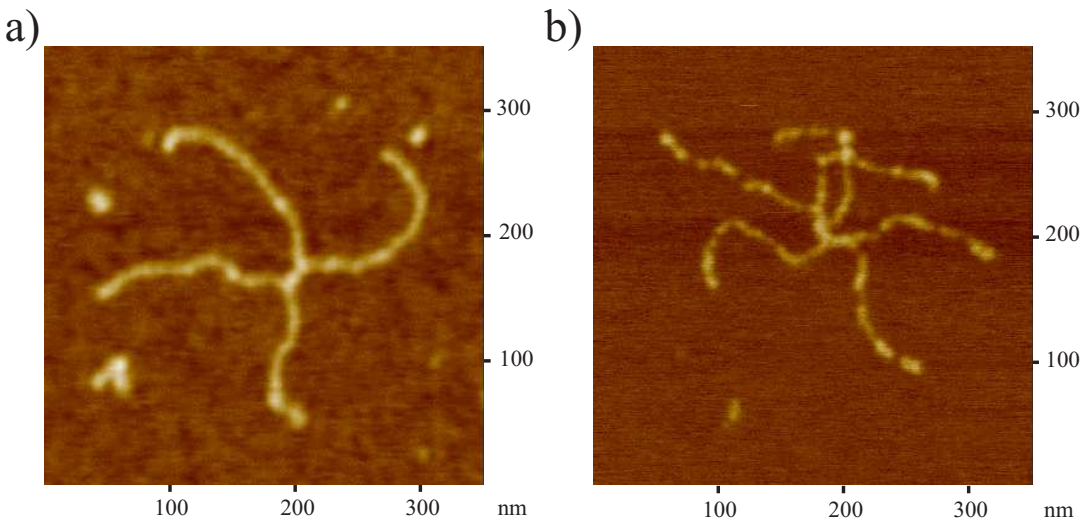

Figure 2.11: SFM of a 4-armed (a) and a 6-armed (b) DNA junction. Height scale is 5 nm.

have in solution, is of great interest [67, 68]. Using SFM data to solve the problem might seem a bit difficult, as only the planar structure of the adsorbed molecule can be observed. However, one can use the fact that in the tetragonal form the end to end distance of two adjacent arms as well as the angle between them is smaller than in the planar one. A 3-armed junction, where the all arms have the same length, is not helpful as in both cases the mean angle measured by SFM will always be 120°. However, an asymmetric junction with one shorter arm leads to a mean measured angle between the longer arms of smaller than 120° [67, 68]. The same situation is found for the 4-arm junction, consisting of two 3-armed branching points. Here, the angle between adjacent arms on one 3-armed linker is significantly smaller than 120°, which should be expected for a planar structure. For the 4-armed junction the symmetry is as well broken as one 3-armed linker has one short arm connecting the next linker and two long arms. Therefore the measured angle in the SFM data should be approximately the angle found for the real tetragonal structure in solution. Thus, it points to the fact that the structure of the 3-arm junction is not planar in agreement with the previously mentioned studies [67, 68].

Excluding technical problems, the proposed construction scheme for n-arm junctions with $n > 3$ allows the assembly of junctions with any number of arms with low effort. Once the sequence of the initial 3-armed linker is designed it is sufficient to build up all the linkers with more arms. This is an advantage to the construction scheme where n-armed linkers are hybridized from n semi-complementary oligonucleotides, where all sequences have to be new designed for a given n. Furthermore, the number of oligomers with different sequences is lower for the scheme based on 3-armed linkers. For the 3-armed linker of course 3 oligomers are necessary. For the

Linker arms	3	4	5	6	7	8	9	10	11	12	13	14	15	16	17	18
Strands	3	4	5	6	7	7	8	8	10	9	10	10	10	10	11	11

Table 2.1: Minimum number of DNA strands with different sequences needed for the assembly of an n-armed linker.

4-armed linker 6 oligomers are required, but for the 4 oligomers which couple the elongations two identical pairs can be taken. Thus the number of different oligomers is 4, two to couple the elongations and two to couple the 3-armed linkers. For the 6-armed linker one needs 6 different oligomers. Three oligomers for the central 3-armed linker and 3 oligomers for the 3-armed linker which can couple the elongations. So it seems that one can not decrease the number of different oligomers to less than n. However, the number of strands with different cohesive ends does not increase linearly with the number of arms for $n > 7$. To double the number of arms for any n-arm junctions with $n \geq 3$, one needs only three different strands more and only one new cohesive end pair has to be added. The strands terminated by ○ sticky ends, which bind the elongations (Fig. 2.8, p. 34) have to be replaced by strands with the new sticky end, suppose a ◁ which symbolizes any sequence, which is different from the previously used ones. Up to this point the number of different sequences did not increase. Then another 3-armed linker, consisting of three supplementary oligomers, is added, which has a $<$ end complementary to the ◁ end, as well as two ○ ends to couple the elongations. Thus, each arm of the previous n-armed linker splits into two new arms, the number of arms is doubled and one gets a $2n$-linker. This means, that an linear increase of strands leads to an exponential increase of arms. However, for n which are not simple factors of two and three, the situation is more complicated as here the radial symmetry of the linker has to be destroyed. But nevertheless the number of strands does not increase linearly with the number of arms. For n up to 18 the minimum number of necessary strands with different sequences is given in table 2.1.

2.3 Attachment of colloids to the junction center

In Chapter 1 a construction scheme for a DNA based circuit was proposed. One step of the procedure is the specific deposition of functional elements on predefined locations. Such "functional elements" on the nanometer scale could for example be carbon nanotubes, which can be coupled to DNA [69], but also metallic or semiconducting nanoparticles. Such nanosized clusters could serve as quantum dots in a design of a single electron transistor. A condition, which limits the size of such a quantum dot, is that the charging energy, i.e. the increase in energy after an electron is added to the dot, is larger than the thermal fluctuations k_BT. At room

temperature this restriction is valid for cluster sizes up to 5 nm.

Several work has already been done to fabricate nanoparticle-DNA assemblies including the (i) the formation of nanoparticle dimers and trimers by coupling the particles via a DNA strand [7, 63], (ii) the electrophoretic separation of particles with a distinct number of attached DNA strands [70, 71] (iii) the 3D assembly of nanoparticles by using DNA as a selective adhesion material [8], (iv) the formation of supramolecular aggregates by self-assembly of DNA-streptavidin adducts [61] and (v) the assembly of nanoparticle arrays on 2D DNA lattices [72]. All these methods are based on short synthetic oligonucleotides. Therefore, the length scale of DNA branches in these hybrid structures is only a view nanometers. For the integration of such hybrid structures into electrode arrays as well as for the subsequent metallization, branch lengths of more than 100 nm are required, which has been already discussed in Chapter 2. Suitable templates, which meet this criteria are the n-armed junctions, which synthesis is described before. In the following, it will be shown, how streptavidin coated 5 nm gold colloids can be attached near the branching point of a biotin functionalized junction, which is fabricated by slightly modifying the previously demonstrated method.

To incorporate biotin at or near the junction center one can not use synthetic oligomers which are biotinylated at one of their ends, as the biotin is attached to either the 3'- or the 5'-end and would prevent subsequent ligation. The biotin can therefore not be attached to the DNA backbone. The only further possibility is to use an anchor to the DNA bases, which can be easily done due to the availability of biotinylated nucleotide triphosphates. Without changing the general synthesis procedure described in section 2.1, the easiest way to incorporate biotinylated bases is during the fill-in step of dATP into the 5'-overhang of the elongations by exchanging dATP with biotin-14-dATP. The successful biotinylation of the elongations is proven with magnetic beads similar to the method described later in Section 3.1.1, but using *Hin*fI instead of *Hin*dIII restriction enzyme. It clearly shows a successful biotin modification of all fragments. The resulting junction, which is formed by using biotinylated elongations, is depicted in Figure 2.12. In a 3-armed junction three biotin molecules are incorporated at a distance of 16 bp (5.3 nm) from the branching point of the junction. In principle this structure should be able to accommodate also three 5 nm colloids. To bind the streptavidin coated colloids to the junctions, those were mixed in a slight excess of colloids to the number of available biotin bind-

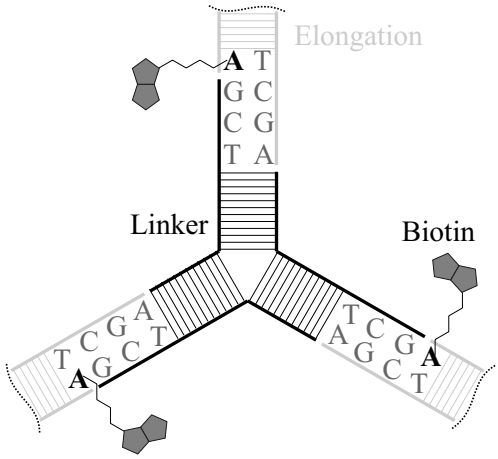

Figure 2.12: Scheme of the biotin modification of a DNA junction.

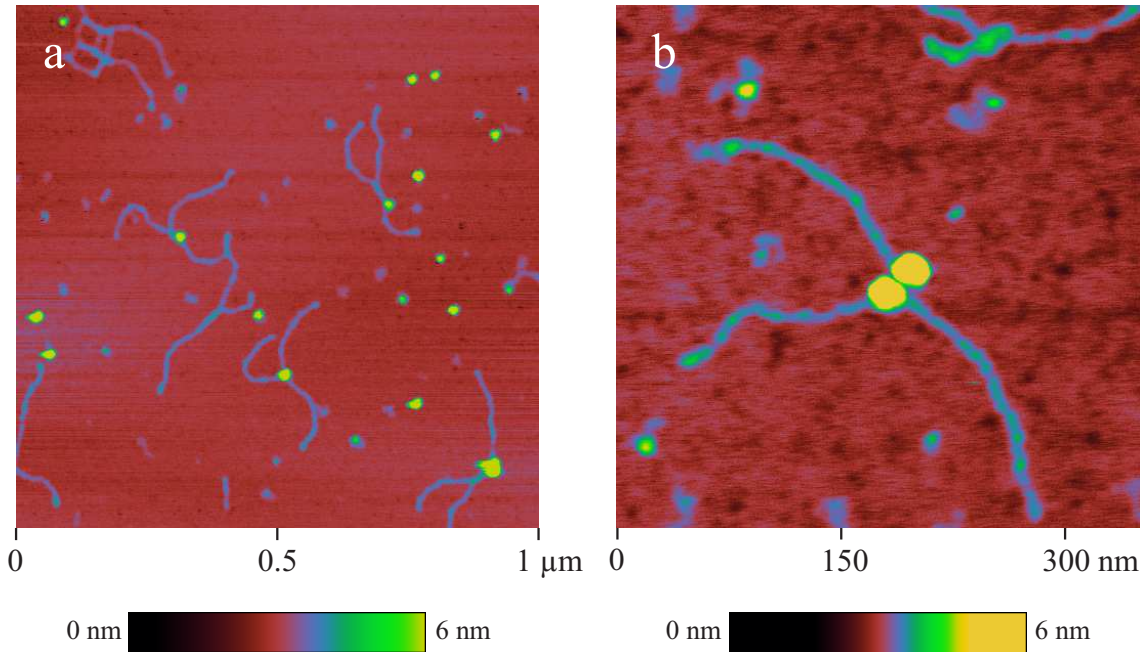

Figure 2.13: 5 nm gold colloids specifically immobilized at the branching point of DNA junctions.

ing sites. SFM shows that this sample consists of a large number of free colloids, which are not bound to any junction (not shown). Separating the junctions from the colloids using a commercial DNA clean-up kit (Qiaquick, Qiagen Inc.) shows, that most of the junctions do not carry colloids. Further analysis suggests, that a lot of free streptavidin must be present in the used colloid solution (Sigma-Aldrich), which prevents binding to the DNA junctions. Therefore, the colloids are cleaned by filtration (Microcon 100, Millipore). Mixing the cleaned streptavidin colloids with the biotinylated DNA junctions gives a much better result. On most of the junctions one colloid is attached at the branching point (Fig. 2.13a). The measured height of the particles is within a small tolerance 5 nm, which allows clearly to distinguish the colloids from other components of the sample, like e.g. free streptavidin. No unspecific binding of colloids to the DNA away from the branching point is observed. Some of the DNA junctions have two attached colloids (Fig. 2.13b). The binding of three colloids to one junction molecule is not observed.

This means, that the site-specific attachment of nanoparticles at the branching point of a DNA junction is successfully demonstrated. It also shows the general suitability of the method for the specific deposition of nanoobjects. As the incorporation of biotin does not change the general setup of the junction synthesis, it is easily possible to attach nanoparticles site-specifically also to junctions with more than three arms. The absence of junctions with more than three bound colloids

is probably due to free streptavidin, which is still present after filtration, and it is maybe the main problem of using biotin-streptavidin interaction to bind particles to DNA in comparison to the thiol chemistry, which is widely used [7, 8, 70, 72]. However, the use of qualitatively better streptavidin conjugated colloids or a more extended filtration should prevent these difficulties.

3 Integration of DNA into microstructures

The integration of DNA molecules onto microstructured surfaces aims two subjects. On the one hand, microstructures can serve to connect the anchored DNA template structure to the outer world. For example metal contact pads can establish an electrical contact to the DNA structure. On the other hand, a structured surface can itself act as a structure forming element, which guides the form of the resulting DNA network. For instance, with DNA strands, which are stretched between microstructured dots forming a periodic array, a large DNA network can be formed.

In order to develop methods for these tasks, the easiest problem, which can be solved, is to stretch a linear DNA molecule between two microstructured elements. In this work it will be the establishment of a DNA bridge between two gold electrodes. For this, a functionalization of the DNA ends and/or the substrate is required, which is specific to the microstructure and excludes unspecific binding of DNA to the surface areas in-between the contacts. Furthermore, it is necessary to manipulate and stretch DNA, in order to position the molecule and drive it from the random coil structure to a linear conformation. In the following sections the used functionalization techniques and the experimental setup for stretching DNA molecules in a hydrodynamic flow and for their observation with fluorescence microscopy are described. Thereafter, the results of the experiments are presented and discussed.

3.1 Experimental setup

3.1.1 Functionalization of gold electrodes and DNA ends

If one wants to form a DNA bridge between two electrodes, the system includes two DNA ends - one has to bind to the first contact and the other to the second contact. To solve this task straight forward, one can design a DNA/substrate functionalization in a way that end 1 of the DNA binds exclusively to electrode 1 and end 2 binds exclusively to electrode 2. This experiment has been done for the

first time by Braun *et al.* [15], who deposited with the help of microcapillaries a thiol modified oligomer complementary to end 1 of λ-DNA to electrode 1 and correspondingly a thiol modified oligomer complementary to end 2 to electrode 2. This method addresses the single DNA ends differently. However, the technique requires a site-specific functionalization of the contact pads, which is difficult to obtain. For covering few micrometer large pads with the oligomer solution, droplets in the range of picoliters have to by applied, which requires large effort, especially if one wants to bind many molecules in parallel. In order to avoid the electrode specific functionalization, it is also possible to use the same modification for both electrodes and address both DNA ends sequentially. Let us assume that a DNA molecule is bound with one end on such an electrode. To accomplish the bridging to the next electrode one needs a force not only for stretching the DNA but also for dragging the second end away from the first electrode to prevent the binding there. The success of this method depends on the kinetics of binding versus the time, which is necessary for removing the second end. As this method requires less effort, it is chosen for the experiments of the next section.

Several used techniques to anchor DNA to structured and non-structured surfaces are described in Section 1.3.2. As there is in most cases no affinity between DNA ends and surface, a bifunctional linker molecule is commonly applied, which binds with one end to the surface and with the other end to the DNA. Thiol groups bind specifically to noble metals. Therefore, they can be used to form one side of the linker between biomolecule and a gold surface. The other side can be formed either by amine groups, oligomers complementary to the DNA sticky ends or by biotin. The use of a certain anchor depends on the particular application. In the following four different DNA-substrate modifications are discussed.

(1) The use of thiolated oligomers for anchoring a single DNA end.

(2) Amine modified electrodes for electrostatic binding of DNA as a simple system for double-sided DNA binding.

(3) Biotinylation of DNA ends and gold electrodes.

(4) Fabrication of *BT*-DNA possessing one biotinylated and one thiolated end.

The use of **thiolated oligomers** to anchor λ-DNA is simplified by the fact that this commercially available DNA possesses already two 12 bp overhangs, which are complementary to each other (Fig. 3.1). Thus, one only has to synthesize a 12 bp long thiol modified oligomer, which is complementary to one of the ends, and to bind it to the electrode structure by incubation in a salt containing solution. Then the λ-DNA can be applied which is bound only on one side. The disadvantage of this method is that the rupture force of this bond is only several pN and therefore

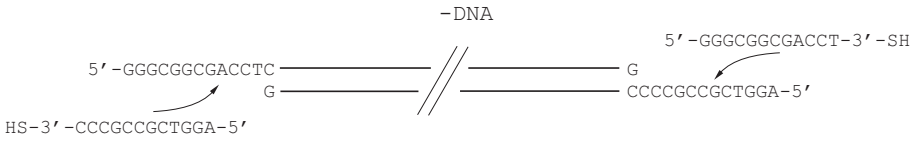

Figure 3.1: The two sticky ends of λ-DNA and the corresponding complementary thiolated oligomers used to anchor the DNA to gold surfaces.

quite low (Section 1.3.2). The 12-mer can be fixed at the λ-DNA end by closing the single stranded nick remaining after hybridization by ligation. This process will be explained in detail at the end if this section where the fabrication of *BT*-DNA is described.

The molecular combing technique of Bensimon *et al.* uses **electrostatics** to bind DNA to surfaces (Section 1.3.2). This method, however, has only been used on homogeneously covered surfaces but never to structured ones. Application to microstructures requires the selective deposition of amine groups. For the modification of gold contact pads a molecule called aminoethanethiol, which consists of a thiol and an amine group connected by a short carbohydrate spacer, was taken [73]. Deposition onto the contacts is easily made from an ethanol solution [74]. In comparison to stretching on amine modified glass surfaces [51] the pH as well as the ionic composition of the DNA solution has to be modified and tuned in order to achieve end-specific binding on the gold surface. This is due to the probably different density of amine groups on both substrates as well as changed surface charges. The advantage of this method is its simplicity - an easy chemical modification of the electrodes and its applicability to any type of unmodified DNA.

By contrast to the two previously explained methods, the **anchoring of biotinylated DNA** to a surface requires modification of both - substrate and DNA. To achieve an affinity of biotin to the substrate one has to deposit streptavidin there. For this, a method invented by Zimmermann *et al.* [57] was applied. There, first a gold surface is biotinylated with a biotin-thiol linker and subsequent streptavidin is attached on the biotin (Fig. 1.17b, p. 24). Then the biotinylated DNA can be bound on the unoccupied binding sites of streptavidin. Biotinylation of the DNA ends was carried out as described previously by filling the 5'-overhangs of λ-DNA using Klenow polymerase and biotinylated dCTP (Fig. 1.11b, p. 14). Addition of the remaining three nucleotides (dTTP, dATP, dGTP) to the reaction mix leads to biotinylation of both DNA ends. One end carries six biotin molecules the other one four (Fig. 3.2a). If the fill-in reaction is carried out without dATP, it stops at the thymine site at the 5'-overhang. Thus, one end of λ-DNA remains unchanged whereas the other one is filled with 8 bases among them two biotinylated cytosines (Fig. 3.2b). This way a single DNA end can be functionalized with bi-

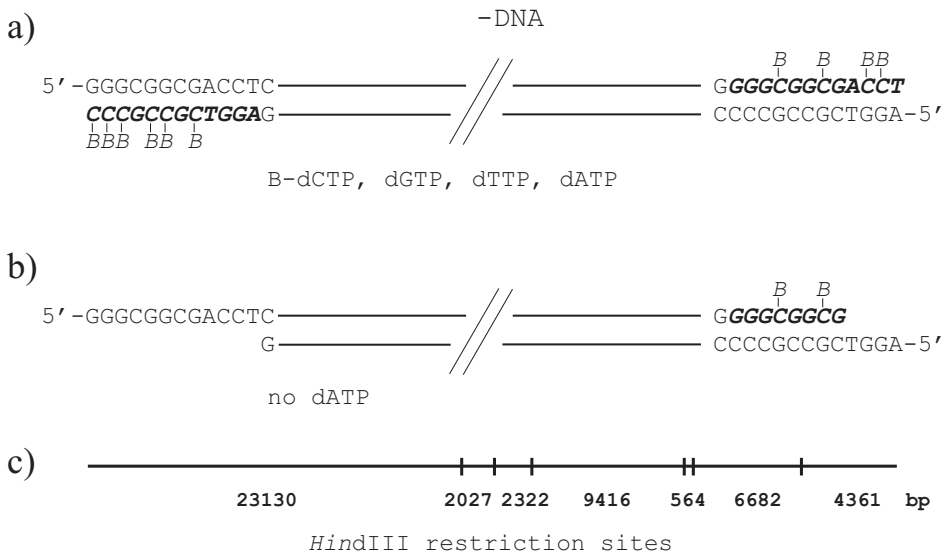

Figure 3.2: Biotinylation of λ-DNA by fill-in of the recessed ends with biotinylated dCTP. a) Biotinylation of both ends (2B-DNA) and b) of one end (2B-DNA). c) Map of the *Hin*dIII restriction sites of λ-DNA.

otin. The successful biotinylation can be proven using streptavidin coated magnetic beads and gel electrophoresis [57]. If λ-DNA, which is biotinylated at both ends (2B-DNA), is digested with *Hin*dIII restriction enzyme, it is cleaved into several non-biotinylated fragments and the both 23.1 kbp and 4.3 kbp long biotinylated end fragments (Fig. 3.2c). Streptavidin coated magnetic beads are used to separate these end fragments from the remaining strands. For this, the entire biotinylated DNA is bound to the beads. Then the beads with the attached DNA are incubated with *Hin*dIII restriction enzyme. The DNA is digested, the non-biotinylated fragments are released but the 23.1 kbp and 4.3 kbp strands remain at the beads (Fig. 3.3a). If a magnetic field is applied to the suspension, the beads are collected in a pellet. The supernatant contains now all restriction fragments except the 23.1 kbp and 4.3 kbp long ends. Thus, after electrophoretic separation of the supernatant, all fragments except the two 23.1 kbp and 4.3 kbp strands should be present, which is indeed found in experiment (Fig. 3.3b). The same proof can be done for the DNA biotinylated on one end (1B-DNA). Here only the 4.3 kbp long end fragment is biotinylated and therefore missing in the gel (Fig. 3.3b).

It is also easily possible to combine two different DNA functionalizations. Thus, using the methods described above, one can synthesize **BT-DNA which is biotinylated on one and thiolated on the other end** (Fig. 3.4a). This DNA modification can be very useful if one wants to couple a small object, like a small bead or microtubles [75] via a DNA strand to a contact pad. The thiol group estab-

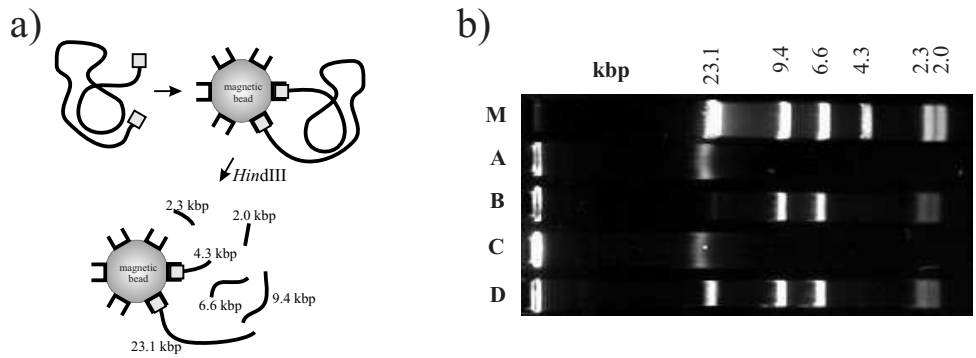

Figure 3.3: Proving the successful biotinylation of λ-DNA by using streptavidin coated magnetic beads. a) Schematic representation of the separation procedure. b) Gel electrophoresis of biotinylated λ-DNA bound to the beads. M) λ-DNA *Hin*dIII digested as molecular weight marker. A) 2B-DNA which is not bound to the beads. B) Released fragments of 2B-DNA bound to the beads after *Hin*dIII digestion. C) 1B-DNA which is not bound to the beads. D) Released fragments of 1B-DNA bound to the beads after *Hin*dIII digestion.

lishes the linkage to the gold surface whereas the biotin is used to tether the streptavidin coated object. During the synthesis, the DNA is biotinylated on the 4.3 kbp end as described above without having dATP in the reaction mix. The thiol modification is done by hybridization of the appropriate thiol oligomer to the 23.1 kbp end of λ-DNA (Fig. 3.1) and subsequent ligation of the remaining single stranded nick [15]. However, before hybridization two other reactions have to be carried out. First, as the oligomer is not phosphorylated at its 5'-end, a phosphate has to be added there in order to enable the ligation of the 5'-phosphorus of the oligomer to the 3'-hydroxyl group of the λ-DNA using T4 polynucleotide kinase (Fig. 1.16, p.23). Second, the λ-DNA has to be dephosphorylated using alkaline phosphatase. It has a phosphate on both 5'-ends and the ligase could couple different λ-DNA molecules to multimers. This can be prevented by the dephosphorylation reaction. The successful synthesis of *BT*-DNA can again be proven by gel electrophoresis. The biotinylation of the 4.3 kbp end is tested using magnetic beads. Exactly the fragment is not released after *Hin*dIII digestion of *BT*-DNA, which was bound to streptavidin coated beads (Fig. 3.4b). The thiol modification is shown by binding a small 5 nm gold colloid to the thiolated end of the DNA. As the colloid is very small in comparison to the large λ-DNA molecule it does not change the running behavior of the DNA which can be seen in the fluorescence image of the gel (Fig. 3.4b). In order to proof that the band is really formed by DNA-colloid complexes it is stained with a meta-stabile gold enhancement solution [17], which enlarges specifically the gold colloids. After some time a visible band appears in the gel (Fig. 3.4b). This band is only present if the DNA carries a thiol group. Incubation of the colloids

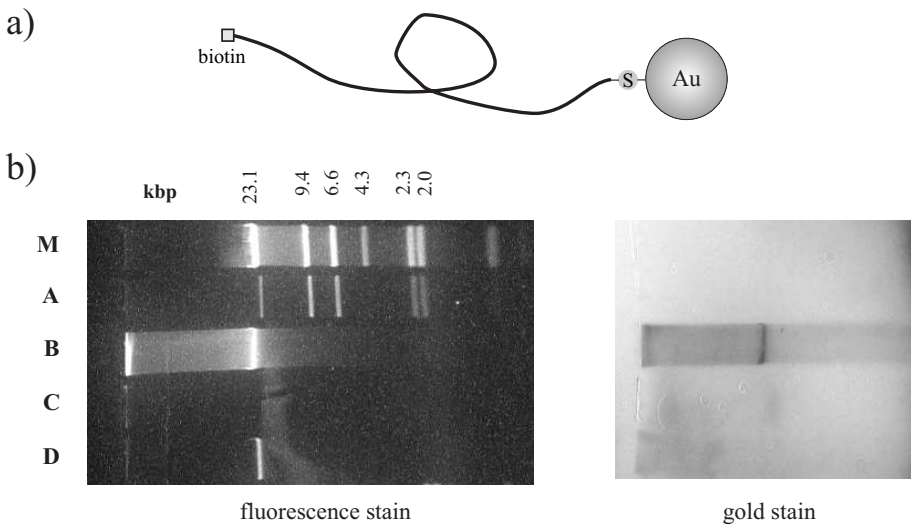

Figure 3.4: Proving the synthesis of *BT*-DNA. a) A 5 nm gold colloid is bound to the thiolated end. b) Gel electrophoresis. The two images are obtained by subsequent fluorescence and gold staining of the same gel. M) λ-DNA *Hin*dIII digested as molecular weight marker. A) Released fragments of the *BT*-DNA bound to streptavidin coated magnetic beads after *Hin*dIII digestion. B) *BT*-DNA with 5 nm gold colloids. C) *BT*-DNA which is not bound to the magnetic beads. D) λ-DNA with 5 nm gold colloids.

with native λ-DNA results in a band after fluorescence staining but no band after the gold staining. Thus, the successful synthesis of *BT*-DNA is proven.

3.1.2 Flow cell and fluorescence microscopy

For the integration of DNA into microstructures it is necessary to stretch DNA in solution. Stretching can be done by several methods, like hydrodynamic flow [15,57, 76], electrostatic field [57,77] and even molecular motors [75]. Using electrostatics one has to deal with problems arising from electrochemistry. Therefore, the simplest system to operate is hydrodynamic flow. If the flow is generated within a tube-like structure, the flow velocity, and correspondingly the stretching force, goes at the chamber walls down to zero according to the law of Hagen-Poiseuille. Therefore, a setup using microcapillaries was chosen (Fig. 3.5). The advantage is that the flow can be directed onto the surface, which assures higher flow velocities at the surface. Furthermore, both microcapillaries are connected to a micromanipulator system allowing their movement independently in X, Y and Z direction. Thus, the flow direction can be fine tuned and altered.

The behavior of a flexible polymer in flow remains a subject with lots of open questions [76]. However, in order to estimate the molecule extension as a function of

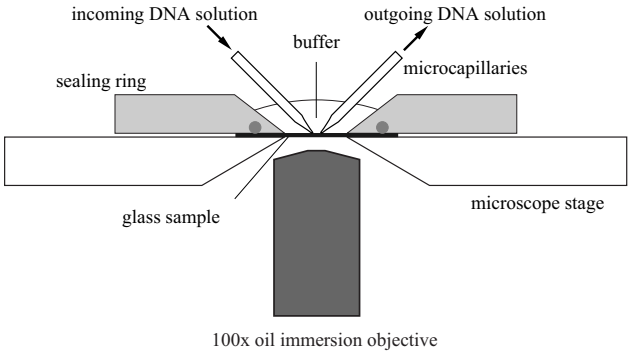

Figure 3.5: Experimental setup of DNA stretching using a hydrodynamic flow.

the flow velocity and to calculate the applied force, some simple models work with surprisingly precision. Almost 70 years ago KUHN developed a model where the polymer is treated as an elastic "dumbbell" in which a spring connects two beads representing the free ends of the molecule [78]. For a tethered DNA molecule there is just one free end at which the drag forces act. Thus, a "half dumbbell" model has to be applied [76]. The drag force can be written as $F = \xi \cdot v$ where ξ is the friction coefficient and v the flow velocity. Experimental data shows that for DNA molecules of the length $16\,\mu\text{m} < L < 150\,\mu\text{m}$ the relative extension x/L scales with the reduced velocity v/D [76]; D is the measured center-of-mass diffusivity, which is for λ-DNA $0.47\,\mu m^2 s^{-1}$ [79]. D is related to the translational drag coefficient $\xi_{coil} k_B T$ of the undeformed molecule by the fluctuation-dissipation theorem, $\xi_{coil} = 1/D$ [76]. If the drag forces do not exceed 20 pN, the stretching force F_{spring} of the DNA, which counteracts the drag, is given by the force-extension relation from the wormlike chain model (Eq. 1.15, p. 20). Thus, one obtains

$$\frac{F_{drag}}{k_B T} = \frac{\xi v}{k_B T} = f \xi_{coil} v = f \frac{v}{D} = \frac{1}{a}\left[\frac{1}{4}\left(1 - \frac{x}{L}\right)^{-2} - \frac{1}{4} + \frac{x}{L}\right] = \frac{F_{spring}}{k_B T}, \quad (3.1)$$

from where the relation between relative extension x/L and reduced velocity v/D can be extracted (Fig. 3.6a). a denotes the persistence length of the DNA, f is a scaling factor. If f is set to 0.73, this equation, based on the "half-dumbbell" model, is in remarkable agreement with experimental data [76]. However, it does not provide the right values for experimentally obtained stretching forces. A more elaborate model which assumes a continuous distribution of drag forces along the molecule can be applied to calculate the right forces. The continuous drag forces are responsible that the mass distribution along the stretched molecule has a maximum at its end [76] where also the highest lateral fluctuations of size $d \sim (k_B T/\eta v)^{1/2}$ are located [80]; η is the viscosity of the surrounding liquid. In order to calculate the stretching forces, in a simple assumption the stretched molecule is considered as a rod of length L and diameter d and the stretching force results for $(L - x) \ll L$

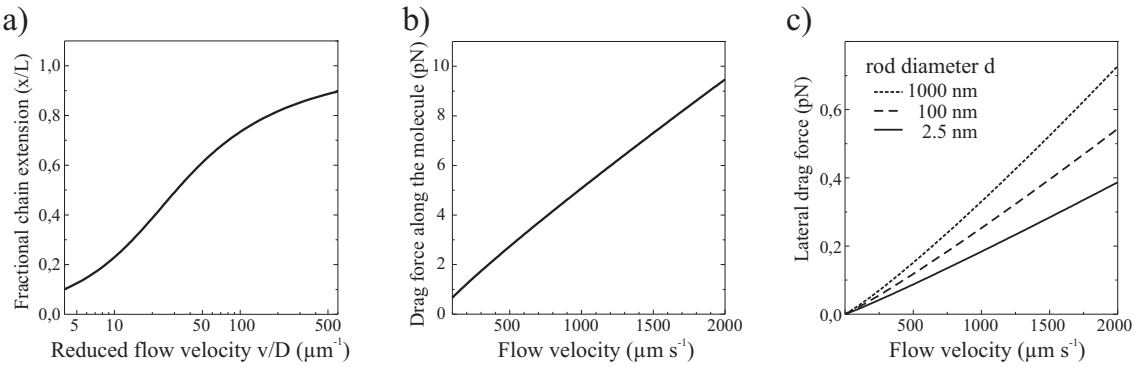

Figure 3.6: a) Relative extension of a DNA molecule as a function of reduced flow velocity v/D. Factor f from eq. 3.1 is set to 0.73. D for λ-DNA is $0.47\,\mu\mathrm{m}^2\mathrm{s}^{-1}$. b) Drag force acting on a single λ-DNA molecule along its axis as a function of flow velocity taken from eq. 3.2. c) Drag force acting on a single λ-DNA molecule perpendicular to its axis as a function of flow velocity taken from eq. 3.3. The molecule is assumed as a rod and curves were calculated for different diameters. For the viscosity the value for water $\eta_{H_2O} = 0.243\,10^{-3}$ $\mathrm{Ns\,m}^{-2}$ was taken.

to [80]

$$F_{drag} = \frac{2\pi\eta L v}{\ln(L/d)}. \tag{3.2}$$

The resulting curve can be seen in Figure 3.6b. In order to stretch the DNA sufficiently, flow velocities of at least $100\,\mu\mathrm{m\,s}^{-1}$ are required, which corresponds to forces in the pN range.

The lateral drag force, acting on a DNA molecule stretched between two anchor points in a flow perpendicular to the molecule axis, is estimated by considering the DNA as a cylinder of diameter d [81]:

$$F = \frac{2\eta L v}{\pi(\ln\frac{8\eta}{\rho d v} - 0.0772)}. \tag{3.3}$$

Due to lateral fluctuations of the molecule the effective diameter, which is "seen" by the flow, is likely to be larger than the real diameter of DNA of 2 nm. The drag force as a function of the flow velocity was therefore calculated for different diameters (Fig. 3.6c). As the drag is approximately proportional to the logarithm of the rod diameter d, it changes only a little at large variations of d. Thus, even at an assumed diameter of 1000 nm the lateral drag force is a factor of 10 smaller than the drag along the molecule axis. This is quite surprising and might indicate that the lateral drag force cannot be described with such a simple model. Indeed, lateral drag forces derived from the experiments described later on are significantly higher than the values obtained from Equation 3.3.

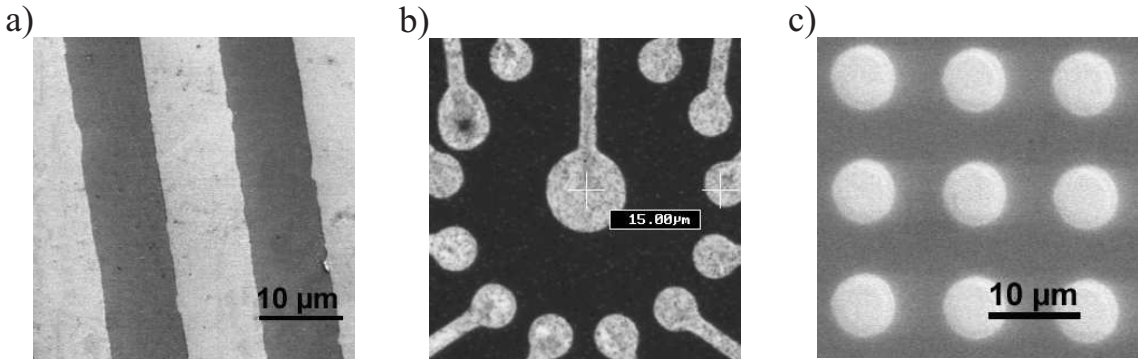

Figure 3.7: Gold microstructures used for DNA stretching experiments. a) SEM image of gold stripes (bright lines) on silicon[1]. b) Laser scanning microscope image of a clock-like electrode structure on a glass support[1]. c) SEM image of a gold dot array on silicon.

In the experiments the flow is generated using a hose pump, which generates rates from $10\,\mu l\,s^{-1}$ up to more than $2000\,\mu l\,s^{-1}$.For an inner diameter of the microcapillaries of 0.58 mm this corresponds to flow velocities from $40\,\mu m\,s^{-1}$ up to several thousand $\mu m\,s^{-1}$.

The setup with an open flow cell and and the flow manipulation with microcapillaries coming to the sample from above requires observation on an inverted microscope, where the objective is located below the sample (Fig. 3.5). Therefore the sample has to be made on a glass support and consequently all applied gold microstructures were fabricated on glass. Three different types of microstructures were used, which are depicted in Figure 3.7. For the purpose of imaging the gold structures with scanning electron microscopy (SEM) they were also fabricated on silicon, but for the DNA stretching experiments only samples on glass supports were applied.

Single DNA molecules were observed by fluorescence microscopy. For this, a 100x oil immersion objective with a numerical aperture of 1.4 was used, which combines high resolution as well as high light yield. Imaging was done with a peltier-cooled CCD camera Zeiss Axiocam HR. The DNA was fluorescence labelled with YOYO1 dye, which is exited with blue light at 480 nm and has a green emission with a maximum at 511 nm. The dimeric molecule binds strongly to double-stranded DNA and the fluorescence quantum yield of the bound dye is about 1000-fold higher than when free in solution [82]. This results in an extremely low background fluorescence, thus enabling imaging of single DNA molecules [15, 76]. YOYO1 has two different binding modes to DNA: (i) at high nucleotide-to-chromophore ratios it is bis-intercalated and strongly fluorescent, and (ii) at low nucleotide-to-chromophore ratios it binds externally and is weakly fluorescent [83]. A disadvantage of YOYO1

[1]Obtained from Ingolf Mönch, IFW Dresden.

is that it induces single-stranded photocleavage, which leads to enhanced double-stranded cleavage due to the dimeric structure [82]. To minimize the problems arising from this, the DNA is very low stained with a ratio of 80 bp per YOYO1 molecule. Under these conditions the DNA remains intact over hundreds of seconds and is still visible in the microscope although photo bleaching is accelerated and the signal to noise ratio is decreased. The slight staining of the DNA has furthermore the advantage that it should not change the mechanic properties of the DNA to much. Dimeric nucleic acid stains like YOYO1 have been found to unwind the DNA double helix locally resulting in a larger contour length[2] as well as a larger persistence length at high labelling ratios of 6 bp per dye molecule [76]. In the following experiments, low labelling conditions are used. Therefore, values for contour and persistence lengths should be only slightly larger than for unstained DNA. However, this issue will further be discussed in Section 3.2.2.

3.2 *In-situ* manipulation of single DNA molecules

3.2.1 Stretching of DNA between microstructures

In the following different experiments are described where DNA is stretched on microfabricated surfaces. All the different anchoring procedures, which were described in the Section 3.1.1, have been applied. The experiments are ordered by the type of surface attachment.

Single-sided binding of λ-DNA via thiolated oligomers

Binding specifically just one end of the DNA to gold electrodes is accomplished by using a thiolated oligomer, which is complementary to one of the 5'-overhangs of λ-DNA. Both ways of hybridization of the oligomer to the λ-DNA were tested; (i) hybridization of λ-DNA to oligomers, which are already attached at the gold surface as well as (ii) hybridization in solution followed by ligation and subsequent anchoring of the thiolated λ-DNA to the gold surface.

Hybridization at the surface is accomplished by incubating the gold electrode structures with thiolated oligomer of the sequence 5'-GGGCGGCGACCT-3'-SH. After that a solution containing λ-DNA molecules is flown over the electrodes and binding of single molecules is observed. Figure 3.8 shows an image sequence a λ-DNA molecule tethered with one end to an electrode. The exclusive binding on one end is shown by applying different flow velocities which leads to different stretching lengths. In Figures 3.8a-c a small flow velocity of about 40 μm s^{-1}was applied which stretches the DNA to about 8 μm corresponding to half of the contour length. The

[2]For labelled λ-DNA a contour length of 22 μm was found instead of 16.3 μm for native DNA.

DNA is still very coiled, showing therefore large lateral fluctuations. Increasing the

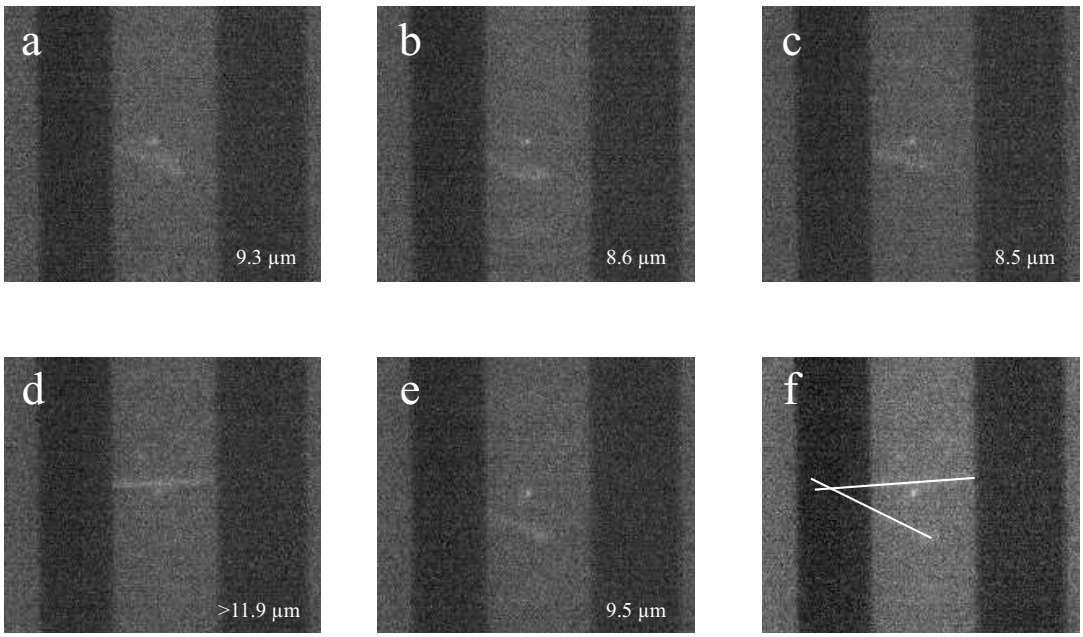

Figure 3.8: Image sequence of a single λ-DNA molecule attached via a thiolated oligomer with one end to a gold electrode at varying flow speeds. The black stripes are the gold electrodes. The small withe line is the DNA. a-c) Low flow velocity. d) High flow velocity. e) Again, lower flow velocity and different flow direction. f) Interpolated anchor point of the DNA molecule from images d and f. The numbers at the images indicated the length of the stretched molecule.

flow velocity to about $160\,\mu\mathrm{m\,s^{-1}}$leads to much better stretching of the molecule (Fig. 3.8d). The length of the DNA is measured to be at least $11.9\,\mu$m, but it can be larger as not the whole molecule can be seen. By changing flow direction and velocity it can be proven that the DNA is only bound on a single end as it is not stuck to the second electrode Fig. 3.8e. Thus, it is shown, that by using electrodes covered with oligomers which are sticky to a single end of λ-DNA, an attachment of the DNA on a single end can be established. The achieved stretching forces vary from about 0.1 pN at $8\,\mu$m extension to at least 0.4 pN at $11.9\,\mu$m extension. A disadvantage of the used microscopy setup is that, as the DNA can not directly be observed on the gold electrodes, i.e. the anchoring point can not be seen. However, by superimposing two images where the DNA was stretched into two different directions the anchor point can be determined by interpolation (Fig. 3.8f). Only this enables the length measurements - the stretching lengths depicted in the images are obtained by this method.

Binding of thiol modified λ-DNA was simply done by flowing the DNA solution

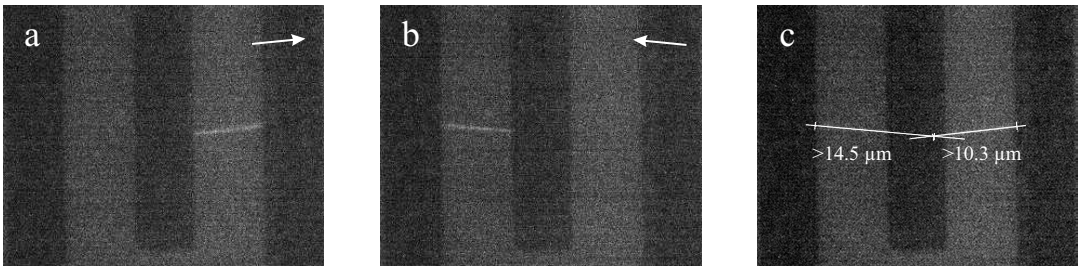

Figure 3.9: λ-DNA attached with one end to a gold electrode (black stripes) at changing flow directions indicated by the arrow in the upper right corner of each image a) Flow from left to right. b) Flow from right to left. c) Interpolated anchor point of the DNA molecule from the previous two images.

over clean gold electrodes. Again binding of single DNA molecules to the electrodes is observed. Figure 3.9 shows an image sequence were a molecule is attached at the middle gold electrode. In this case the flow direction is changed. It was several times switched from left to right and backwards from right to left and the molecule follows exactly the given flow. This shows again the successful attachment of only one DNA end. Furthermore, from the two stretching directions of the DNA, the anchor point can be easily extrapolated. Thus, length measurements can be done, which confirm that the DNA is at least stretched to 14.5 μm which corresponds to a force of about 2 pN.

Double-sided binding of λ-DNA between electrodes using electrostatics

The electrostatic binding of DNA to amine modified glass surfaces has already been shown previously [51]. However, up to now it has neither been demonstrated on gold surfaces nor on microstructured gold electrodes. The surface properties of amine modified glass are supposed to be different in comparison with amine modified gold regarding the density of amine groups and the related surface charge. Therefore, the particular stretching conditions like pH and ionic composition of the solution are different as well. In order to obtain a good stretching result for gold surfaces, the buffer system has to be optimized, i.e. different buffers adjusted to different pH values have to be tested. For this, a droplet of the particular buffer solution containing the DNA is placed onto a gold film deposited on a silicon support. Then the gold surface is covered with a cover slip; thus spreading the droplet over the whole sample and generating a flow. The result is imaged under the fluorescence microscope. The best conditions, where the DNA is only bound with the ends, are found for 100 mM Tris buffer at pH 8.0, which is different in comparison to glass (10 mM AMPSO, pH 8.8). Figure 3.10 shows a stretched DNA molecule on an amine modified gold surface. It is bound to the surface only at the ends as the image

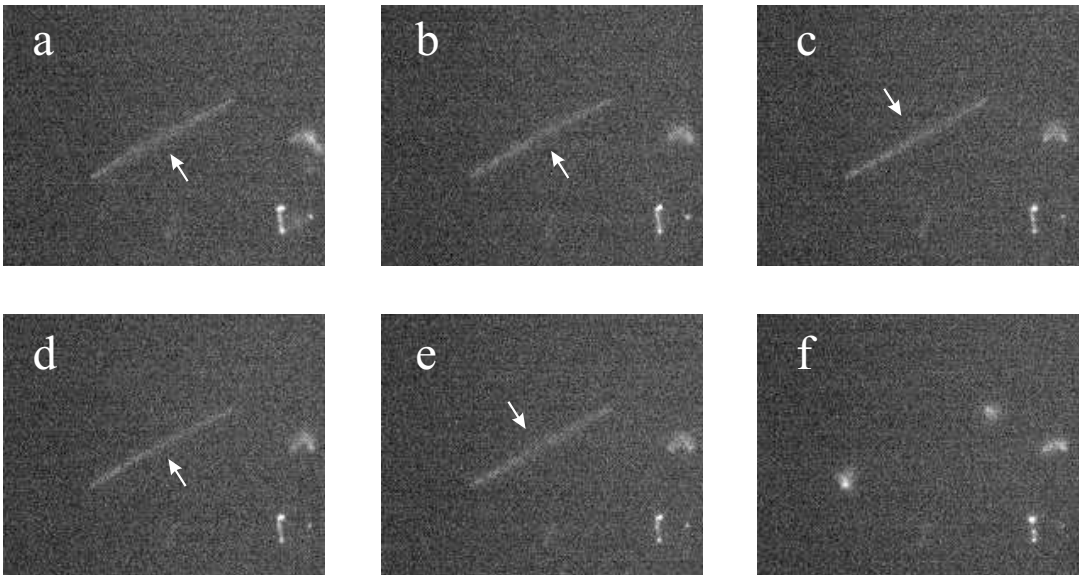

Figure 3.10: Image sequence of a stretched λ-DNA molecule bound electrostatically with both ends to an amine-coated plain gold surface. The molecule length is 12.5μm. The arrows indicate the bending direction of the molecule due to lateral vibrations of the DNA. Image f shows the photocleaved molecule. Photocleavage was induced by YOYO1 staining.

sequence shows. Note the lateral fluctuations of the molecule similar to a guitar string, which proof that the DNA midsegment of the DNA is freely moving. Finally the DNA breaks due to fluorescence induced photocleavage (Fig. 3.10f). The two parts of the molecule recede immediately back to the anchor points into the coiled form. That is, why they are only to be seen as two dots. It furthermore shows, that the DNA is nowhere else bound than at its ends. Thus, it is possible to bind DNA end-specifically on amine modified gold surfaces.

In order to get stretched DNA molecules bridging two electrodes, the amine modification is now applied to micropatterned gold films. In analogy to the plain gold films the microfabricated surfaces are covered with aminoethanethiol. Then the DNA in the same buffer, which was previously used, is applied in flow. Figure 3.11 shows an image sequence of a couple of DNA molecules bound with both ends to the electrodes by using this method. The hose pump, which is used to generate the flow, makes a short pulsation after each half turn of the rotor. This leads to short periodic deviations of the flow direction which can be observed in the experiment. The normal flow direction can be seen in Figure 3.11a on the molecule in the lower right corner, which is attached at only one end. Within such a flow deviation the second end of the molecule is moved to the other electrode and binds there (Fig. 3.11b). After a second flow deviation more molecules bind with the second end to the opposite electrode (Fig. 3.11c). As after the short flow deviations the flow

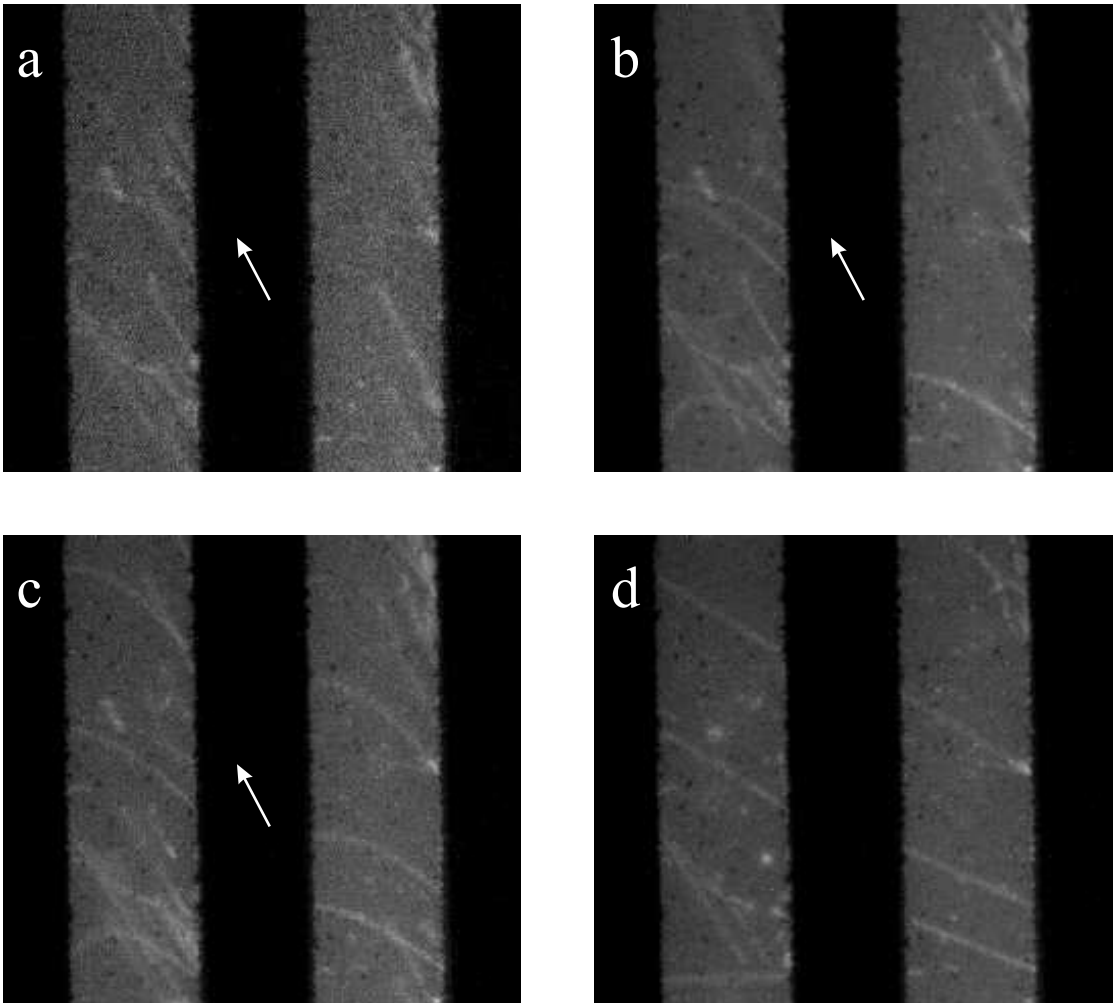

Figure 3.11: Image sequence of single λ-DNA molecules bound with both ends between amine modified gold electrodes. The arrow in the first three images indicates the flow direction. In the last image the flow is shut of. Note that the each of the images b-d are obtained by averaging 5 single images. The electrode spacing is 8.3 μm.

points into the original direction, the attached DNA molecules are affected also by hydrodynamic drag from the side. Thus they are not straight but reveal a bow-like form. By switching the flow off, the drag becomes zero and the molecules recede into the linear form (Fig. 3.11d). This again shows, that the DNA ends bind only at the gold electrodes and the midsegment of the DNA can freely move on the glass substrate, which means that the applied method of substrate modification can be successfully used to stretch DNA molecules between two different gold electrodes.

Up to this point it is shown that a DNA bridge between two electrodes can be formed using aminoethanethiol for the gold substrate modification. In order to in-

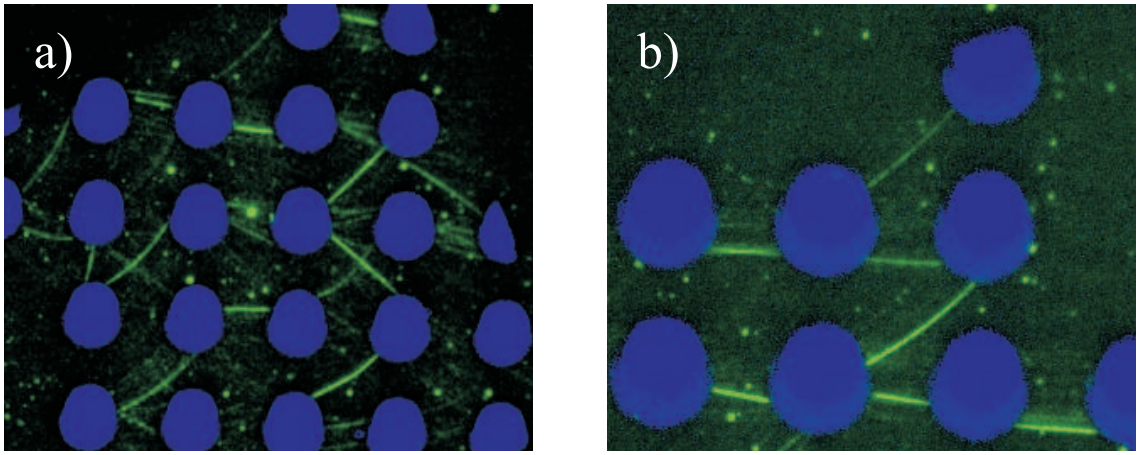

Figure 3.12: DNA network formed by single DNA molecules stretched on an array of gold dots. Both images are obtained by overlaying the dot image with the DNA image in two different color channels. The blue channel is the inverted transmission light microscopy image of the gold dots. The green channel is the fluorescence image of the DNA.

crease the complexity of the resulting DNA structure stretching of DNA is done on a periodic array of gold dots (Fig. 3.7c). Connecting the single dots of the array by DNA molecules should result in a complex network structure. In order to do this, different flow directions have to be applied on the sample. Otherwise only connections between dots lying in the direction of the flow would be obtained. Therefore, the position of the microcapillaries is changed during the binding procedure of the DNA to the electrodes. The result of this experiment can be seen in Figure 3.12. Clearly, DNA networks can be obtained by connecting the dots of the array with DNA molecules. Variation of the flow direction leads to the formation of horizontal as well as vertical connections between the dots. Furthermore DNA bridges connecting the diagonal opposing dots of a quadratic dot cell are apparent. Thus, a large random network is created. A problem is still the control over the assembly process. How can only a single connection between each pair of adjacent dots be established? At the moment, in order to get connections between all dots, it is necessary to bind more molecules to the array than required for single molecule connections. In this case some dots are linked by several DNA molecules. In order to avoid problems from this, enzymes could be applied to remove the unwanted connections. Another possibility could be to decrease the size of the electrodes. On the other hand, it might even not be necessary to remove the additional connections. This depends on the subsequent application if it is robust enough to tolerate an additional number of connections.

In conclusion, the developed method using aminoethanethiol to bind DNA electrostatically between electrodes is a quite simple but reliable and robust method for

DNA network assembly.

Double-sided binding of λ-DNA via biotin-streptavidin bridges

λ-DNA which is biotinylated at both ends can also be used for establishing a bridge between two streptavidin modified gold electrodes. Figure 3.13 shows the dynamics of stretched molecules at changing flow velocities. Differently attached molecules can be seen in the image. Some, which are bound only at one end are to short to bind at the other electrode. At decreasing flow speed, their lengths are decreasing, too. Other molecules are stretched to the other electrode, but not all of them bind their. When the flow is shut off only the molecules which are really attached at both ends remain stretched (Fig. 3.13d). One of them is attached at one end inbetween the electrodes. This unspecific binding can be to the glass substrate, however it can also be due to failures of the microfabricated structures. The gold lines are produced by etching trenches into a gold layer covering the whole glass substrate. Uncomplete etching can result in gold dots between the electrodes which then serve as attachment points for the DNA. But fortunately this faulty binding is quite rare in comparison to the number of DNA molecules which bind with both ends to the gold (see for example Fig. 3.14).

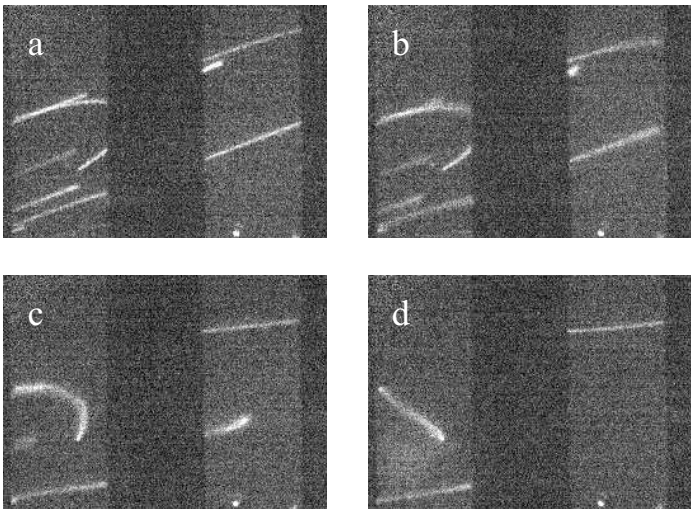

Figure 3.13: Single stretched DNA molecules attached via streptavidin-biotin anchors to gold electrodes. The flow velocity is stepwise decreased to zero from image a to d. The electrode spacing is 8.3 μm.

An interesting behavior of the biotin-streptavidin procedure is that many molecules are bound with both ends at one electrode, thus forming a U-shape (Fig. 3.14). This is seldom observed for the aminothiol procedure. A possible explanation is the faster binding of the biotin to the streptavidin coated surface in comparison to the electrostatic attachment. If the binding is faster,the probability is higher, that, if once a biotinylated end is bound, the second end is not dragged away by the flow but binds nearby.

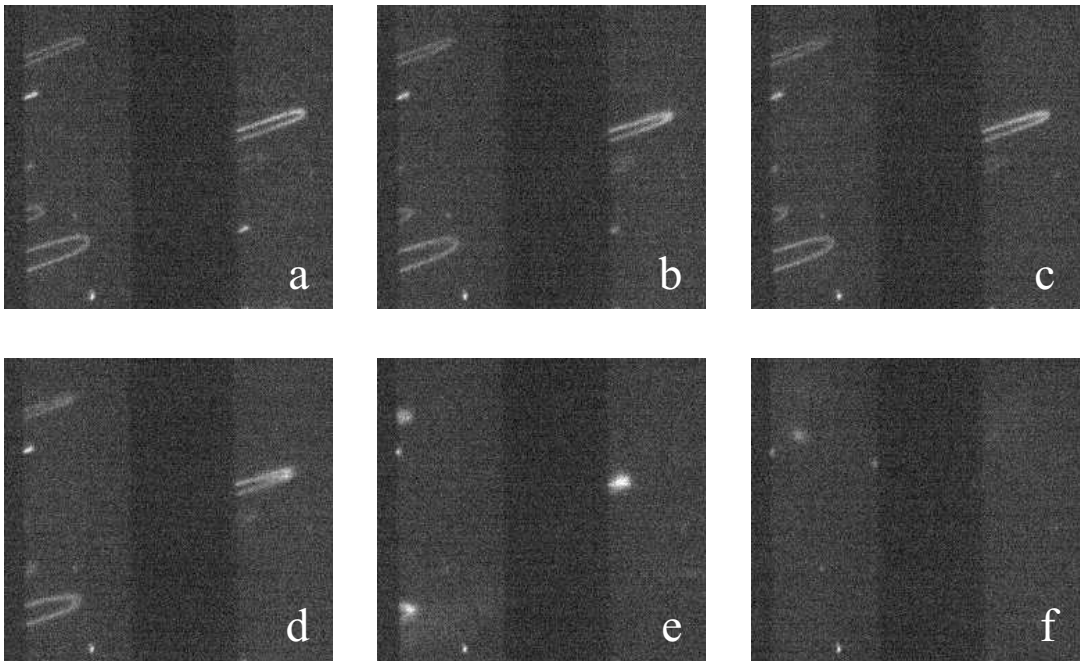

Figure 3.14: Single U-formed DNA molecules attached via streptavidin-biotin anchors to gold electrodes. The flow velocity is stepwise decreased to zero from image a to f. The electrode spacing is 8.3 μm.

Anchoring biotinylated DNA to streptavidin coated microparticles

A simple random microstructure can be easily formed by spherical microbeads which are adsorbed unspecifically to the glass substrate. These beads consist e.g. of polystyrene and are available with different diameters ranging from the submicrometer scale to several micrometers. Furthermore differently functionalized spheres can be purchased. By using streptavidin coated beads, biotinylated DNA can be easily attached there [47, 76]. Figure 3.15 shows DNA molecules which are bound to adsorbed streptavidin microspheres. By using DNA, which is biotinylated only at one end, single sided binding is accomplished and the molecules can be stretched in flow

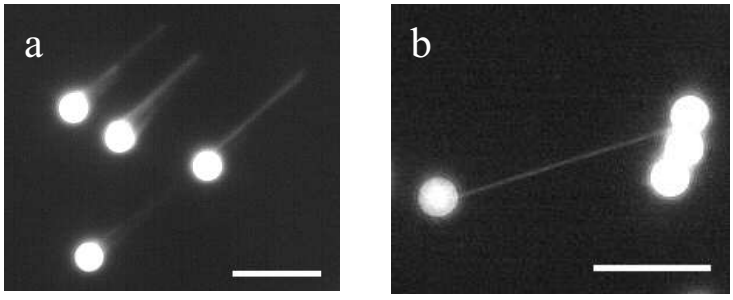

Figure 3.15: a) DNA biotinylated at one end bound to immobilized streptavidin coated beads and stretched in flow. b) DNA molecule biotinylated at both ends stretched between two beads. Scale bars are 10 μm.

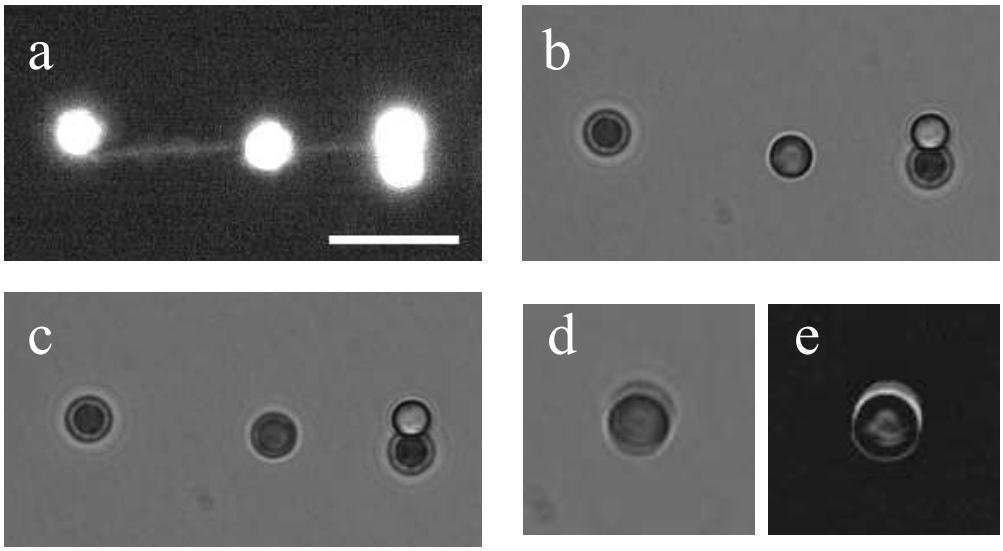

Figure 3.16: Two biotinylated DNA molecules trapping a free streptavidin coated bead. a) Fluorescence image. The bead in the center is not bound to the surface but only bound to the two DNA molecules, which are attached to the immobile beads on the image edges. Scale bar is 10 μm. b), c) Two phase contrast images at different times. d) Superimposition of both phase contrast images e) Difference image of the phase contrast images.

(Fig. 3.15a). By applying DNA biotinylated at both ends, the formation of bridges between two separated dots can be observed (Fig. 3.15b). In this case a stretching of up to 19.4 μm length is observed. The question, whether it is overstretching or just the result of an increased contour length, will be discussed in the following section.

An interesting feature, observed with DNA biotinylated at both ends, is the trapping of non-adsorbed beads by two DNA molecules. One molecule which is attached with one end to an immobile bead can trap a second mobile bead from solution. To this trapped bead again a second DNA molecule can bind which then can form a bridge to another immobile bead. Figure 3.16a shows the fluorescence image of such a trapped bead, which is located in the center of the image. Clearly the two DNA strands connecting the bead to the outer immobile beads can be seen. To verify that the central bead is indeed not bound to the surface, a time series of phase contrast images of the beads was taken. Figures 3.16b,c show two images of the series. By superimposing both images one can clearly see the different positions of the bead in both images Figure 3.16e. The difference image shows that only the position of the central bead is changed (Fig. 3.16e), whereas the immobile beads do not provide any contrast. The fluctuation of the position of the central bead is due to the Brownian motion of the particle. As larger the forces, which act on the bead from the DNA molecules, as smaller are these fluctuations. Thus, the average quadratic displacement of the bead is a measure of these forces.

3.2.2 Determination of stretching forces

In order to determine the forces which last the anchors of the DNA molecules, the forces acting on stretched DNA molecules will be estimated in the following. The focus will be on the hydrodynamic drag forces acting on stretched DNA molecules in a flow, which is not along the stretching direction. There, the DNA takes on a bow-like form (Fig. 3.11, p. 56). Furthermore, the forces acting on the bead trapped by two DNA strands (Fig. 3.16) will be determined.

Forces of stretched DNA molecules in a lateral flow

The bow-like shape of the DNA molecules, which are exposed to a lateral flow resembles the problem of a free hanging chain of length L between two anchor points under the influence of gravity. There, the external acting gravity force is at each point of the chain proportional to the length dl of a small segment. Assuming this proportionality the problem is analytically solvable as it is shown in the Appendix A.1.1.

In the case of the DNA molecules, a better description of the external drag force dF_D should be to split the force into two parts. One is the hydrodynamic drag along the molecule the other one is the drag perpendicular to the DNA, which both will assumed to be proportional to the projections dx, dy of the segment dl. Thus, $dF_D = C_1 dy + C_2 dx$ with a flow direction parallel to either the y- or the x-axis, although here for the force component parallel to the flow the DNA is assumed as a rod instead of sphere hanging on a rope like in the half-dumbbell model. However, applying this relation the problem is not analytically solvable, anymore. Thus, in order to simplify the problem arising from that, the external force is, like for a chain, assumed to be proportional to the length segment dl. This approximation is probably quite correct for slightly curved molecules, as in this case the external force is dominated by the drag perpendicular to the DNA. However, for strong curved molecules with a higher part of drag force along the DNA, this relation gets probably wrong.

Assuming $F_D = C\,dl$ and a flow parallel to the y-axis, one can directly take the solution from the chain problem for the shape $y(x)$ of the DNA (Eq. A.6, p. 110):

$$y = 1/B\{\cosh[B(x - x_0)] - 1\} + y_0. \tag{3.4}$$

Fitting the shape of the bow-like DNA by using this equation, the values for B, x_0 and y_0 are obtained.

To obtain the drag force, the force constant C has to be determined. This is done by using the fact, that DNA has an entropic elasticity. If the extension L' along the bow of the DNA is near the contour length L, one can simplify the force-extension

relation of the DNA (Eq. 1.15, p. 20) to

$$F = \frac{k_B T}{a}\frac{1}{4}\left(1 - \frac{L'}{L}\right)^{-2} \quad \Longrightarrow \quad \frac{L'}{L} = 1 - \sqrt{\frac{k_B T}{4aF}} = \frac{dl'}{dl}, \tag{3.5}$$

where dl'/dl is the local stretching, which has to be considered, because the force along the stretched DNA molecule in a lateral flow is not constant. The sum of all segments dl must result in the contour length L of the DNA. Thus,

$$L = \int_0^L dl = \int_0^{L'} \frac{dl'}{1 - \sqrt{\frac{k_B T}{4aF}}} = \int_{x_1}^{x_2} \frac{\sqrt{1 + y'^2}}{1 - \sqrt{\frac{k_B T}{4aF}}}\, dx, \tag{3.6}$$

with $dl' = \sqrt{1 + y'^2}\, dx$. The force along the DNA is given by the solution for the free hanging chain $F_{chain} = C/B \cosh[B(x - x_0)]$ (Appendix A.1.1). Together with Equation 3.4 this results to

$$L = \int_{x_1}^{x_2} \frac{\cosh[B(x - x_0)]}{1 - \sqrt{\frac{k_B T}{4aCB^{-1}\cosh[B(x - x_0)]}}}\, dx. \tag{3.7}$$

From this relation the force constant C can be finally extracted. To obtain it for a particular molecule, the value of C has to be found, for which the integral in Equation 3.7 equals the contour length L of the DNA. As the integral is not analytical solvable, the force constant C is determined numerically by a home-made software.

Figure 3.17 shows four molecules attached via biotin-streptavidin to the surface, which shape was fitted by using Equation 3.4. In the upper row of the figure the curves are depicted, which describe the real shape of the molecules. In the lower row the result of the fit is shown. As presumed for the molecules, which are strongly bent (molecule 1 and 2), the fitted curve shows larger deviations from the real curvature. This means, that an assumed linear dependency of the drag force on the length of small segment dl' is only a quite rough approximation. A nearly perfect agreement of the fitting function with the shape of the molecule is found for molecule 4, which is only slightly bent. For this molecule the drag force is probably well described by the linear relation $dF_D = C dl'$. From the fit, the values for B (Tab. 3.1) and x_0 are obtained. Note, that the molecules 1, 2 and 4 are approximately fully extended to the contour length (Tab. 3.1).

By a numerical procedure the values for the force constant C are obtained for which the integral in Equation 3.7 results to the contour length. The drag force acting at the DNA molecule is then obtained by $F_D = C \cdot l'$. The horizontal force, which represents the lowest tension along the DNA, results to $F_H = C/B$ according to Section A.1.1. It is located at the local minimum of the curve at (x_0, y_0). The results for the forces calculated for the four molecules are shown in Table 3.1. Using

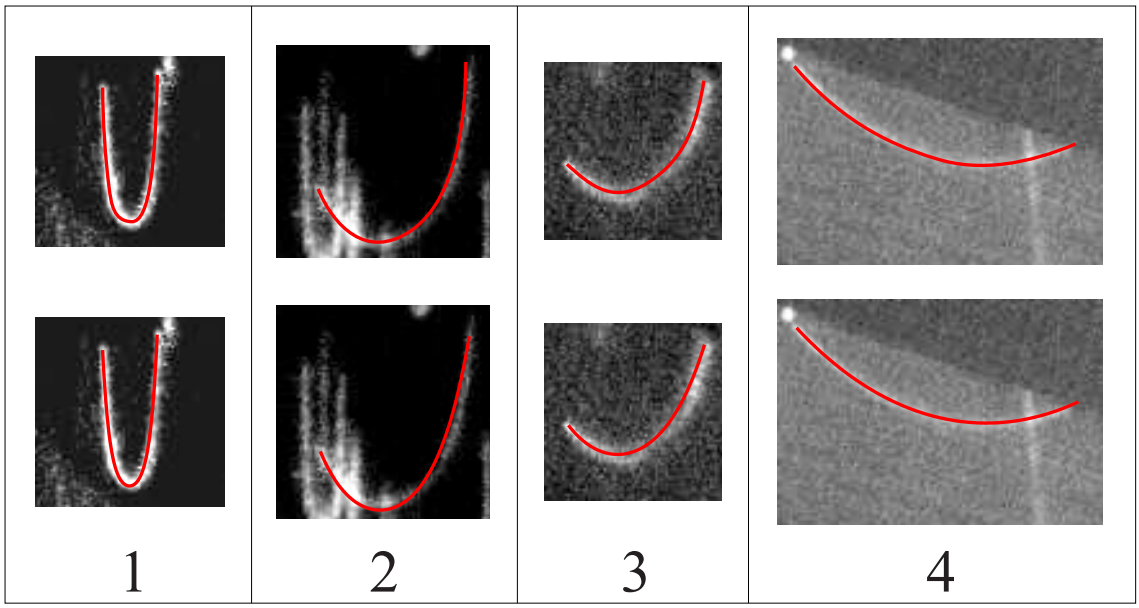

Figure 3.17: Bow-shaped DNA molecules. The flow direction is from top to the bottom. In the images in the top row the curves, which describe the real shape of the molecules, are shown (red line). In the images in the bottom row the curves obtained by the fitting procedure are depicted (red line). All images have the same scale. For end-to end distances of the molecules see Table 3.1.

the persistence length and the contour length of native DNA ($L = 16.3\,\mu$m, $a = 53\,$nm) for two molecules tremendous drag forces of more than 300 pN are obtained, which is obviously much to large, as it is already much beyond the force necessary to overstretch DNA. The reason for the incorrect forces is that the force-extension equation from the worm-like-chain model is not precise for extensions around the contour length as it approaches infinity at this point. Thus, for molecule 2, which is extended beyond the contour length to $16.5\,\mu$m no forces at all can be calculated. In order to avoid problems with the singularity of the relation, modified values for L and a were obtained by fitting experimental force-extension data from Ref. 47 (Fig. 1.15, p. 21) with the simplified force-extension relation of Equation 3.5. Thus, fictive values of $a = 18\,$nm and $L = 18.3\,\mu$m were obtained which describe the measured forces better for a relative extension around 1. Using the new parameters, reasonable drag forces between 5 and 50 pN for the three fully extended molecules are obtained. These forces correspond to the values to stretch the DNA to its contour length. Therefore, with the new parameters much better estimations of the real forces are obtained for the three molecules which are extended to about the contour length.

The total force acting at a single anchor point $x_i (i = 1, 2)$ of the DNA can be

	Molecule	**1**	**2**	**3**	**4**
	B [μm^{-1}]	2.56	0.53	0.43	0.096
	EED[μm]	3.0	10.3	8.1	15.0
	L' [μm]	16.0	16.5	10.5	16.1
$a = 53$ nm	C [pN μm^{-1}]	22	-	**0.044**	19
$L = 16.3\,\mu$m	F_D [pN]	352	-	**0.46**	306
	F_H [pN]	8.6	-	**0.10**	198
$a = 18$ nm	C [pN μm^{-1}]	**1.5**	**2.3**	0.091	**0.35**
$L = 18.3\,\mu$m	F_D [pN]	**24**	**38**	0.95	**5.6**
	F_H [pN]	**0.58**	**4.3**	0.21	**3.6**
	$F_{A\,max}$ [pN]	**12.6**	**27.8**	0.71	**5.3**
$a = 73$ nm	C [pN μm^{-1}]	0.087	0.064	0.015	0.017
$L = 22.0\,\mu$m	F_D [pN]	1.4	1.1	0.16	0.27
	F_H [pN]	0.034	0.12	0.035	0.18

Table 3.1: Fitted curve parameters and force constants for bow-shaped DNA molecules in a lateral flow. The molecules, which are given by their number, correspond to the molecules depicted in Figure 3.17. EED denotes the end-to-end distance, L' the extension along the bow. $F_{A\,max}$ is the maximum total force at the anchor point. The forces were calculated for three different sets for the contour length L and the persistence length a. The force values in bold provide the best agreement with the real forces.

calculated by:

$$F_A = \sqrt{{F_H}^2 + \left(F_D \frac{\sinh[B(x_i - x_0)]}{BL'}\right)^2}. \tag{3.8}$$

This leads to a maximum anchor force of about 28 pN for molecule 2 (Tab. 3.1), which has to be lasted by the streptavidin biotin linkage consisting of a maximum number of 4 or 6 connections. For molecule 3 the forces are best described with the correct values of L and a for the native molecule, as the extension L' is with 10.5 μm significantly lower than the contour length. Here a drag force half about 0.5 pN is obtained.

The flow velocities in the experiments did not exceed 500 μm s^{-1}. Using Equation 3.3 (p. 50) for the lateral drag force on a cylinder with a diameter of 1 μm, a force constant of about 0.01 pN μm^{-1} is obtained. This value, however, is much below the experimentally obtained force constants in Table 3.1. Thus, the lateral drag can probably not described by the simple cylinder model.

For completion, forces are also calculated for $L = 22\,\mu$m and $a = 73$ nm which have been found for highly fluorescently labelled DNA [79]. However, as it was stated previously, the DNA used in this experiments is only low labelled with 80 bp per dye molecule. Therefore, the obtained drag forces, which all lie in the pN and

sub-pN range are probably much to small. However, they give a lower limit for the real stretching forces.

In conclusion one can say, that the simple model, which was proposed to describe the forces at bow-shaped DNA molecules in flow, works quite well, if the molecules are not strongly bent. It could be shown that the biotin-streptavidin linkage used to couple the DNA to the surface, which consists of a maximum number of 4 or 6 biotin-streptavidin bridges, lasts forces of several 10 pN. Furthermore, it demonstrates that forces in this range can be generated with the hydrodynamic flow technique.

Forces acting on a bead trapped by two DNA strands

In the following, the forces acting on the bead in Figure 3.16, p. 60, which is trapped by two DNA strands will be determined. As it is commonly done in magnetic tweezers techniques, the Brownian fluctuations of the bead are analyzed [47]. The longer the DNA molecules, which are attached to the bead, are stretched, the stronger are the forces, which act on the bead, and the smaller are the fluctuations of the bead. The average potential energy of the oscillation perpendicular to the stretched DNA strands (x-direction) can be directly gained from the equipartition theorem with $E_{Px} = k_B T/2$ [84]. The force in x-direction is proportional to small displacements Δx of the bead (Fig. 3.18), which is in analogy to the case of the pendulum:

$$F_\perp = -2\frac{F_\parallel}{L}\Delta x =: -k_\perp \Delta x. \tag{3.9}$$

Thus, the average potential energy can be written as $E_{Px} = k_\perp/2\ \delta x^2$ with the average quadratic displacement of the bead of $\delta x^2 = \langle x^2\rangle - \langle x\rangle^2$. With $k_\perp = 2F_\parallel/L$ (Eq. 3.9) it leads to

$$F_\parallel = \frac{k_B T L}{2\,\delta x^2}, \tag{3.10}$$

and gives a direct relation between the average quadratic Brownian fluctuation δx^2 and the stretching force $F_\parallel$ of the DNA molecules.

δx^2 is determined by recording a time series of 121 images. These images are arranged into a single image in an 11x11 array. The bead position is then determined by calculating the correlation function between array image and the image of the first bead of the series, which serves as the reference.

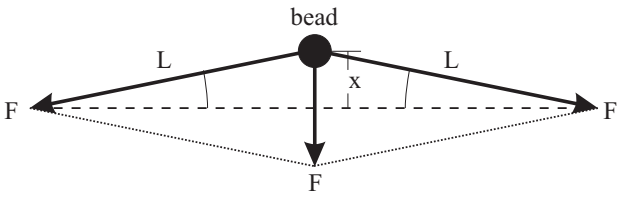

Figure 3.18: Forces at the bead trapped by two DNA strands.

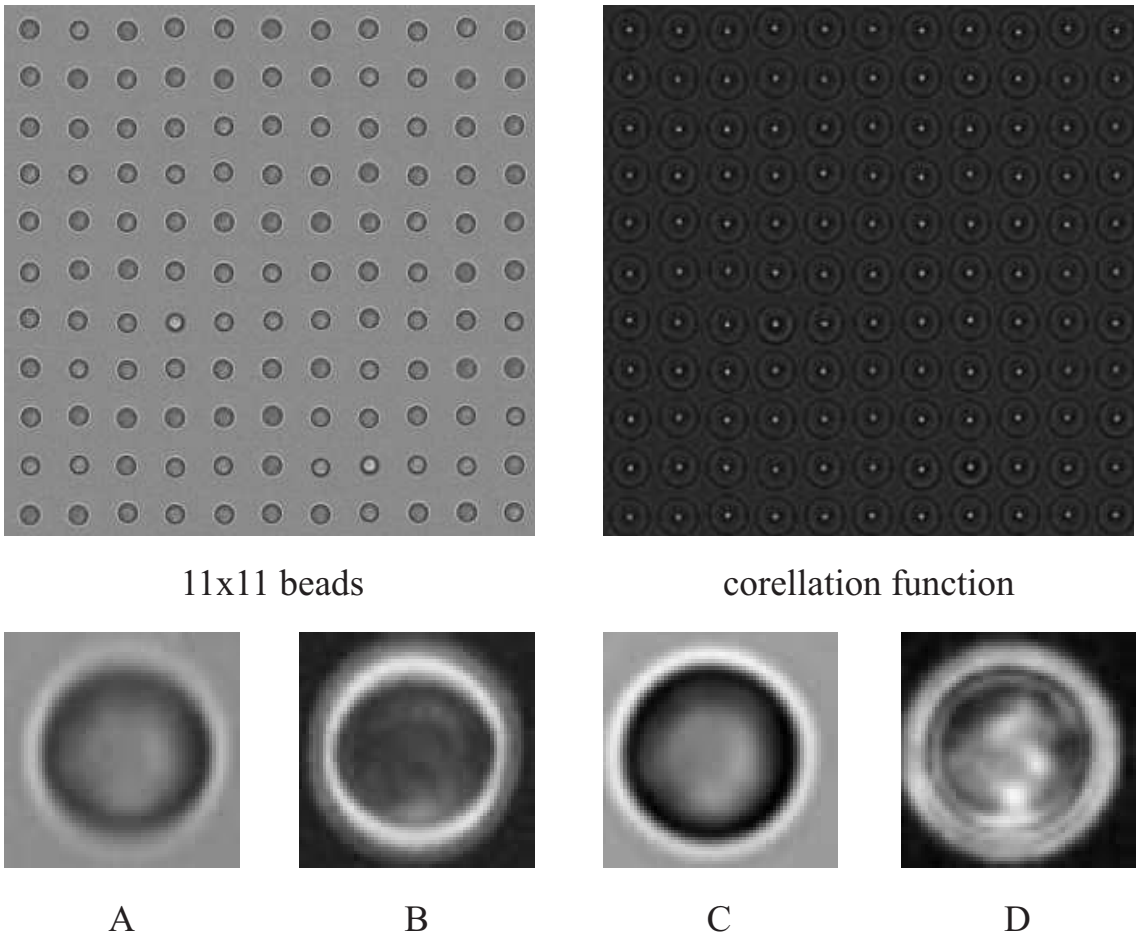

Figure 3.19: Time series of 121 images of the bead arranged to an 11x11 array together with the corresponding correlation function with the first image of the series. A) Average image of all beads. B) Variance image of all beads. C) Correlation average of the all bead images. D) Variance of the correlation average.

The correlation C is defined by

$$C = \sum_{n,m} (OP_n - RP_m)^2, \tag{3.11}$$

were OP denotes the points of the original image and RP the points of the reference image. At points of high correlation between both images C has a local extremum. The correlation function, which is obtained from C after a scaling procedure, was obtained by using a commercial software[3]. Figure 3.19 shows an 11x11 bead image

[3]SPIP - Scanning Probe Image Processor for Windows, V2.21, Image Metrology ApS, Kopenhagen

Series	$\sqrt{\delta x^2}$ [nm]	$\sqrt{\delta y^2}$ [nm]	$F_{\parallel,L=12.5\,\mu m}$ [pN]	$F_\parallel/L$ [pN/μm]	L_{corr} [μm]	F_{corr} [pN]
1	205	71.3	0.61	0.049	13.4	0.66
2	187	69.6	0.73	0.059	13.7	0.80
3	192	77.5	0.69	0.055	13.6	0.75

Table 3.2: Average quadratic fluctuations and forces for the bead trapped by two DNA strands for three image series. δx and δy are the fluctuations perpendicular and parallel to the stretched DNA, respectively. $F_{\parallel,L=12.5\,\mu m}$ is the force for the measured DNA extension L of 12.5 μm. L_{corr} and F_{corr} are the corrected values, if the value for $F_\parallel/L$, which directly results from Equation 3.10, is applied to the WLC model.

array with the corresponding correlation function. Furthermore, the average image of all bead images was calculated, which shows that the bead fluctuations are mainly perpendicular to the DNA strands, as the bead edge of the average image appears more smeared in that direction. This is better to be seen in the variance image, which is defined as the standard deviation of the pixel gray scale values of all images from the average image. As brighter the pixels in the variance image are, as larger are the fluctuations at this point. The bright ring in the image (Fig. 3.19B), where the fluctuations are concentrated is broader along the axis perpendicular to the DNA strands. Thus, the fluctuations are mainly there. Image C shows the correlation average of all bead images. It is the average considering the changing bead position, which is determined from the correlation function. Therefore, no smear or other asymmetries referring to the bead center are seen here. In image D the variance from the correlation average is depicted. The large fluctuations there arise from the changing height of the bead along the optical axis of the objective.

After this qualitative analysis of the bead movement the average quadratic fluctuations are calculated from the bead positions determined from the correlation function. Table 3.2 shows the obtained averaged fluctuations perpendicular (δx) and parallel (δy) to the stretched DNA molecules, which are in x direction about a factor of three larger than in y direction. In order to calculate the stretching force of the DNA molecules $F_\parallel$ using Equation 3.10, the DNA extension L is still required. However, as the beads are highly fluorescent, the anchor points of the DNA can not be seen and the length can not be exactly measured (Fig. 3.16, p. 60). L has to be at least 12.5 μm, which is the length measured for the DNA strand, which appears longer in the figure. Applying this value one gets a lower limit for the stretching force of about 0.7 pN (Tab. 3.2). A more precise way to get the force, is to calculate $F_\parallel/L$, for which only δx^2 is required, and to find the value for L for which $F_\parallel/L$ fits into the WLC model (Eq. 1.15, p. 20). Doing this, one obtains a corrected extension between 13.4 and 13.7 μm. The corresponding forces, which act on the bead from the stretched DNA strands, lie thus between 0.66 and 0.80 pN. These values should

provide a more precise result for the real acting forces.

4 Platinum cluster chains along DNA

The challenge in the development of a new metallization procedure of DNA templates is to establish a method where continuous nanowires with a diameter below 10 nm can be fabricated. The demand on such a DNA metallization is that it is highly specific, i.e. metal deposition should take place selectively at the DNA, but not in the surrounding medium. However, under experimental conditions one always deals with both processes - the heterogenous reaction at the biotemplate as well as the homogeneous reaction, which leads to unwanted background metallization. These two metallization routes are competing. Therefore, in order to avoid the background process, methods have to be developed, where the heterogeneous reaction channel at the biotemplate is strongly favored compared to the homogeneous reaction channel.

One approach for an enhanced heterogeneous metallization at the biomolecular template is the formation of effective nucleation centers at the DNA, which catalyze and therefore accelerate the further metal deposition. Simultaneously, the background metallization is kinetically suppressed. The quality of such a metallization procedure depends very much on the properties of the nucleation centers and the subsequent metal growth process. In previous investigations, nucleation centers at the DNA were formed by binding metal ions, like silver [15], cadmium [16] and palladium [18], to the biomolecular template. However, these examples still possess some disadvantages, for example high background or coarse metallization (see Section 1.3.3).

In order to find a metallization method, which is more specific and results into the formation of thinner structures, platinum turns out to be an interesting material. Platinum complexes are known to bind strongly to DNA [85]. Additional to that, the binding depends on the sequence of the DNA. The growth process of platinum clusters upon reduction of platinum complexes is autocatalytic [86]. Furthermore, First Principles Molecuar Dynamics investigations of the formation of platinum clusters show that already an initially formed Pt dimer can serve as nucleation center because its formation is the limiting step during the whole reaction [87, 88].

The hope of using Pt complexes for the metallization of DNA is to promote heterogeneous cluster nucleation from single complexes, which are bound to the DNA. If the nucleus formation at the bound complexes is favored to the homogeneous nucleation, a highly specific metallization of the DNA could be achieved and due to the sequence-dependent binding of Pt complexes to DNA even a sequence-dependent metallization could become possible.

In the following the DNA metallization using platinum complexes is studied. In Section 4.1 the binding of Pt complexes to DNA is investigated as it is the initial step of the procedure. In order to compare homogeneous and heterogenous nucleation, in Section 4.2 the cluster formation in the absence of DNA is studied. It is followed by the detailed investigation of cluster formation in the presence of DNA in Section 4.3. It will be shown that for a successful metallization, i.e. the formation of cluster chains along the template, the DNA must be densely covered with bound $PtCl_4^{2-}$ complexes. In Section 4.4 it is demonstrated that synthesized cluster chains along DNA templates can be enhanced to form continuous wires.

4.1 Binding of $PtCl_4^{2-}$ complexes at DNA

Among the large number of different platinum complexes, the chloro-ammine complexes are of great interest for the application in DNA metallization. The binding of K_2PtCl_4 and cisplatinum is studied in the following. The tetrachloro species K_2PtCl_4 was successfully used in our group to metallize other biomolecules like microtubules [9, 10] and bacterial surface layers (S-layers) [13, 14]. It binds to the aminoacids of these biotemplates and can thus initiate a cluster growth at these proteins. Furthermore, it is known to bind strongly to DNA [89, 90]. Cisplatinum (cis-platinum(II)diammine dichloride, cis-$[Pt(NH_3)_2Cl_2]$) is probably the best investigated platinum complex, as it is widely used as an anti-cancer drug [85]. The binding to DNA takes place in a several step process by replacing the chlorine ligands with the N^7 nitrogen of guanine or adenine [91]. However, this ligand exchange does not occur directly, but involves a previous hydrolysis of the complex, where the chlorine ligand is exchanged with a water molecule. Hydrolysis takes place in a time scale of hours. Subsequently, the water can be easily replaced by the N^7 of a DNA base with a typical reaction time of several minutes [91]. Thus, the kinetics of the binding process is limited by the hydrolysis of the platinum complex. After the complex is bound to the DNA by a single bond, which is called *monofunctional adduct* a second bond can be established by exchanging the second chlorine ligand with water, which takes again place within several hours. Then the N^7 of a neighboring base can comparable quickly bind by replacing the water. This *bifunctional* adduct is most favorable formed between two guanines, but it also formes at a adenine-guanine sequence [92]. Due to the very specific binding of cisplatinum to

DNA, it is possible to bind the platinum complex at specific positions to DNA, by designing a DNA target which has a guanine-guanine sequence at these locations. The binding of platinum complexes to DNA leads to changes of the DNA structure, in particular the base stacking is strongly distorted. The normally parallel base plains are tilted to an angle of up to 90° [93, 94], which leads to DNA bending as well as shrinkage [95].

Due to the structural similarities between cis-Pt$(NH_3)_2Cl_2$ and $PtCl_4^{2-}$, the principle binding mechanism, including the hydrolysis of the chlorine ligand, should be the same for $PtCl_4^{2-}$ as for cisplatinum. For $PtCl_4^{2-}$ the particular binding mechanism to DNA is less known. From early studies, which were conducted also in a large excess of complexes to DNA base pairs, it is known that up to three complexes can bind per base pair, which implies additional binding sites at the DNA bases [90]. The reaction kinetics is dependent on the GC content of the DNA; as higher the GC percentage as faster the process [96, 97]. The total amount of bound complexes does not depend on that. The time to get saturation of the DNA with complexes lies in the range of several hours [89]. An interesting difference to cisplatinum is, that at a ratio of one complex per base pair the platinated DNA precipitates for the cis-species whereas for $PtCl_4^{2-}$ no precipitation is observed even at a ratio of 50:1. This points to the fact, that the structural changes, which are induced by $PtCl_4^{2-}$ are not as strong as for cis-Pt$(NH_3)_2Cl_2$. Indeed, in metallization experiments it turned out that the structural changes and the DNA precipitation induced by cisplatin are so tremendous that cisplatin could not be used for a successful metallization.

Therefore, in the following it will be mainly focused on DNA metallization using $PtCl_4^{2-}$. As the binding of this platinum complex to DNA is not well investigated, it is studied in more detail under the conditions, which are subsequently used for the DNA metallization. The main subjects are (i) the hydrolysis dependence of the binding, (ii) the time scale of the reaction and (iii) the conformational distortions of the complexes to the DNA helix. It is known that platinum complexes lower the melting temperature of DNA, which is for native λ-DNA only 37°C in an aqueous surrounding [98]. Therefore, it is also clarified, whether the DNA is still in the double-stranded conformation after complex binding or denatured to the single stranded form.

4.1.1 UV/VIS spectroscopy

One way to investigate the binding of $PtCl_4^{2-}$ complexes and its hydrolysis products to DNA are UV/VIS absorbance measurements. As already mentioned in Section 1.1, distortions of the DNA base stacking due to the melting transition from double-stranded to single-stranded DNA can be quantified at 260 nm wavelength. But, such distortions in the base stacking can also arise from the binding of molecules to the DNA bases. As the platinum complexes are known to tilt the base plains

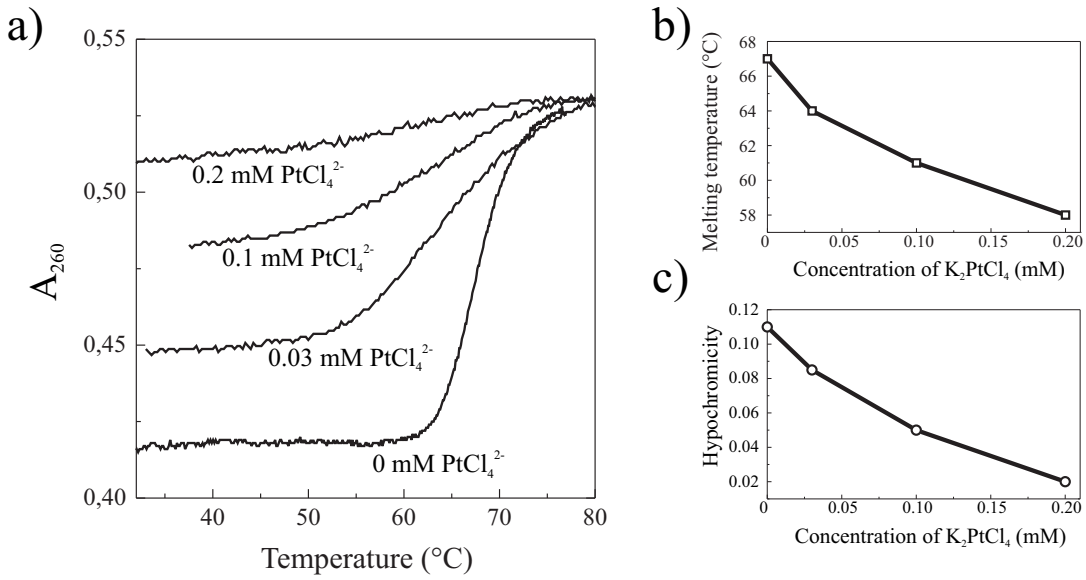

Figure 4.1: DNA melting for different concentrations of $PtCl_4^{2-}$. a) Melting curves of 20 μg/ml salmon DNA in 5 mM $NaSO_4$ incubated 16 h with different concentrations of $PtCl_4^{2-}$. A_{260} denotes the absorbance at 260 nm b) Melting temperature as a function of the $PtCl_4^{2-}$ concentration as obtained from the melting curves (Section 1.1). c) Hypochromicity, which is defined as the A_{260} difference after and before melting, as a function of the $PtCl_4^{2-}$ concentration.

against each other [93, 94], binding of them should therefore result in an increase of A_{260}. From this absorbance increase, however, one does not know, whether it comes exclusively from the distorted base stacking due to complex binding or from local denaturation of the DNA induced by the complexes, as both effects result in an increase of A_{260}. If the DNA would be denatured by the complexes, no melting transition could be observed in experiments. Therefore, in order to separate the two effects, DNA melting temperature studies were performed in the presence of different concentrations of $PtCl_4^{2-}$. For this, the DNA was incubated overnight to insure complete complex binding. Figure 4.1 shows two effects caused by complexes bound to the DNA: (i) The A_{260} is already increased before melting has started. The higher the complex concentration the higher is the increase, i.e. the hypochromism is shrinking (Fig. 4.1c). For $PtCl_4^{2-}$ concentrations larger than 0.2 mM no hypochrome absorbance decrease could be detected anymore, i.e. the base stacking is completely vanished. (ii) The melting temperature is lowered (Fig. 4.1b). However, even for the highest complex concentration of 0.2 mM it is much above room temperature. Thus, from these investigations one obtains that the $PtCl_4^{2-}$ complexes indeed distort the base stacking, resulting in an A_{260} increase. At room temperature these distortions are caused by tilted base plains and not by local DNA denaturation up

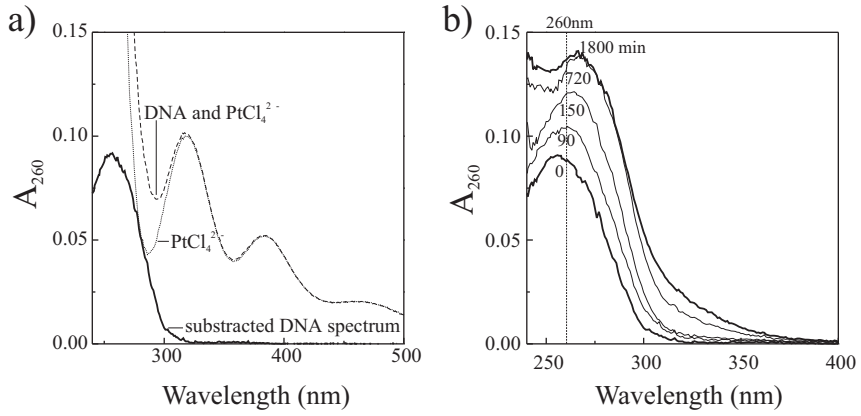

Figure 4.2: Time course of the breakdown of DNA base stacking due to $PtCl_4^{2-}$ binding. a) Spectra of a 1 mM $PtCl_4^{2-}$ solution and a solution containing 1 mM $PtCl_4^{2-}$ and 5 μg/ml λ-DNA immediately after mixing. Substraction of both spectra provides the pure DNA spectra with a maximum at about 260 nm. b) Spectra of DNA incubated with $PtCl_4^{2-}$ obtained at different times of the binding process. Note the absorbance increase around 260 nm indicating the breakdown of the DNA base stacking.

to a concentration of 0.2 mM $PtCl_4^{2-}$ corresponding to a complex-to-base-pair ratio (C/B ratio) in solution of 6 complexes per base pair.

For the melting studies the DNA was incubated overnight with the complexes, resulting in an final A_{260} increase. However, monitoring the A_{260} increase of the DNA over time should provide information about the time scale in which the distortion of the base stacking, and therefore the binding of $PtCl_4^{2-}$ takes place. However, the A_{260} of DNA can not be directly measured in the spectrometer, as it is overlapped by electronic excitations of the Pt complexes (Fig. 4.2a). Moreover, the $PtCl_4^{2-}$ spectrum changes over time due to hydrolysis, which changes also for an equilibrated complex solution, when it is mixed with the DNA solution as it is diluted. Therefore, in order to obtain the pure DNA spectrum, a reference solution is measured over time additional to the DNA-$PtCl_4^{2-}$ sample solution. This reference contains only $PtCl_4^{2-}$ in the same dilution as the sample. Subsequent substraction of sample and reference spectra gives thus the DNA spectrum (Fig. 4.2a). All parts of the spectrum, coming from the platinum, are successfully eliminated, if the DNA spectrum shows no absorbance for wavelengths larger 320 nm. Application of the substraction procedure to a series of sample and reference spectra in time, allows to record the time course of the DNA helix breakdown, which is caused by the binding of the $PtCl_4^{2-}$ complexes. Figure 4.2b shows the time evolution of the DNA spectrum obtained this way. It clearly shows that the helix breakdown occurs in the range of hours and is completed after about 12 h. This means, that also the complete binding of $PtCl_4^{2-}$ to DNA proceeds at least in this time. In this case complete binding

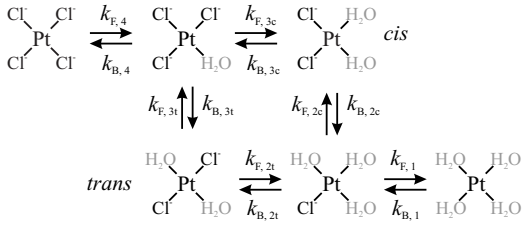

Figure 4.3: Reaction model of the hydrolysis of $PtCl_4^{2-}$ according to Ref. 99

	K_{eq} (mM)	k_F (s^{-1})	k_B ($s^{-1}M^{-1}$)
4	12.6	$3.6{\cdot}10^{-5}$	$2.8{\cdot}10^{-3}$
3c	0.8	$6.0{\cdot}10^{-5}$	$7.5{\cdot}10^{-2}$
3t	0.6	$2.8{\cdot}10^{-8}$	$4.6{\cdot}10^{-5}$
2c	0.18	$3.0{\cdot}10^{-7}$	$2.0{\cdot}10^{-3}$
2t	0.22	$1.0{\cdot}10^{-4}$	0.5
1	0.01	$3.0{\cdot}10^{-7}$	$3.0{\cdot}10^{-2}$

Table 4.1: Equilibria and rate constants for the hydrolysis of $PtCl_4^{2-}$ from Ref. 99.

means the maximum possible loading of the DNA with about three complexes per base pair, which is achieved at the applied C/B ratio of 130 [90].

For cisplatinum the time scale of the binding depends very much on the hydrolysis of the complex [91]. For $PtCl_4^{2-}$ it is interesting to know, whether the binding to DNA is hydrolysis limited, too. To investigate this, one needs exact information about the percentage of the different hydrolyzed species in a $PtCl_4^{2-}$ solution. The hydrolysis of $PtCl_4^{2-}$ is slightly different to cisplatinum, as four chlorine ligands can be exchanged by water. The model for the involved reactions is depicted in Figure 4.3. In principle all four chlorine ligands can be replaced by water. However, from the rate constants one sees that the formation of *trans*-$[PtCl_2(H_2O)_2]^0$ as well as of $[PtCl(H_2O)_3]^+$ from the *cis*-complex is very slow. Considerable amounts of these two species are only found for reaction times times larger than 100 h in very dilute solutions [99]. Therefore, a solution of $PtCl_4^{2-}$, which is aged overnight, contains only $PtCl_4^{2-}$, $[PtCl_3H_2O]^-$ and *cis*-$[PtCl_2(H_2O)_2]^0$. The time for the hydrolysis of these complexes is in the order of 10 h. Therefore, taking the equilibrium constants for the two reactions involved in the formation of the three complexes, it is possible to calculate the percentage of complexes after overnight aging (Fig. 4.4). One can see, that the fractions of the three complex species can be varied over a large range

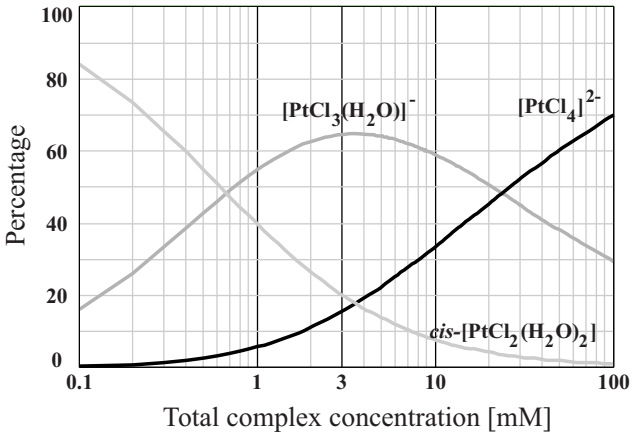

Figure 4.4: Percentage of the different complex species after 16 h hydrolysis of $PtCl_4^{2-}$. The calculation is explained in the Appendix A.1.2.

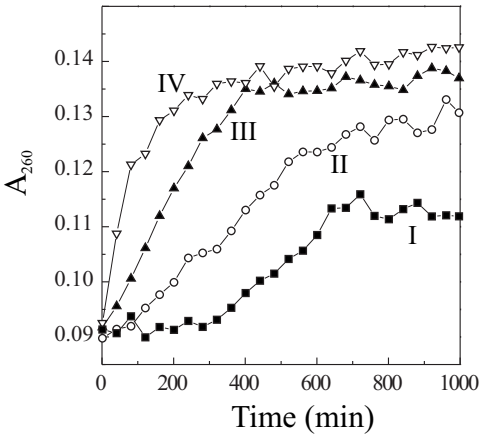

Solution	I	II	III	IV
Stock (mM)	10*	100†	10†	1.5†
$[PtCl_4]^{2-}$	1	0.70	0.35	0.17
$[PtCl_3H_2O]^-$	0	0.29	0.59	0.56
$[PtCl_2(H_2O)_2]$	0	0.01	0.06	0.27
$t_{\Delta A_{260}/2}$ (min)	440	350	190	70

[*] fresh, [†] 16 h aged

Figure 4.5: Time course of the breakdown of DNA base stacking due to $PtCl_4^{2-}$ binding dependent on the hydrolysis. The breakdown of the DNA base stacking was recorded at 260 nm for four different hydrolyzed $PtCl_4^{2-}$ solutions, which were prepared directly before the experiment started by dilution to 1 mM from I) fresh and 16 h aged II) 100 mM, III) 10 mM and IV) 1.5 mM $PtCl_4^{2-}$ stocks. The fraction of the different hydrolyzed species can be seen in the table. It was calculated as described in the Appendix A.1.2. $t_{\Delta A_{260}/2}$ (min) denotes the time after the half of the total A_{260} absorbance change is reached.

by changing the total concentration of the complexes. This opens a way to prepare differently hydrolyzed complex solutions with the same molarity of complexes, just by dilution of differently concentrated aged stock solutions. For the investigation of the hydrolysis-dependent binding of $PtCl_4^{2-}$ to DNA, four 1 mM solutions with different fractions of hydrolyzed species are used (Table in Figure 4.5). Solution I, which contains only non-hydrolyzed complexes, is prepared by diluting freshly dissolved salt. The other solutions are diluted to 1 mM from 100 mM, 10 mM and 1.5 mM stock solutions, which have been previously aged for 16 h. These dilutes contain now the same fractions of hydrolyzed complexes as their stocks, because the hydrolysis of $PtCl_4^{2-}$ is a quite slow process and changes only in the range of hours (Appendix A.1.2). Thus, if the experiment is started immediately after dilution, one knows the exact state of hydrolysis at the beginning of the investigation.

To study the hydrolysis dependence of $PtCl_4^{2-}$ binding, the breakdown of the DNA base stacking was observed for each of the four solutions. As one can see in Figure 4.5, the binding of the Pt complexes to DNA is very much affected by the hydrolysis. Like in the case of cisplatinum, a higher degree of hydrolysis leads to a much faster breakdown of the base stacking, i.e. to a faster binding process. This means that the binding of $PtCl_4^{2-}$ to DNA is hydrolysis dependent, from which one may conclude that the binding mechanism is very similar as for cisplatinum. Another consequence from this experiment is, that in the following metallization experiments only previously aged stock solutions of complexes are used, in order to ensure a complete binding of $PtCl_4^{2-}$ to DNA during an overnight incubation. The

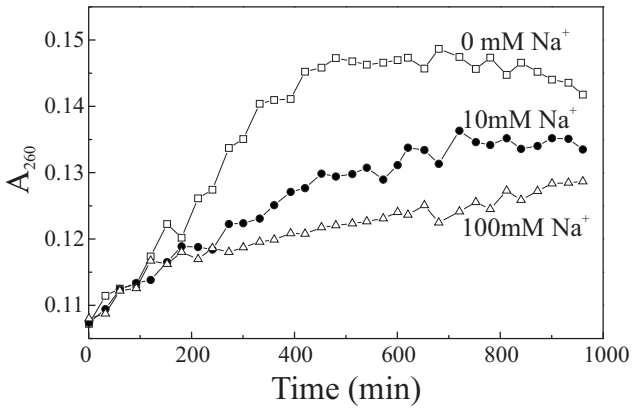

Figure 4.6: The time course of the breakdown of the DNA base stacking due to $PtCl_4^{2-}$ complex binding in the presence of Na_2SO_4.

typical stock concentration was 10 mM.

As one could see in the previous investigations, the DNA base stacking is completely vanished during the binding of the Pt complexes. This means, that large distortions of the DNA structure must be present. Up to 0.2 mM $PtCl_4^{2-}$ the DNA is still double-stranded at room temperature, but it is not clear, if this is still the case for higher complex concentrations. SFM studies, described later on, confirm heavy structural changes. These distortions are not desirable, as they alter also the morphology of the DNA template network structures. One way to avoid them is the additional stabilization of the DNA during complex binding. An increased ionic strength of the solution, for example by addition of monovalent ions, is known to increase the melting temperature, i.e. to stabilize the DNA (Eq. 1.1, p. 8). Different buffers and salts are tried, whether they can stabilize the DNA upon $PtCl_4^{2-}$ binding. Doing this, one problem is, that $PtCl_4^{2-}$ turns out to be very reactive with all kind of buffers and anions, taking them as new ligands instead of chlorine. It changes the whole properties including the reactivity with DNA and the reduction potential. Therefore, one requirement to any additive is that it shall not react with the Pt complexes, which can be easily checked by measuring the UV/VIS spectrum of $PtCl_4^{2-}$ after incubation with the additive. It turns out, that all buffers used in this experiment (Hepes, Tris-SO_4^{2-}, Mes) change tremendously the complex spectrum and can thus not be applied for DNA stabilization. Furthermore, the additive shall not contain Cl^- ions, as they shift the hydrolysis balance towards the non-hydrolyzed species and prevent the binding this way. An appropriate salt, showing no reaction with $PtCl_4^{2-}$ was found with Na_2SO_4. The helix breakdown during $PtCl_4^{2-}$ binding was therefore studied in the presence of different concentrations of Na_2SO_4 (Fig. 4.6). At the beginning no retardation of the helix breakdown due to Na^+ is visible. However, at larger reaction times the collapse of the base stacking becomes slower with increasing Na^+ concentration. The final increase A_{260} in the presence of Na^+ is smaller than without salt addition and furthermore significantly less than the absorbance increase, which is obtained by denaturing double stranded to single stranded DNA. This points to the fact that the base stacking is partially

preserved in the presence of Na_2SO_4. Thus, the distortion of the DNA double helix due to the reaction of $PtCl_4^{2-}$ with DNA can be reduced upon addition of Na^+. However, with this investigation it remains unclear, if the sodium ions affect the complex binding to the DNA. The origin of the stabilization can either be an increased helix stability or a reduced binding, whereas the latter case is not desired. The reduced binding can even be caused by the increased helix stability, which leads to sterical hindrance of the complexes. The similar kinetics after the start of the binding points to the fact, that Na^+ does not affect the binding at the beginning of the reaction.

4.1.2 Gel electrophoreses

From the UV/VIS studies it is known, that binding of $PtCl_4^{2-}$ to DNA leads to the complete destruction of the DNA base stacking for high C/B ratios. From this investigations, however, it is not clear if the base pairing is still preserved or if the DNA denatures upon the complex binding. The maintenance of the double-stranded configuration is, however, very important, for example, for the metallization of DNA junctions or DNA which is anchored between electrodes. Denaturation would destroy these template structures.

In order to investigate the DNA configuration a series of investigations using gel electrophoresis was done. Here, the fact was used that long single-stranded DNA, in contrast to double-stranded DNA, does not run in a sharp band but only in a smear in non-denaturing agarose gels. If DNA covered with platinum complexes would be denatured, it should therefore not run in a band. For the reason of comparison, both, single- and double-stranded DNA, was incubated with $PtCl_4^{2-}$ for 16 h. In order to look at differently long DNA fragments, λ-DNA as well as λ-DNA digested with *Hin*dIII was applied. The single-stranded form of the fragments was obtained by heating the DNA for 5 min at 95°C and subsequent cooling on ice in order to avoid reassociation. A problem, which still remains, is the visualization of the DNA in the gel, as the bound complexes prevent staining of the DNA with fluorescence dyes. Therefore, the platinated DNA is, previously to the gel electrophoresis, incubated with a small amount of a reducing agent (dimethylammine borane, DMAB). It is not sufficient to reduce all platinum in solution, but large enough to form few small clusters at the DNA. After running the gel, the DNA is visualized by enhancing the small Pt clusters with the gold stain, previously applied to proof the thiol modification of the DNA (Fig. 3.4, p. 48). The result of this experiment is shown in Figure 4.7. Lane A shows the single-stranded λ-DNA complexed with $PtCl_4^{2-}$. As expected, only a smear can be seen in the gel. By contrast, the double-stranded λ-DNA, which was before incubated with $PtCl_4^{2-}$ for 16 h, runs in a sharp band. This means, that the double-stranded configuration is with bound complexes maintained, although the helix structure is largely disturbed. This fact is even supported by the shorter frag-

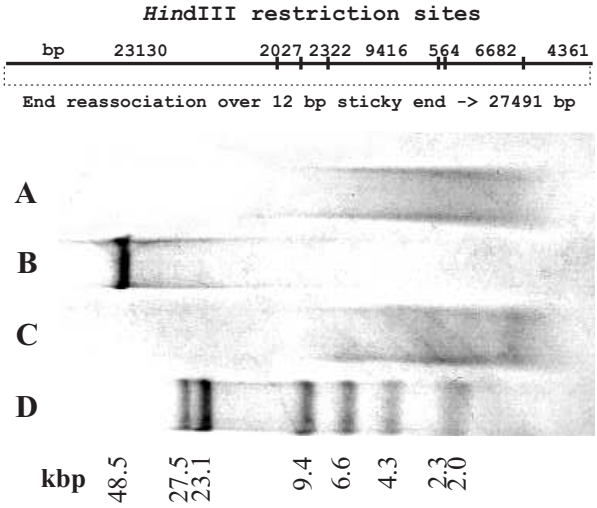

Figure 4.7: Gel electrophoresis of single and double stranded DNA after 16 h incubation with $PtCl_4^{2-}$. (A) Single stranded λ-DNA. (B) Double stranded λ-DNA.(C) Single stranded, *Hin*dIII digested λ-DNA. (D) Double stranded, *Hin*dIII digested λ-DNA.

ments of *Hin*dIII digested λ-DNA, where the same result is obtained. Denatured fragments complexed with $PtCl_4^{2-}$ run in a smear. Double-stranded fragments down to 2 kbp run in bands after $PtCl_4^{2-}$ incubation, showing that the double-stranded configuration is also preserved for these short DNA strands. In the *Hin*dIII restriction site map in Figure 4.7 one can see that the largest fragment should have a length of 23.1 kbp. However, another band on the large molecular weight side is apparent. This band can also be observed for native, non-platinated fragments, where molecular weight estimations gave a length of about 28 kbp. The reason for this is that the both ends of λ-DNA have complementary, cohesive 5'-overhangs, which can rehybridize to form the original plasmid. The melting temperature of this connection is about 59°C and thus stabile at room temperature. If the two end fragments of *Hin*dIII digested λ-DNA reassociate, a 27.5 kbp long fragment is formed as depicted in the restriction site map (Fig. 4.7). The high molecular weight band is, therefore, attributed to this construct. Supported is this explanation by the fact, that after heating *Hin*dIII digested λ-DNA to 65°C, followed by rapid cooling on ice, the band can not be seen in the gel anymore, as the 12 bp long link is denatured. Furthermore, if a strong 27.5 kbp band is be found, the intensity of the 4.3 kbp fragment is significantly lowered. Observing the 27.5 kbp construct also for DNA, which is fully loaded with $PtCl_4^{2-}$, points to the fact, that even the 12 bp long link stays double-stranded. It is a particular sequence, formed by 10 GC and 2 AT base pairs, but it proofs that the double-stranded configuration is even maintained on a length scale of a few bases, and that no larger denaturation takes place.

4.1.3 SFM studies

The structural changes which DNA undergoes upon $PtCl_4^{2-}$ binding can be visualized by SFM. Figure 4.8a shows one complete native λ-DNA molecule. The molecule

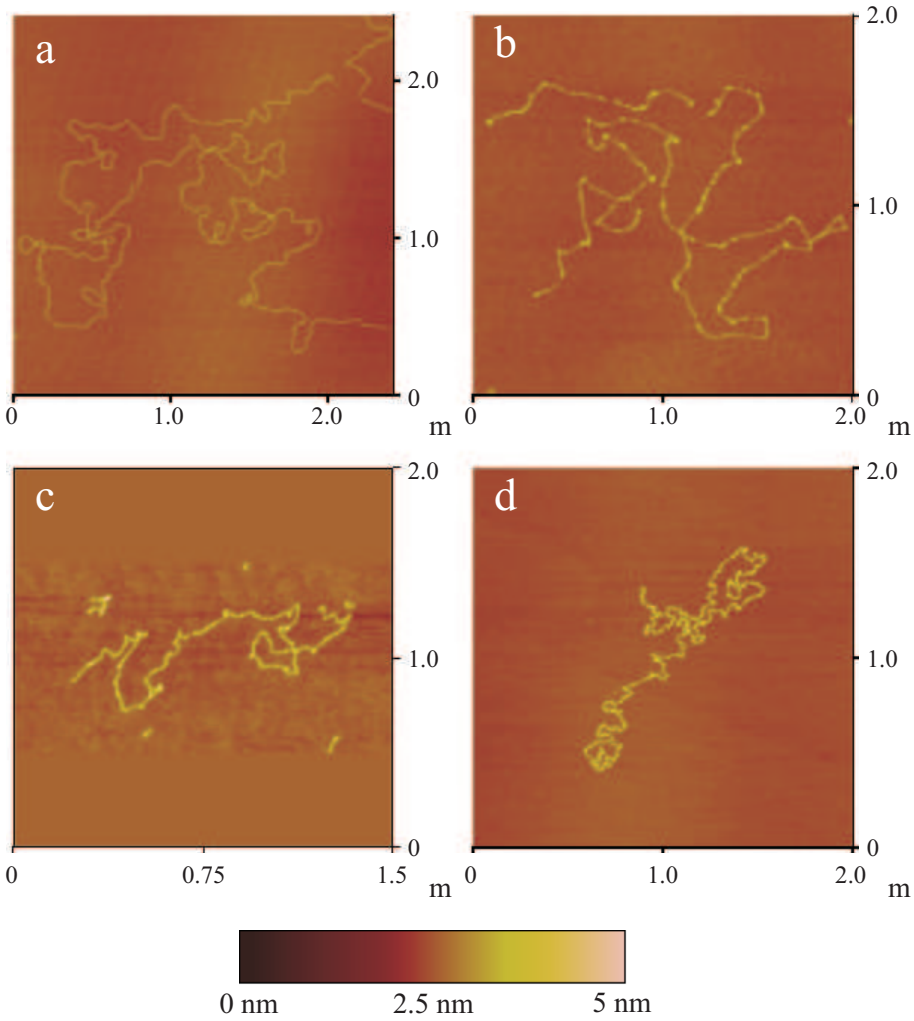

Figure 4.8: SFM images of DNA complexed by $PtCl_4^{2-}$. **a**) Native λ-DNA. **b**) λ-DNA after 1 h of $PtCl_4^{2-}$ incubation. **c**) λ-DNA after 16 h of $PtCl_4^{2-}$ incubation. **d**) λ-DNA after 16 h of $PtCl_4^{2-}$ incubation with additional 100 mM Na^+.

appears naturally coiled, but only on a larger length scale of more than 100 nm. The height of the adsorbed DNA is with about 0.5 nm the same along the whole molecule. After 1 h of incubation with $PtCl_4^{2-}$ sharp kinks and shorter coils can be seen in the DNA structure (Fig. 4.8b). Furthermore, dots with a height up to 1.5 nm become visible at the molecule arising from kinks out of the image plain. In Figure 4.8c the DNA morphology is shown after 16 h incubation with $PtCl_4^{2-}$. The density of kinks with a larger height is much higher. Thus, there are no regions anymore with the height of native DNA of 0.5 nm. The distortions cover the whole molecule. Together with the overall height increase, the length of the molecule appears shrinked. Length

	molecule length
native λ-DNA	16.0 - 16.4 μm
λ + 16 h $PtCl_4^{2-}$	1.5 - 2.9 μm
λ + 16 h $PtCl_4^{2-}$ + 100 mM Na^+	3.5 - 9.7 μm

Table 4.2: Averaged DNA length as obtained from SFM images for native λ-DNA and λ-DNA complexed by $PtCl_4^{2-}$ with and without Na^+.

measurements of about 20 molecules show that the average length is reduced by about a factor of 8 (Tab. 4.2). The shrinkage agrees to observations of Onoa and coworkers [95]. The shrinkage of the DNA length can not be explained by the rapture of single molecules, because otherwise in the electrophoresis experiment no sharp band indicating a unique molecule length would be obtained. The SFM investigation agrees nicely with the spectroscopic data concerning the time scale of the binding process. It clearly shows, that the largest structural changes still occur after 1 h of binding.

As already explained previously, it is desirable to avoid the large distortions induced by $PtCl_4^{2-}$ to the DNA structure. In the spectroscopic investigations of the binding process, it is shown, that the Na^+ ions from added Na_2SO_4 can reduce the distortion of the DNA base stacking. Figure 4.8d shows λ-DNA after 16 h incubation with $PtCl_4^{2-}$ in the presence of 100 mM Na_2SO_4. As one can see, large distortions are still visible. Also the overall height increase of the DNA is found. However, the length of the molecule seems to be larger than in the case without Na_2SO_4. This is confirmed by length measurements of a larger number of DNA molecules, where the average length is found to be about three times larger than in the absence of Na_2SO_4 (Tab. 4.2). This means, the addition of Na^+ can stabilize the DNA structure although it cannot completely avoid distortions.

4.1.4 Conclusions about the binding of $PtCl_4^{2-}$ to DNA

Investigated was the binding of $PtCl_4^{2-}$ to λ-DNA in a large excess of Pt complexes to DNA base pairs. In particular a C/B ratio of 130 was applied in most of the experiments.

(1) It is found that the $PtCl_4^{2-}$ complexes induce tremendous structural distortions on the DNA. The melting temperature is lowered, the DNA base stacking is completely distorted, i.e. the helix structure breaks down, and lots of kinks are induced into the linear structure of the molecule.

(2) The distortions of the DNA structure do not cause denaturation of double-stranded DNA. The double-stranded configuration is maintained at least down to a length of 12 bp.

(3) The time scale of the helix breakdown is in the range of several hours. Thus, the complete binding process, leading to a coverage of the DNA with 3 complexes per base pair [90], proceeds at least this time.

(4) The binding depends strongly on hydrolysis. Therefore, a similar binding mechanism as in the case of cisplatinum is likely. It involves a hydrolysis step, before a bond to the DNA bases can be established. To ensure rapid and complete binding of $PtCl_4^{2-}$ to DNA, for the following metallization experiments a 10 mM stock solution, which was aged for 16 h, was used.

(5) The structural distortions can be decreased by addition of Na_2SO_4 during the binding process. This additive stabilizes only the DNA but does not react with the Pt complexes.

From the performed experiments the quantity of bound complexes remains unclear. Thus it is possible, that the binding of further complexes still proceeds after the breakdown of the base stacking. However, it can also be the case that the binding is complete before and that the breakdown process is driven by the establishment of additional bonds of Pt complexes to the DNA. For example monofunctional Pt adducts become bifunctional and increase therefore the distortion of the DNA structure. Measurements of the quantity of bound complexes are necessary to gain in future better insight into the interaction between $PtCl_4^{2-}$ and DNA.

4.2 Cluster formation without DNA

Metallization using $PtCl_4^{2-}$ requires chemical reduction of these complexes. In our group the reducing agent dimethylammine borane (DMAB) has been successfully applied to metallize microtubules [9, 10] as well as DNA [18]. It turned out to be well compatible with these biomolecules. It is known to be also an efficient reducing agent for the chloro complexes of platinum [100]. Therefore, DMAB was chosen as reducing agent in the following metallization experiments.

Before the metallization of DNA is investigated, experiments about the cluster formation without DNA are carried out. These experiments are done under the same conditions and concentrations like the following preparations in presence of DNA. The experiments in the absence of DNA serve as a reference. Only from the comparison with the studies performed in the presence of DNA one can determine the influence and the role of the DNA during the cluster formation process.

The result of Pt cluster formation from $PtCl_4^{2-}$ and DMAB without DNA is shown in Figure 4.9a. The sample contains only about 50 nm large polycrystalline agglomerates, similar to the results reported in Ref. 100. Two conclusions can be gained from this experiment. First, DMAB is able to reduce $PtCl_4^{2-}$ without additional heterogeneous nucleation centers. The cluster formation takes place via

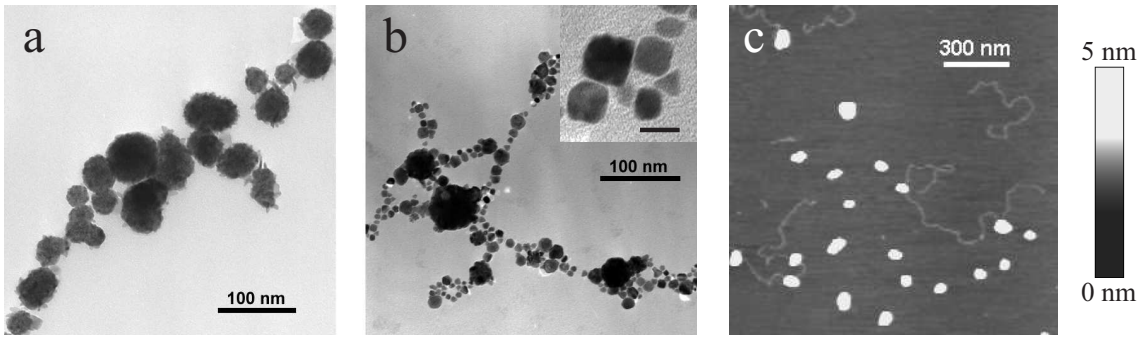

Figure 4.9: Pt particle formation by chemical reduction of $PtCl_4^{2-}$ in the absence of DNA. Electron micrographs of Pt particles formed from 1 mM $PtCl_4^{2-}$ and 1 mM DMAB: (a) In the absence of citrate, (b) in the presence of 0.5 mM citrate. The inset shows an enlarged area of the image. The scale bar is 10 nm. c) SFM image of Pt particles prepared without citrate. DNA was added 5 min after the chemical reduction was started.

spontaneous, so-called *homogeneous* nucleation in solution followed by the growth of small particles. Second, the presence of only 50 nm large polycrystalline agglomerates is caused by the agglomeration of smaller particles into bigger agglomerates in the absence of any capping agent. Small particles possess a very large surface energy due to a high ratio between surface and volume. This surface energy is reduced by agglomeration leading to a stabile state. Only by the use of capping agents it is possible to stabilize the small crystallites and prevent their aggregation.

It is widely known in the literature that citrate acts as a strong capping agent for Pt colloids [101]. Depending on the stoichiometric ratio between metal complexes and citrate, monodisperse, single-crystalline nanoparticles can be obtained. The synthesis of Pt clusters from $PtCl_4^{2-}$ and DMAB in the presence of citrate results also in the formation of small single-crystalline clusters (Fig. 4.9b). Here, a $PtCl_4^{2-}$ to citrate ratio of 2:1 was used. As the inset shows, these particles are often of tetragonal or polyhedral shape, which is typical for citrate stabilized Pt clusters. This experiment shows that, in order to obtain small, separated Pt crystallites, a capping agent is needed. The capping impact of citrate during the DMAB reduction is not complete, because the resulting colloid suspension does not contain monodisperse particles. The size of the small crystallites varies from 5 to 10 nm. Furthermore, some larger agglomerates as in the absence of citrate are found, which might be caused by the much faster reaction kinetics of less then 30 min for DMAB in comparison with the slower process using hydrogen as reducing agent [101]. As stated at the beginning, the experiments without DNA serve only as reference and no work is done to tune the conditions here to synthesize monodisperse citrate stabilized colloids. It is noteworthy that the morphology of the randomly formed cluster aggregates in the presence of citrate is already partly chain-like without DNA. The

length of the chains where one cluster follows another is, however, restricted to less than 100 nm.

To investigate the interaction between DNA and clusters formed in the absence of DNA by homogeneous nucleation, DNA was added to the cluster suspension after the cluster preparation. Here, it is not sufficient to use TEM for imaging as only clusters, consisting of metal, can be seen, but not the DNA formed of light organic molecules. However, one can apply SFM in order to visualize both, clusters and native DNA, as Figure 4.9c shows. The bright dots in the image are the aggregates of homogeneously nucleated particles, as their height of more than 20 nm shows. There is a certain, but rather low affinity between these aggregates and the DNA molecules found in the image. This shows, that the particles are already sufficiently stabilized due to aggregation and do not require an additional capping agent.

4.3 Cluster formation in the presence of DNA

In general, the Pt cluster nucleation in the presence of DNA can happen in two ways: (i) spontaneous in solution (homogeneous nucleation) or (ii) directly at the DNA template (heterogeneous nucleation). In principle both processes could be used for DNA metallization. This means, it should also be possible to achieve a metallization by adsorption of homogeneously nucleated Pt clusters to the DNA. However, from the previous section it is known that aggregation of these particles is very strong. Therefore, the obtained metal structures should be irregular and coarse. The better way, which should prevent the aggregate formation and should lead to a more homogeneous coverage of the DNA with metal, is the heterogeneous nucleation of clusters at the DNA, i.e. the direct growth of particles at the template.

The aim of the following metallization experiments is to initiate the cluster growth at the DNA. This will be done by *activating* the DNA with the $PtCl_4^{2-}$ complexes, i.e. by densely covering the DNA with bound complexes, which shall serve in the subsequent reduction step as nucleation centers. The hope is that the heterogeneous nucleation at the activated DNA is kinetically favored to the homogeneous process in solution, which should lead to the suppression of the latter one. Probably, it is impossible to hinder the nucleation in solution completely, as there will always be a balance between heterogeneous and homogeneous nucleation. But, by carefully adjusting the reaction parameters it should be possible to shift the balance in the desired direction.

In order to investigate the contributions of both reaction ways, it is necessary to compare both processes. Therefore, in the following the cluster formation in the presence of native, i.e. non-activated, DNA, which should be dominated by homogeneous cluster formation, will be compared with the cluster formation in the presence of activated DNA.

4.3.1 Cluster formation with native DNA

Cluster formation in the presence of native DNA is achieved by simultaneous mixing of $PtCl_4^{2-}$, DNA and reducing agent. The result is shown in the TEM micrograph in Figure 4.10a. One can see about 5 nm large platinum clusters forming partly chainlike aggregates but as well large aggregates with about 50 nm in diameter. To get further insight in the morphology of the cluster aggregates, SFM samples were prepared (Fig. 4.10b). For this, a reduced amount of DMAB was applied, in order to leave enough free DNA, which is not covered with clusters. It again shows that the formed particles consist of 5 nm clusters as well as large aggregates with diameters of about 50 nm. Additional to the TEM image, it can be seen, that the small clusters are located directly at the DNA and that the large aggregates are surrounded by lots of DNA strands. This leads to a few conclusions: (i) The large aggregates show that homogeneous nucleation takes place and is even a dominating process during the particle formation in the presence of native DNA. (ii) Aggregation leads to inhomogeneous metal distribution along the DNA strands. The clusters are located at the DNA strands, but chains of single clusters are rather short. (iii) The DNA acts as a good capping agent or protecting polymer for platinum clusters, as it is able to hinder the aggregation of small clusters to large particles. This particle stabilization by DNA was already found for CdS particles [102]. The origin of these small clusters on DNA, seen in the SFM, remains still unclear. They could be grown from first bound Pt complexes at the DNA or homogeneously nucleated and subsequently trapped by the DNA before they can aggregate.

The addition of DNA during cluster formation changes also the kinetics of the process. This is already visible by eye. Without DNA the solution starts to turn black already a few seconds after addition of the reducing agent. With DNA a remarkable turbidity can be seen only after several minutes. To determine the kinetics of the cluster formation quantitatively, the UV/VIS absorbance increase at 600 nm was measured. At this wavelength the extinction is not overlapped anymore by the electronic excitations of $PtCl_4^{2-}$ or DNA and only absorbance and light scattering at the growing Pt particles is observed. Figure 4.11 shows the development of the 600 nm absorbance (A_{600}) upon time for different amounts of added native DNA. The more DNA is added, the slower is the absorbance increase. Whereas in the absence of DNA the particle formation process is finished after about 3 min, maximum absorbance is reached for the highest DNA concentration only after 20 min. At about 100 μg/ml DNA the maximum delay is reached and no further retardation is obtained by increasing the DNA amount. The value for the maximum absorbance of about 2 is also interesting. If the platinum particle suspension would contain only spherical particles smaller than 20 nm, which do not aggregate, the absorbance can be calculated using the Mie theory. For a 1 mM solution of $PtCl_4^{2-}$, where all the complexes are reduced to colloidal platinum, a value of 0.35 is obtained for the ab-

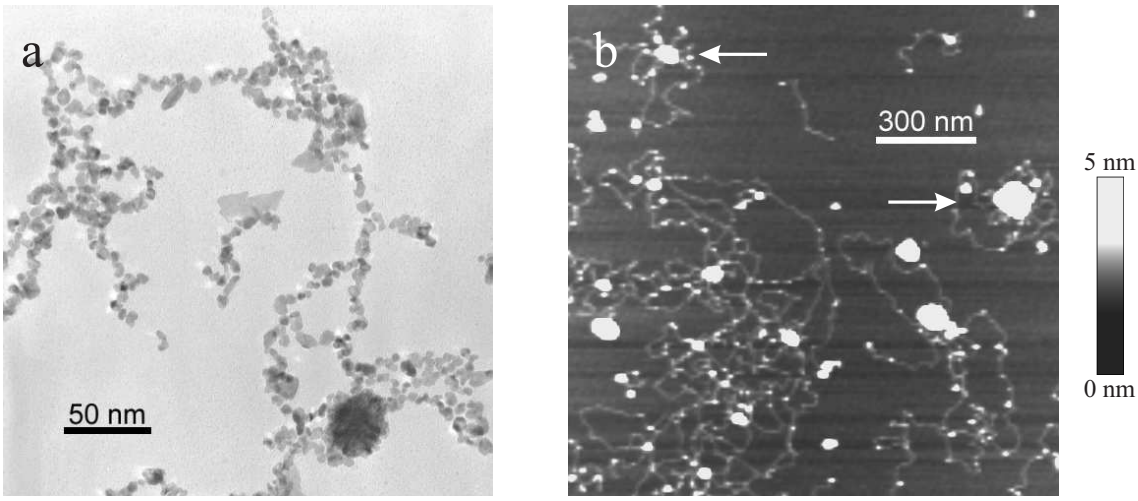

Figure 4.10: Pt cluster formation in the presence of native λ-DNA. The concentrations are 1 mM $PtCl_4^{2-}$ and 5 μg/ml λ-DNA. a) TEM micrograph of the reduction with 1 mM DMAB. b) SFM image obtained by reduction with 0.2 mM DMAB. The arrows indicate DNA coils around large cluster agglomerates.

sorbance, which is independent from the diameter of the particles (Appendix A.1.3). This means, that the obtained absorbance of 2 reflects mainly the aggregation of small clusters into big particles, which is consistent with other investigations [86]. The decreased maximum absorbance for the highest DNA concentrations indicates therefore a decreased number and size of large agglomerates.

Where does the strong retardation of the cluster formation due to the DNA come from? In the absence of DNA particles are free to agglomerate. After an agglomeration center is formed, it attracts faster and faster, more and more small clusters. As one can see in the SFM image (Fig. 4.10b), DNA can stabilize the small clusters and prevent their aggregation. Therefore, the formation of aggregation centers as

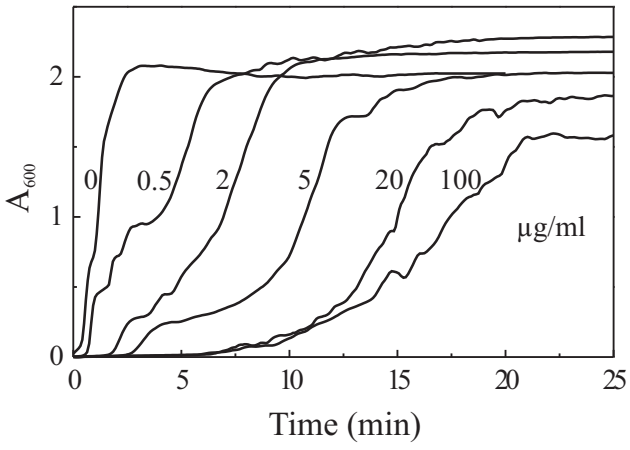

Figure 4.11: Kinetics of Pt cluster formation in the presence of non-activated DNA for varying amounts of DNA. DNA concentration is given in μg/ml. The concentrations for $PtCl_4^{2-}$ (1mM) and DMAB (1 mM) are kept constant.

well as the further aggregation is hindered and therefore retarded. Furthermore, DNA stabilizes also the large agglomerates, which can be seen from the DNA coils found around them. This should decrease the affinity of the large particles for small clusters and additional lead to a slower aggregation.

4.3.2 Cluster chain formation at activated DNA

Pt cluster formation in the presence of activated DNA is carried out by incubating λ-DNA 20 h in an aged solution of $PtCl_4^{2-}$ with a complex to base pair ratio of 130:1, in order to allow the dense coverage of the DNA with bound complexes. Subsequently, colloidal platinum is formed by starting the chemical reduction. The result, obtained for activated DNA, is strikingly different to the case of native DNA. Chains of platinum clusters, where one cluster follows the other, with cluster diameters between 3 and 5 nm are found (Fig. 4.12a). The cluster chains reach a length in the micrometer range (Fig. 4.12b). Furthermore no large aggregates or other background, but exclusively small clusters forming chains are obtained. High resolution transmission electron microscopy (HRTEM), which is able to resolve the lattice plains of the formed clusters (Fig. 4.12c), confirms the monocrystalline character of the clusters. The lattice plane distances can be easily extracted in the power spectrum of the HRTEM image. They are in good agreement with the values for bulk platinum along the [111], [200] and [202] directions, confirming the formation of metallic platinum. In Figure 4.12c one can furthermore see, that the clusters are partly grown together, connected via grain boundaries. Thus, a continuous wires with a length up to 100 nm and a maximum diameter of 5 nm are formed. These regions of continuous metal coverage are, however, separated by a few nanometers large gaps. Interesting is also the non-spherical, sometimes oval shape of the particles indicating that the growth proceeds along the DNA. In order to proof directly, that the clusters are located at the DNA, SFM imaging was performed on cluster chains synthesized with 1/5 of the normal amount of reducing agent (Fig. 4.12d). The cluster density is therefore lower. This way uncovered DNA and clusters can be seen in one image. It shows clearly, that the clusters or only found at the DNA and not anywhere else. Furthermore, the clusters cover the whole DNA equally and no longer parts without metal coverage is found, which is in contrast to the case of native DNA.

From the investigations of the morphology of the formed cluster chains one can conclude: (i) All the small crystallites with a lateral dimension smaller 5 nm, are located on DNA strands, because no additional capping agent beside DNA is present in solution. Otherwise large spherical aggregates should be observed. (ii) DNA is an excellent capping agent. A DNA concentration of 15 μM nucleotides is sufficient to obtain a stable suspension of 5 nm crystallites, whereas 500 μM citrate still leads to aggregation. (iii) The cluster chains can only be synthesized with activated DNA,

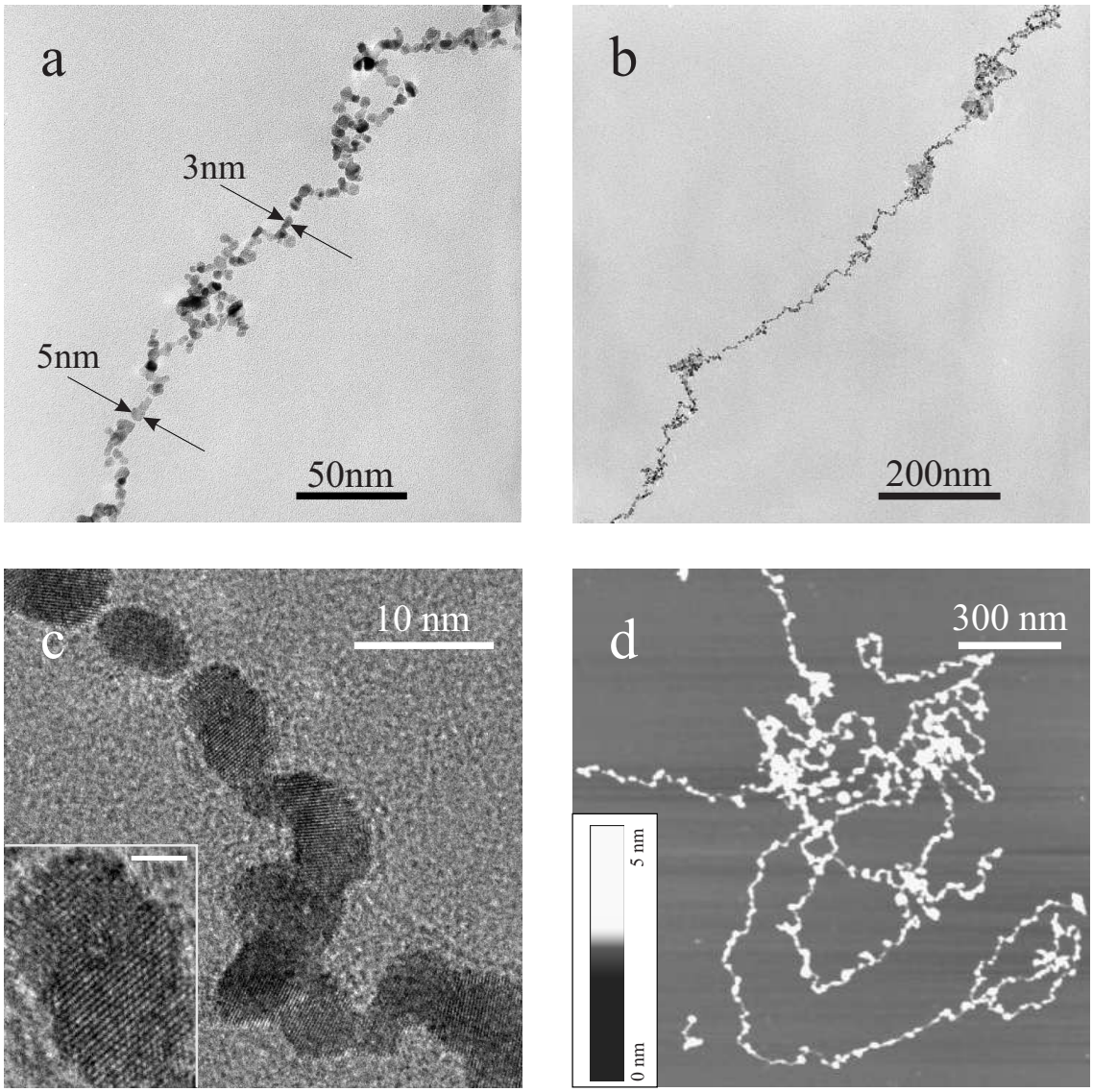

Figure 4.12: Pt cluster formation in the presence of activated DNA. a) TEM micrograph on a part of a cluster chain formed by 20 h activation of 5 μg/ml λ-DNA in 1 mM $PtCl_4^{2-}$ and subsequent reduction with 1 mM DMAB. b) Large scale view on the same chain. c) HRTEM image of the cluster chain. The scale bar in the inset is 2 nm. d) SFM image of clusters grown at activated DNA with a reduced amount of DMAB of 0.2 mM.

which is densely covered with complexes! This proves, that cluster nucleation takes place heterogeneously at the bound complexes. (iv) The absence of aggregates consisting of homogeneously nucleated, unstabilized cluster shows, that homogeneously nucleation is hindered and even completely suppressed. (v) Over all, the existence

of stabile, densely covered cluster chains along DNA is remarkable, as investigations of positively charged colloids, which bind electrostatically to DNA, revealed, that only a small fixed number of colloids can adsorb at the DNA [64]. There, further attempts to load the DNA with more colloids resulted in an instable phase and aggregation of the particles. This is another point, which shows that the cluster chains are not formed by an adsorption process, but by cluster nucleation at the template.

To investigate in more detail the role of the bound complexes for activated DNA, the kinetics of the platinum reduction was measured in presence of DNA, which was differently activated for different times (Fig. 4.13a,b). It can be clearly seen, that the longer the DNA is activated, the faster the cluster formation process. This can be quite easily understood by making use of the morphology studies of the cluster chains formed from activated DNA. They suggested a preferred heterogeneous nucleation at the DNA and a suppressed homogeneous nucleation. This means, with the complexes, bound to the DNA, nucleation sites are introduced into the solution, which promote the cluster growth and make it much faster. This is exactly seen in the development of the reduction kinetics upon DNA activation.

The time which is necessary to achieve complete activation is about 20 h. This is quite well in correspondence to the time scale in which binding of the complexes to the DNA occurs and supports once more the finding that the complexes bound to the DNA promote the heterogeneous nucleation at the biotemplate. The maximum absorbance after cluster formation is for activated DNA about the same as for non-activated DNA. For the latter one the height of the absorbance value was explained by the dominating influence of the large cluster aggregates. For activated DNA only small crystallites are found. On a first view one could think that the final absorbance should equal 0.35 - the value obtained by the Mie theory. However, Mie theory is valid only for spherical particles. The cluster chains consist of oval cluster, which are additional grown together, and therefore probably better described as rods. Gans extended the model of Mie to ellipsoids [103]. Application of of this theory to particles with an aspect ratio of 1:5 leads to a four times increased A_{600} in comparison with spherical clusters [104], which may explain the high absorbance value for the cluster chains. These chains are strictly spoken also agglomerates, however, agglomeration is here restricted to “one dimension”.

In Figure 4.13c the kinetic curves for the cluster formation without DNA, with native and with activated DNA are summarized. The fastest process is the pure agglomeration of small particles into large aggregates in the absence of DNA. Addition of native DNA leads to a retarded reaction, as the Pt crystallites are stabilized by the DNA, which hinders their aggregation. Introducing nucleation centers in the form of activated DNA into the platinum solution results again in an accelerated cluster formation, although it is due to the cluster stabilization by the DNA not as fast as the process without DNA.

In the framework of the investigations of the cluster chains formed from activated

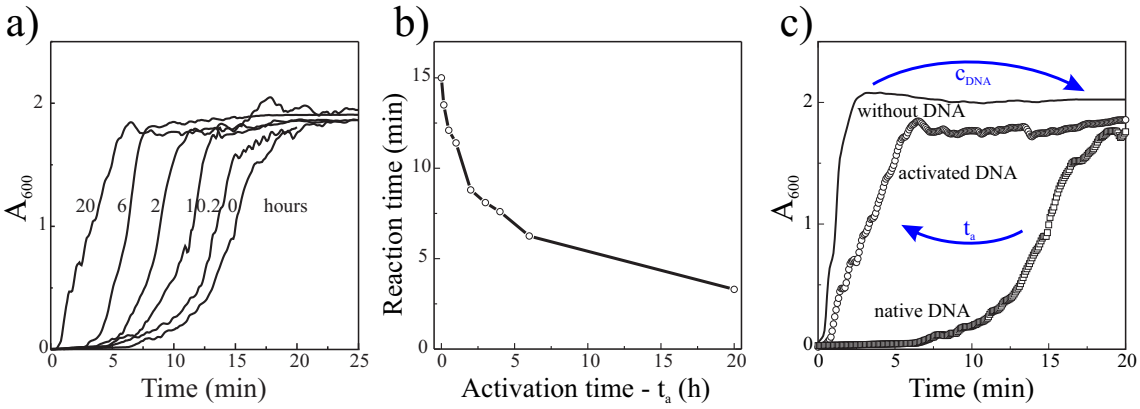

Figure 4.13: Kinetics of Pt cluster formation in the presence of DNA after different activation times t_a. a) Time evolution of the absorbance at 600 nm of a 1 mM $PtCl_4^{2-}$ solution during reduction with 1 mM DMAB in the presence of 20 μg/ml DNA, which was activated for different times t_a. b) Reaction time as a function of the activation time, extracted from the absorbance curves in (a). The reaction time was defined as the time, when half of the maximum absorbance is reached. c) Comparison of the reaction kinetics for the cluster formation without DNA, with non-activated DNA and with 20 h activated DNA.

DNA, a method was developed, which allows TEM and SFM of one and the same object. It therefore combines the advantages of both techniques. With TEM only the metal clusters can be seen and it provides the highest resolution. With SFM metal particles and biomolecule can be imaged simultaneously. The method was made possible by using Maxtaform finder grids, which copper support possesses a view small wholes. At these spots the carbon film was enough stabilized by the copper mesh that vibrations during tapping mode imaging with the SFM did not occur. Figure 4.14 shows a SFM and a TEM image of one and the same cluster chain. With the SFM one can proof that no free DNA is located around the chain. However, it is impossible to proof, if the DNA is covered with metal and if the cluster coverage is dense or even continuous, although SFM is frequently applied in literature for exactly that purpose [21, 22]. However, single clusters of a chain can excellently be resolved with TEM, showing also that the clusters cover the DNA densely. The limited resolution of the SFM comes mainly from the rather large tip radius compared to the tiny cluster structures. Single particles of the cluster chains are broadened to such an extent that they are not resolvable. From the images one can estimate the tip radius with a simple model where the cluster chain is assumed to be a rod of diameter r and the tip is approximated by a semisphere of diameter R. The height of the SFM tip h follows along horizontal deviations x from the center of the cluster chain at x_o the equation:

$$h = \sqrt{(R+r)^2 - (x-x_0)^2} + r - R, \qquad h \geq 0. \tag{4.1}$$

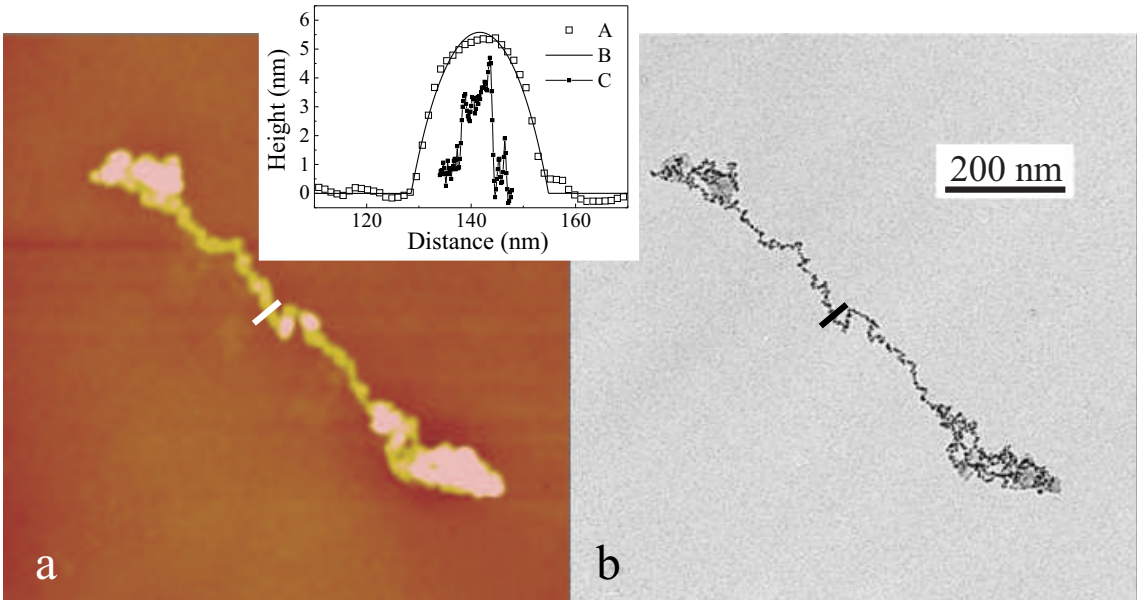

Figure 4.14: SFM and TEM images of a single platinum cluster chain grown along a DNA molecule a) SFM image. As substrate, a carbon-coated TEM grid was used. The height scale is 20 nm. b) TEM image of the same chain. Inset: (A) section cut in the SFM image along the small white line; (B) fitting function for the cut in A; (C) intensity profile in the TEM image along the small black line.

A fit was performed along the section cut that is indicated by the small white line in Figure 4.14. The profile of the cut is plotted in the inset of Figure 4.14. The height of the cluster chain at the section cut is 5.6 nm. This value is taken for the object diameter r. The fit of the section cut with the model curve, which is now only dependent from the tip radius R, gives the best result for $R = 17.3\,\text{nm}$, which is comparable to values found in the literature [105]. For better visualization of the object broadening due to the tip, the inset of Figure 4.14 contains also the intensity profile of a cluster located at the same place in the TEM image. Here, a width of about 6 nm is obtained, which is in good agreement to the height measured in the SFM image. Note, the intensity profile shows only gray scale values, which do not represent the cluster height.

4.3.3 DNA sequence specificity of the cluster nucleation

In the previous section it could be shown that the selective growth of platinum cluster at the DNA by chemical reduction of $PtCl_4^{2-}$ is only possible in the presence of activated DNA. From the investigations, carried out to study the synthesis process, it could be concluded, that the nucleation of the platinum clusters must

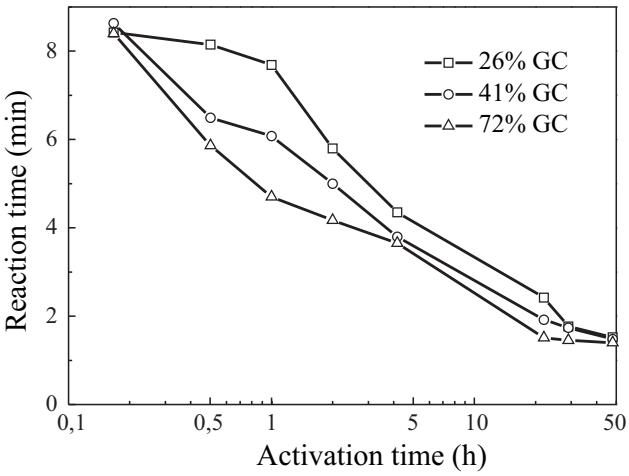

Figure 4.15: Influence of the GC content of the DNA on the cluster formation kinetics. Reaction time as a function of the activation time for three types of DNA possessing a different percentage of guanine-cytosine (GC) base pairs. The used DNA was extracted from *Clostridium perfringens* (containing 26.5% of GC base pairs), salmon testes (41.2% GC) and *Micrococcus luteus* (72% GC).

take place heterogeneously at the DNA. The only possible heterogeneous nucleation centers were found to be the $PtCl_4^{2-}$ complexes, bound densely along the activated DNA. With increasing activation time more and more of these nucleation sites are introduced to the DNA and the cluster formation becomes accelerated.

From binding studies of $PtCl_4^{2-}$ to DNA it is known that the kinetics of the binding process depends on the sequence of the DNA [90, 96, 97]. At short binding times it is found that, the higher the percentage of guanine-cytosine base pairs (GC contents) of the DNA the more complexes can be found at the DNA. For long binding times the amount of complexes does not anymore depend on the GC contents of the DNA.

This binding behavior can now be used to design an experiment, which demonstrates the sequence specificity of the nucleation of platinum clusters at DNA. If the platinum complexes, which are bound to the DNA bases, really promote the heterogeneous nucleation at the DNA, than at low activation times the cluster formation process should be accelerated with increasing GC contents, where more complexes and thus nucleation sites are present. Three types of DNA with different GC contents, obtained from *Clostridium perfringens* (26.5% GC), salmon testes (41.2% GC) and *Micrococcus luteus* (72% GC), are used in this experiment. In order to proof the previously made assumption, these different types of DNA are used in a series of $PtCl_4^{2-}$ reduction experiments, where the time of the DNA activation is varied and all the other parameters like concentrations and temperature are kept constant. The result of this investigation is shown in Figure 4.15. One can see that it exactly corresponds to the previously made conclusions. Without activation ($t_a = 0$) the reaction time is for all GC contents equal. After short and intermediate activation times of the DNA, where the coverage of the DNA scales with the GC contents, the cluster formation is fastest for the GC-rich and slowest for the GC-poor DNA. After 48 h activation, when all possible binding sites at the DNA bases are occupied, the reaction time is again equal for all three types of DNA. This leads to two important

conclusions: (i) The GC dependency of the cluster formation kinetics can, following the above made argumentation, only be explained by the fact that the platinum complexes, which are bound to the DNA bases (Pt-nucleotide complexes), serve as heterogenous nucleation sites in the cluster formation process. (ii) The strong sequence dependency of the DNA metallization at intermediate activation times opens a possibility for a sequence dependent metallization. This could be done by using an artificial DNA template, which consists alternately of regions composed only by GC and regions composed only by AT base pairs.

4.3.4 Discussion of the nucleation mechanism at DNA

From the experimental investigations it comes out very clearly that the complexes, which are bound to the DNA bases, act as heterogeneous nucleation sites during the cluster formation by chemical reduction of $PtCl_4^{2-}$. How can this experimentally obtained fact be explained?

The electronic properties of the complexes bound to the DNA must be different to the complexes in solution. These differences must be induced by the DNA bases, otherwise for example the observed dependency of the cluster formation on the GC contents could not be explained. This means, the driving force for the DNA promoted cluster nucleation has to be searched on the single molecule level. A powerful tool for such single molecule investigations provides *First-Principles Molecular Dynamics* (FPMD). Parallel to the experiments of the present work, Lucio Colombi Ciacchi from our group in Dresden performed simulations based on the Car-Parrinello method of FPMD, where he investigated the formation of platinum dimers from two $PtCl_4^{2-}$ complexes after reduction as the initial stage of cluster formation. The results obtained from these studies can explain the DNA promoted nucleation of Pt clusters and will be described in the following [87,88,106,107]. First a description of the homogeneous nucleation and afterwards of the heterogenous nucleation at DNA bases is given.

The classical model for the nucleation of metal clusters assumes the reduction of metal ions (Me^{n+}) to their metallic state Me^0, which can, driven by thermal fluctuations, subsequently form a nucleus. The nucleus is only stable, if it exceeds a critical size, i.e. a critical number of metal atoms. Only then it is energetically favorable for the nucleus to grow and to attract more reduced metal atoms. Several experiments, however, are contradictory to this classical model [101, 108]. Furthermore, FPMD investigations suggest a different mechanism [87]. These simulations showed that a stabile platinum dimer is already formed by two $PtCl_4^{2-}$ complexes after reduction with only one electron. This means the two platinum complexes still have an "averaged" oxidization state of 1.5. This Pt dimer is able to grow, i.e. to bind another unreduced complex, thus forming a stabile trimer [106]. Further simulations showed that an unreduced $PtCl_4^{2-}$ complex can bind to a small cluster consisting of 12 Pt(0)

atoms. This binding is even possible, if the Pt atoms of the cluster are not fully reduced [88]. The critical step in the simulated cluster formation process was found to be the initial formation of the Pt dimer [87, 88]. As a consequence the cluster formation mechanism is changed tremendously. The metal ions in solution must not be reduced to oxidization state zero, in order to bind to other metal atoms. Furthermore, already two atoms, which is the smallest possible number, are considered to be the nucleus as they form a stabile dimer, which is able to grow and to attract easier complexes than single platinum complexes in solution. This differed cluster formation mechanism is in better agreement with experimental findings, e.g. the observed autocatalytic growth of platinum clusters, in which the presence of already formed clusters catalyzes the reduction of further complexes [86, 109].

To investigate the heterogeneous nucleation of Pt clusters at the DNA, the FPMD simulations were extended to $PtCl_4^{2-}$ complexes bound to DNA bases. A system consisting of a free complex in solution and a complex bound to one or two bases was first reduced by adding one electron. Subsequently the Pt dimer formation between the two complexes was investigated [20, 107]. As discussed earlier, $PtCl_4^{2-}$ can bind to different bases, where it forms at least monofunctional adducts, but due to the similarities to cisplatinum also bifunctional adducts should exist. At the fully activated DNA, the complexes are therefore bound by several different binding modes. In the simulations the following configurations have been considered: a onefold and a twofold hydrolyzed complex bound to one guanine or to one adenine $[G{\cdot}PtCl_2(H_2O)]$, $[G{\cdot}PtCl(H_2O)_2]^+$ and $[A{\cdot}PtCl_2(H_2O)]$, $[A{\cdot}PtCl(H_2O)_2]^+$ as well as a twofold hydrolyzed complex bound to two stacked guanines $[GG{\cdot}PtCl(H_2O)_2]^{2+}$ (GGP).

Calculations of the HOMO-LUMO energy gap values of the mentioned adducts showed, that the reduction of a platinum complex bound to the DNA is favored over the reduction of a free twofold hydrolyzed complex. The same result was obtained from optimizations of the electronic structure of a system containing the free platinum complex and the bifunctional platinum adduct (GGP), where an added reducing electron was found to be completely localized at the adduct [107].

Because of the higher reducibility of the Pt complexes, which are bound to the DNA, the Pt dimer formation was studied between a free twofold hydrolyzed complex and a reduced Pt·DNA adduct. The reaction for the complex bound to two guanines is depicted in Figure 4.16. It occurs in two steps. First a bond with a Pt-Pt distance of 2.9 Å is formed. Subsequently, a water ligand is released and the Pt-Pt bond is strengthened, which leads to a final bond distance of 2.5 Å. The formation of a Pt dimer proceeds in exactly the same way also for the reduced monofunctional Pt·DNA adducts. Beside the reaction path, where first the Pt·DNA adduct is reduced, the reaction between a reduced free platinum complex and the Pt·DNA adduct was investigated, which is justified by the high excess of free to bound complexes (43:1), which makes the reduction of a free complex probable.

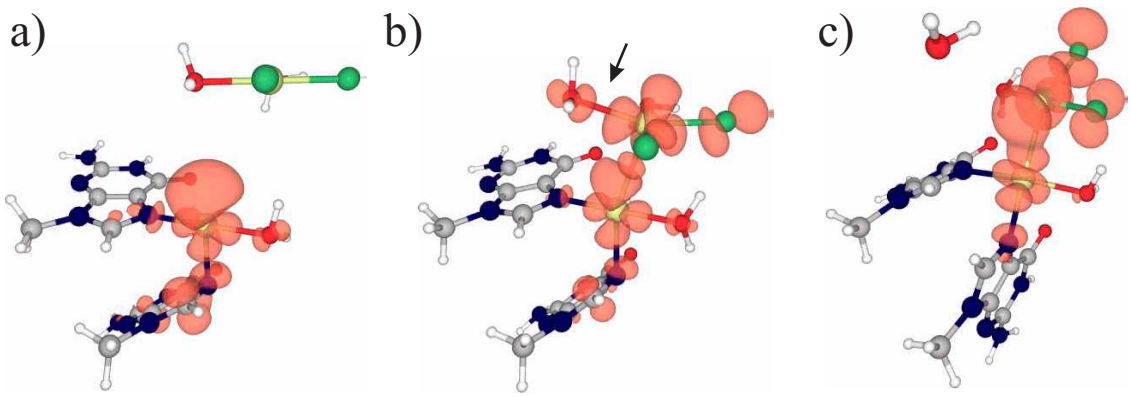

Figure 4.16: Snapshots from a FPMD simulation of the formation of a Pt dimer by the reaction of an unreduced Pt complex with a reduced Pt complex bound to two guanines [107]. Pt: yellow, Cl: green, O: red, N: blue, C: grey, H: white. The orange isodensity surface at 0.002 au represents the particle density of the unpaired reducing electron. a) Initial configuration. b) Formation of an Pt-Pt bond after 200 fs simulation time. c) Final configuration after the release of one water ligand at 2.2 ps.

Similarly to the first reaction path, one water ligand is split up and a final Pt-Pt bond distance of about 2.5 Å is obtained. By contrast, the water release step and the accompanying bond strengthening does not occur for the homogeneous reaction of two free complexes in solution. As a consequence the heterogeneous reaction channel is energetically favored to the homogeneous process. Furthermore, the electron affinity of the Pt dimer, which is bound to DNA bases is higher after the water release step as discussed in Ref. 20. Thus, the heterogeneously nucleated cluster formation is, in comparison to the homogeneous process, energetically favored at three steps during the initial dimer formation: (i) The higher electron affinity of the Pt·DNA adducts. (ii) The stronger bond of the Pt dimer bound to DNA bases. (iii) The further increased electron affinity of the Pt dimer bound to DNA bases. These effects could therefore also lead to a kinetically favored process at the DNA, as the autocatalytic growth process of the cluster is only limited by the initial dimer formation. This argumentation is strongly supported by the experimental findings in Section 4.3.2, where a pure heterogeneous nucleation was found to take place only in the presence of activated DNA.

The energetically favored nucleation, which is induced by the DNA bases, is caused by electron donation from the purines, adenine and guanine, possessing a heterocyclic structure. A possible reason for the increased electron affinity of Pt·DNA adducts is the presence of delocalized π orbital states within the cyclic structure of the DNA bases, which can better accommodate additional electrons [107]. Slight differences between guanine and adenine in the Pt-Pt bond distance point to a slightly increased electron donation from guanine. On the other hand, the bond

energy of a Pt dimer is larger if it is bound to adenine than to guanine. Therefore, no large differences in the ability to promote the heterogeneous nucleation are expected from this data. This is again in accordance to the experimental observations, were a sequence specific cluster nucleation was found to be only caused by the different binding kinetics of $PtCl_4^{2-}$ to guanine and adenine. After long activation times, where independently of the GC contents an equal loading of the DNA with Pt complexes is expected [90], the cluster formation occurs for all types of DNA on the same time scale. Another effect, which is also seen in the experiments is the hydrolysis dependence of the Pt dimerization reaction. The Pt-Pt bond energies are distinctly larger for the dimers obtained from the twofold hydrolyzed Pt·DNA adducts in comparison to the dimers obtained from the onefold hydrolyzed species. This can explain that the reaction time is still decreased for activation times larger than 30 h (Fig. 4.15, p. 91), where the binding process of complexes has already be finished. However, hydrolysis proceeds over longer times, as beside the twofold hydrolyzed cis-complex also the trans as well as a threefold hydrolyzed species are formed after long aging times [99].

In conclusion, it is very remarkable that several mentioned experimentally findings are in accordance with the proposed molecular mechanism for the heterogeneous platinum cluster nucleation at DNA. This strongly supports, that the nucleation takes place via the formation of a Pt(I,II) dimer from a free complex in solution and a complex bound to DNA bases by partially reduction with one electron, where this reaction channel is strongly favored to the homogeneous nucleation in solution.

4.3.5 Influence of control parameters

The heterogenous nucleation of Pt clusters at DNA is governed by the DNA activation. Under certain conditions it is thus possible to synthesize Pt cluster chains. In the following these conditions are investigated in detail. The aim is to understand which parameters affect a successful cluster chain preparation, i.e. allow a selective heterogeneous nucleation at the DNA. Furthermore, conditions are tested, which influence the morphology of the DNA cluster chains and can reduce the shrinkage of the DNA, which was already observed during DNA activation.

Parameters controlling the balance between homogeneous and heterogeneous nucleation

The cluster formation in the presence of native, i.e. non-activated, DNA is dominated by homogeneous cluster nucleation in solution and subsequent aggregation of the small grown crystallites. By contrast, the cluster formation in the presence 20 h activated DNA is dominated by heterogeneous cluster nucleation and subsequent cluster growth at the DNA. The parameter, which splits the two cases is

the activation time t_a. This means with the increasing activation of the DNA the balance between the two cluster formation routes is shifted from almost exclusive homogeneous nucleation towards exclusive heterogeneous nucleation, which is nicely illustrated with the measurements of the cluster formation kinetics dependent on the activation time (Fig. 4.13, p. 89). This means, the first parameter, which affects the heterogeneous nucleation, is the activation time t_a.

The time window, which separates the two cluster formation routes during the synthesis, is about 10 min, as the reaction time for activated DNA is typically 2 min and for non-activated DNA about 12 min. As for activated DNA the heterogeneous process is dominant, the cluster chain formation has finished, before the homogeneous process can start, which is thus completely suppressed. However, if the mentioned time window becomes small enough, the separation between homogeneous and heterogeneous nucleation can vanish. This can be achieved by using a very reactive complex, which is much faster reduced by DMAB. Then the heterogeneous nucleation sites are not as dominating as in the case of $PtCl_4^{2-}$. Complexes, which are very reactive upon reduction with DMAB, are palladium complexes like palladium acetate and $K_2PdCl_4^{2-}$. Due to the structural similarities with $PtCl_4^{2-}$, the chloro complexes of palladium are also supposed to bind to DNA. The characteristic time scale for the reaction of 1 mM $PdCl_4^{2-}$ with DMAB lies below one second, which is much below the time resolution of the UV/VIS measurements. TEM investigations of palladium particles, synthesized by reduction of $PdCl_4^{2-}$ in the absence and in the presence of activated DNA reveal only large aggregates, which possess a dendrite-like structure (not shown). This points to the fact that fast aggregation of homogeneously nucleated particles is the main process, which was also shown in Monte-Carlo simulations [110], and that an eventually occurring heterogeneous process is not anymore dominating. This means, that for the fast reduction process of $PdCl_4^{2-}$ the time window, separating the two nucleation routes, has vanished. However, decreasing the reactivity of the reaction, which means slowing down the cluster formation process, could separate both nucleation routes, as it is the case for $PtCl_4^{2-}$. A slower reaction can be easily achieved by addition of activated DNA and citrate, as a further stabilizer, where the cluster formation takes place within 30 s until maximum 600 nm absorbance is reached. Figure 4.17a shows the morphology of the obtained palladium particles. Clearly, chain-like aggregates, which are not present in the absence of DNA, as well as single palladium clusters can be seen. Doing the same experiment with $PtCl_4^{2-}$ instead of $PdCl_4^{2-}$ reveals only perfectly grown cluster chains with well separated clusters and no free particles around (Fig. 4.17b). The time scale of this reaction is 8 min. Comparison of morphology and kinetics of the reaction with $PdCl_4^{2-}$ and with $PtCl_4^{2-}$ suggests, that, as expected, for $PtCl_4^{2-}$ only heterogeneous nucleation takes place; for $PdCl_4^{2-}$ in the presence of citrate and DNA however, heterogeneous nucleation leading to cluster chains as well as homogeneous nucleation leading to single clusters occurs. This means, that in the latter case

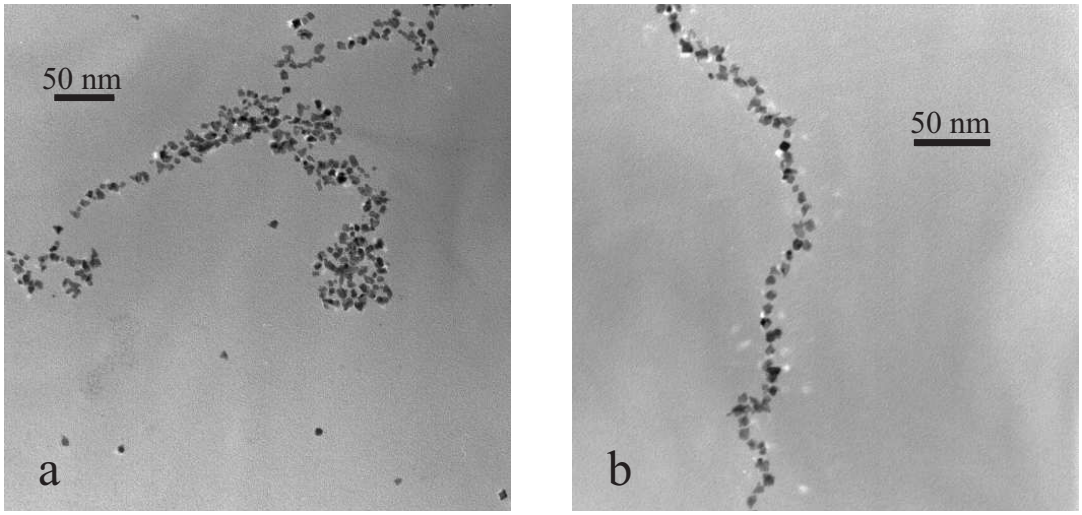

Figure 4.17: Electron micrographs of Pt and Pd particles formed in the presence of 5 μg/ml λ-DNA, 0.5 mM citrate and 1 mM DMAB. a) Pd clusters from 1 mM $PdCl_4^{2-}$ and 16 h activated DNA. b) Pt cluster chain from 1 mM $PtCl_4^{2-}$ and 16 h activated DNA.

the balance could be shifted from purely homogeneous nucleation in the absence of additives towards partly homogeneous and heterogeneous nucleation by varying the reactivity and thus the kinetics of the reduction process, which is another parameter influencing the balance between the two nucleation routes.

Another possibility to change the cluster nucleation is the variation of reagent concentrations. For this, clusters were synthesized for 1/4, 1/2, 1, 2, 4 times of the standard concentrations (1 mM $PtCl_4^{2-}$, 5 μg/ml 20 h activated λ-DNA and 1 mM DMAB. Cluster chains were found of course for the standard concentrations (Fig. 4.18a), which was used as a control. Furthermore, for the double (Fig. 4.18b) and the half (not shown) standard concentrations, cluster chains were obtained. For 1/4 and 4 times of the standard concentrations, however, only aggregates (not shown) were found. This indicates the existence of a relatively small reaction window, where optimal conditions for heterogeneous nucleation and stabilization of the clusters are existent. The concentration dependence of the cluster chain synthesis is a result of a changing homogeneous nucleation. At increased overall concentrations the probability to form spontaneously a homogeneous nucleation center is increased, too. Therefore, the whole process including homogeneous nucleation speeds up and at a certain point the kinetic separation of the two nucleation routes vanishes, like in the case of $PdCl_4^{2-}$. On the other hand, for the cluster synthesis at dilute concentrations, the distance of heterogeneous nucleation sites is increased. Thus, if the diffusion of complexes next to the heterogeneous nucleation center is slower than the homogeneous nucleation, the homogeneous nucleation channel is opened

again. Therefore, only at intermediate concentration the heterogenous nucleation is dominating.

Parameters controlling the morphology

During DNA activation the DNA structure is quite strongly altered. As already previously explained the structural distortions of the DNA are generally not desired. Therefore, investigations are carried out to understand, which parameters influence the cluster chain morphology, and to find ways, to obtain longer chains, where the DNA shrinkage during the activation is reduced.

During the activation the DNA helix structure can be stabilized by addition of Na_2SO_4, which reestablishes base stacking and increases the stiffness of the activated DNA. Therefore, a parameter which should strongly influencing the morphology of the finally formed cluster aggregates should be the rigidity of the DNA. The persistence length, which is the measure for DNA flexibility, is about 100 nm for double stranded DNA in 1 mM low ionic strength solutions used in the present experiments [46]. For single stranded DNA, however, it is only 10 nm. Although the distortion of the base stacking should decrease the stiffness and therefore the persistence length of the DNA, activated double-stranded should still be much more rigid than its single-stranded equivalent. The result of clusters preparation in the presence of activated, thermally denatured, single stranded DNA is shown in Figure 4.18c. In contrast to double-stranded λ-DNA (Fig. 4.18a), only short cluster chain parts forming large aggregates can be seen. Probably, due to the reduced stiffness, the DNA is not anymore able to separate the clusters efficiently, which can now much easier aggregate to stabilize themselves. In order to understand the higher degree of aggregation for single stranded DNA, clusters in the presence of a mixture of the single nucleotides forming the DNA (dGTP, dATP, dCTP, TTP) were prepared. The chemical composition is except the fact that nucleotide triphosphates are used identical to the solutions containing DNA. The only difference is the absence of the DNA backbone connecting the single nucleotides. Figure 4.18d shows the particles formed in this case. No cluster chains are synthesized, but only large ensembles of well separated small clusters and furthermore up to 50 nm large aggregates can be found. Note, that also the shape of the single small clusters has changed. Many of them are polyhedral. The conclusions from this experiment are: (i) Nucleotides are a very efficient capping agent. A concentration of 15 μM leads to 5 nm large crystallites with a much smaller size distribution as formed in the presence of 500 μM sodium citrate. (ii) The presence of large aggregates, however, suggests that cluster stabilization is more efficient in the presence double-stranded DNA, where these large particles are completely missing. This means, the aggregation of the particles is controlled by the stiffness of the template . For double-stranded DNA only cluster chains are obtained, which can be considered as aggregation in one dimension. For

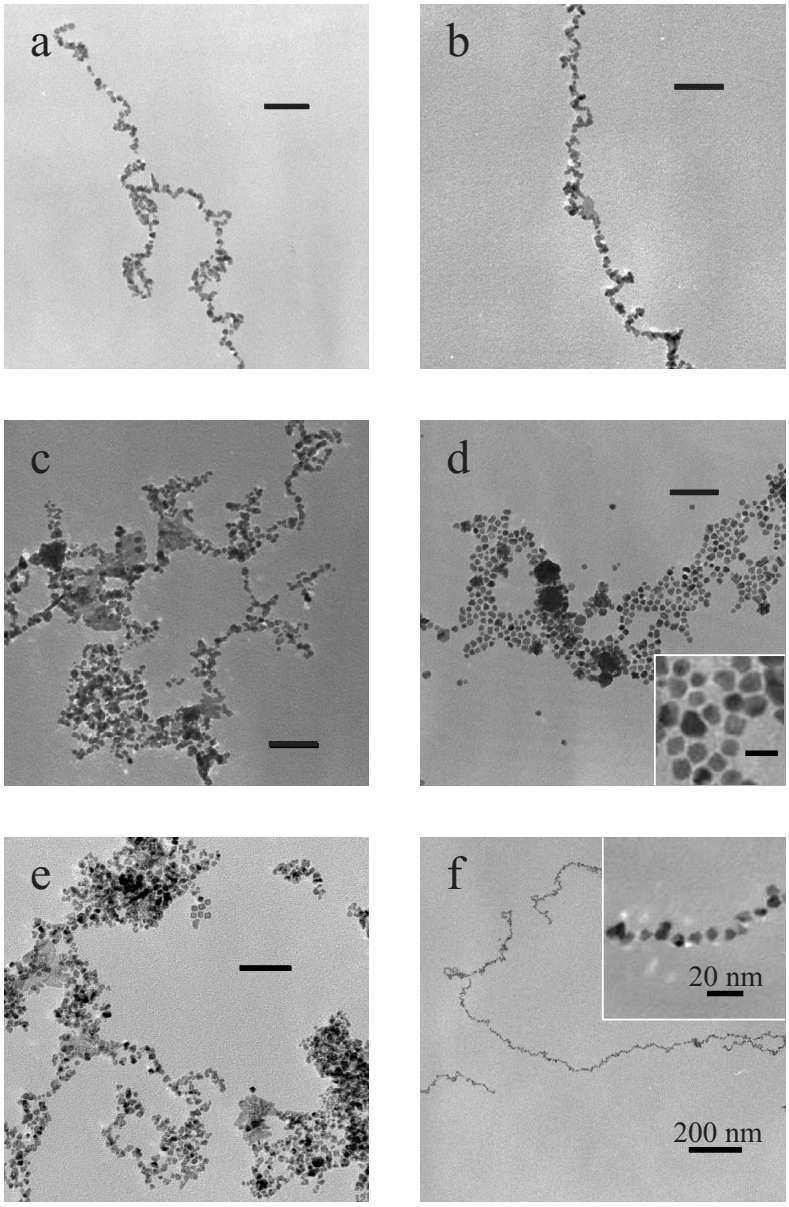

Figure 4.18: Standard Pt cluster formation in the presence of activated DNA versus preparations under changed conditions. a) Standard cluster chain preparation done by reduction of 1 mM $PtCl_4^{2-}$ in presence of 20 h activated 5 μg/ml λ-DNA using 1 mM DMAB. b-f) Preparations under changed conditions: b) Twice of the standard concentrations. c) With single-stranded λ-DNA instead of double-stranded. d) With dNTPs instead of λ-DNA. The nucleotide mix has the same molarity and composition of bases like λ-DNA. The scale bar in the inset is 10 nm. e) With additional 10 mM Na_2SO_4. f) With additional 0.5 mM sodium citrate. If not otherwise stated, the scale bar is 50 nm in all images.

the less rigid single stranded DNA the extend of agglomeration in the other directions is increased, because the more flexible structure is not longer able to separate the single clusters efficiently. Consequently, round aggregates are found for the free moveable single nucleotides as there is no larger superstructure which can prevent their formation. Furthermore, no cluster chains, but large loose aggregates of well separated small cluster are found due to the missing superstructure.

From the previous experiments two possibilities can be thought of, how longer cluster chains, which are less shrinked, could be obtained. One way is to increase the rigidity of the activated DNA. The other way is to stabilize the clusters additionally during their preparation, which should suppress aggregation along the cluster chain and lead to longer chains with well separated particles. Both strategies are tested in the following.

To increase the rigidity of the DNA template, Na_2SO_4 is applied during DNA activation, as it stabilizes the DNA helix structure. The TEM micrograph in Figure 4.18e shows the cluster aggregates obtained for 10 mM Na^+. It is visible that agglomeration of the single clusters takes place upon Na^+ addition, which hinders the formation of cluster chains. The addition of 100 mM Na^+ even increases the degree of aggregate formation (not shown). Whereas the sols with 0 mM and 10 mM Na^+ are stable, the 100 mM Na^+ suspension precipitates, which can be seen in a 600 nm absorbance decrease starting after 3 min. After 1 h a clear solution with a black precipitate on the vessel bottom is obtained. This agglomeration is caused by the fact, that the higher ionic strength decreases the length of electrostatic interactions between the particles in solution, which can thus better agglomerate. This effect is commonly applied to clean and concentrate colloid suspensions by addition of NaCl [70]. Thus, the expected effects by additional stabilization of the DNA with Na_2SO_4 are cancelled due to the increased agglomeration caused by the salt. Therefore, this strategy is not suitable to prepare longer cluster chains.

The other way, the additional stabilization of the clusters during their preparation can be easily obtained by adding citrate together with the reducing agent to the activated DNA solution. Figure 4.18f shows the morphology of the formed cluster aggregates. Only cluster chains are found. The 3-5 nm large clusters are all well-separated as depicted in the inset, which is different in comparison to the preparation without citrate, where continuous regions are observed (Fig. 4.12c, p. 87). The found chains are longer than in the absence of citrate and also the curling of the chains is reduced. Looking at the morphology of the single clusters, one finds that they are often of tetragonal or polyhedral shape, which is a direct influence of the citrate. This means, using citrate it is possible to stabilize the single clusters of a chain and thus the whole cluster chain additionally during its preparation. Furthermore, it is possible to tune the properties of the cluster chains - from chains with continuous metal coverage in the absence of citrate to chains with well-separated single nanoparticles, which are aligned in a row, in the presence of citrate.

4.4 Formation of continuous wires

Up to here the synthesis of Pt cluster chains along single DNA molecules has been shown. The clusters can be grown together, thus forming continuous parts up to 100 nm in length. However, there are still many gaps with a length of smaller than 5 nm present in the metal coverage of a single cluster chain. But, in order to apply metallized DNA for the wiring in electronic circuits, a continuous metal film is required, i.e. a method is searched, which is able to fill these gaps with additional metal.

Platinum clusters have already previously been used as nucleation sites to cover other biomolecules, e.g. microtubules, with a continuous nickel film [9,10]. This was done by electroless metallization, where a metastabile metallization bath is applied, which requires for the reduction of nickel ions catalytic active centers, which are then covered with metal. Because of the suitability of the technique for biomolecules it was applied also for the synthesis of continuous wires at DNA. By a carefully performed metallization, where only the gaps of the cluster chain are filled, it should be possible to obtain wires with a diameter of 10 nm.

The synthesis of continuous wires by further metallization of Pt-DNA cluster chains was done in close and fruitful collaboration with Kinneret Keren, Michael Krüger, Erez Braun and Uri Sivan during a research stay at the Technion in Haifa, Israel. In order to obtain stretched and straight metallized DNA molecules the synthesis of small Pt cluster at the DNA was altered. λ-DNA is incubated overnight with 10 mM $PtCl_4^{2-}$. Then the excess complexes in solution are removed by dialysis against water. Subsequently, DMAB is added, to reduce the bound complexes, DMAB is removed by dialysis and the DNA is again incubated with the $PtCl_4^{2-}$ solution to bind more complexes. After another clean-up of the DNA with dialysis the DNA is stretched in 10 mM AMPSO buffer on amine modified silicon according to the molecular combing technique [51]. The stretching of this DNA is still possible after all the platination steps, although the maximum stretching length was about only the half of the contour length of λ-DNA. After the stretching procedure the complexes, which are bound during the second cycle, are reduced by incubating the sample in a DMAB solution. Subsequently, gold is deposited at the Pt nucleation centers by electroless metallization using a gold enhancement solution [17]. With this method it is possible to obtain straight continuous gold wires with a diameter between 50 and 100 nm (Fig. 4.19a). Reduced reaction times for the gold enhancement times does not result in thinner wires but the structures are discontinuous. Using electron beam lithography, the gold wires can be electrically contacted with gold contact pads (Fig. 4.19a). At the end of the stay in Haifa first electrical measurements were started, showing that the gold wires exhibit conductivity. However, after a certain measurement time the wires were burned out over a certain length, which did not allow the exact determination of

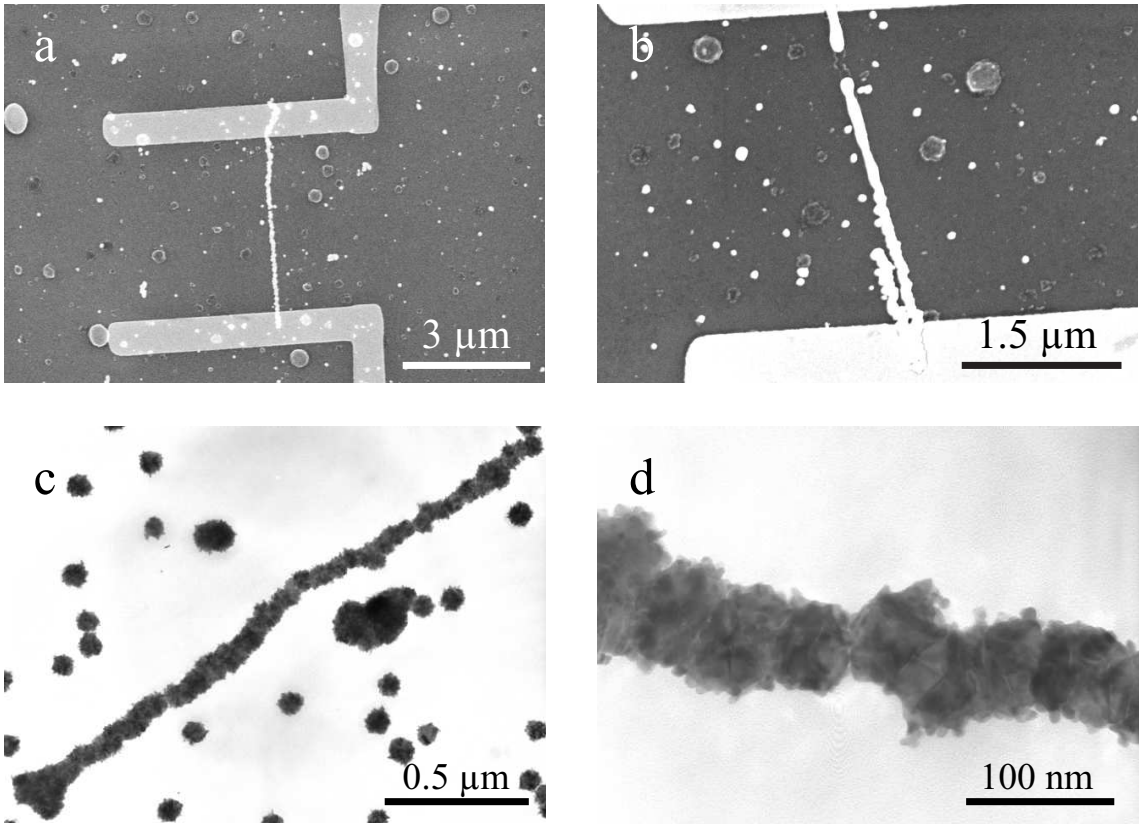

Figure 4.19: Formation of continuous wires by gold enhancement of Pt-DNA cluster chains. a,b) SEM micrographs of gold wires. Pt clusters at the DNA were synthesized by a modified method (see text). Microcontacts to the wires were fabricated using electron beam lithography. The wire in b is burned out after electrical measurements. c,d) TEM micrographs of a gold wire obtained by gold enhancement of a Pt cluster chain, which was synthesized according the standard method.

the electrical resistance (Fig. 4.19b). This instability is caused by grain boundaries within the wire, which have a considerable higher resistance than the parts, which are continuously covered with gold. Therefore, the majority of the electric power is concentrated at these boundaries, which induces overheating and melting. In further work of the group in Haifa, continuous gold wires using the same gold enhancement solution, but silver nucleation centers at the DNA, could be synthesized, which showed ohmic behavior and good conductivity [17]. However, the diameter of these wires could not be substantially decreased.

Using the gold enhancement solution it is also possible to further metallize the Pt cluster chains, which were are synthesized according the standard procedure - DNA activation with subsequent reduction. Figures 4.19c,d show a wire which was

fabricated by depositing cluster chains on a TEM grid and subsequent application of the gold enhancement. The obtained wires are continuous, possess a length of a view micrometers and have a minimum diameter of 50 nm. The zoom of Figure 4.19d shows that the wire is composed of lots of grains.

Summary

The aim of the present thesis was to explore possibilities, how DNA can be used to build up electronic circuitry as an alternative method for structure fabrication in future nanoelectronics. Within the proposed fabrication scheme for a DNA-based circuit several stages turned out to be essential: (i) the assembly of DNA networks, (ii) the integration of DNA into microelectrode structures, (iii) the site-specific deposition of functional elements, and (iv) the metallization of DNA templates. On the way to accomplish these steps, methods were developed, which are summarized in the following.

Construction of multi-branched, functional DNA junctions

A basic element of networks are junctions. Therefore, branched DNA molecules with an arm length of 185 nm were constructed. The assembly of 3-armed DNA molecules was accomplished in a 3-step procedure. First, a small 3-armed linker element was hybridized from three semi-complementary synthetic oligonucleotides. The oligomers were designed in such a way that the assembled linker element possesses short single-stranded 5'-overhangs. In a second step, elongations for the short linker arms were prepared. They were obtained by PCR and subsequent restriction enzyme digestion. The ends of the elongations were treated with Klenow polymerase, in order to obtain 5'-overhangs, which were complementary to the overhangs of the linker. Finally, the elongations were coupled to the linker element by ligation.

Moreover, by carefully choosing the sequences of the 5'-overhangs of the linker elements, it was possible to specifically connect different 3-armed linkers to each other. Thus, n-armed linkers could be synthesized, which were used to assemble n-armed junctions after an elongation step. The formation of junctions with 4 and 6 arms was demonstrated by gel electrophoresis and scanning force microscopy. The developed building-block procedure, where linkers with more than three arms are assembled from 3-armed linkers, allows high flexibility to construct junctions with any number of arms. The number of the arms is for all constructs well-defined and programmed by the sequences of the linker's 5'-overhangs.

As an example how functional elements can be positioned in a DNA network, 5 nm gold colloids were site-specifically attached to the center of 3-armed junctions.

This was accomplished by incorporation of biotin at the ends of the elongations, where the coupling to the linker occurs. Thus, three biotin molecules surrounded the center of the final junction in a distance of 5 nm. By mixing the junctions with streptavidin conjugated 5 nm large gold colloids, hybrid junctions carrying one or two colloids at the center were obtained.

Stretching of single DNA molecules between gold electrodes

Single DNA molecules could be stretched between microstructured gold electrodes. A simple, but nonetheless reliable and efficient method was developed to anchor DNA specifically to the electrodes. The electrodes were modified to be positively charged by coating them with an amino-thiol layer. By careful adjustment of the pH-value of the solution, an end-specific binding of the DNA was accomplished. Using this anchoring method, single molecules could be stretched between two electrodes in a hydrodynamic flow. Applying varying flow directions, whole DNA networks were obtained by stretching single molecules between gold dots forming a large array. The advantage of using amino-thiols is the simplicity of this method - the electrode modification is easy and it is not necessary to modify DNA ends or to rely on the synthesis of a specific DNA end overhang.

Furthermore, other anchoring possibilities of DNA to gold electrodes, like thiol functionalization of DNA with thiol modified oligomers and biotin-streptavidin linkage, were successfully tested. In particular thiol modified oligomers were used to attach only a single end of the DNA to the surface. The construction of bi-functionalized DNA, which is modified on one end with thiol and on the other end with biotin, could beyond that be applied to bind further nanoobjects to DNA anchored with one end to the substrate.

A simple model was developed to characterize the stretching forces acting on U-shaped DNA molecules in the hydrodynamic flow. The biotin-streptavidin anchors were found to last forces up to 28 pN.

Growth of platinum clusters along DNA molecules

A method was developed, which accomplishes the selective growth of platinum clusters at DNA in solution. The synthesis was done by chemical reduction of $PtCl_4^{2-}$ complexes, which were partly bound to the DNA. The result are micrometer long Pt cluster chains with an average cluster diameter of 4 nm. The clusters were found to be partly grown together, thus forming continuous wire-like regions up to 100 nm in length. The cluster nucleation was found to take heterogeneously place at the DNA molecule, if the DNA was activated, i.e. if enough platinum complexes were allowed to bind before chemical reduction. In this case the heterogeneous reaction channel is kinetically favored to the homogeneous cluster nucleation in solution. This leads to the complete suppression of the latter process.

The heterogeneous cluster nucleation at the platinum complexes, which are bound to the DNA, was found to be promoted by the DNA bases, i.e. it is template directed. This is in agreement with First-Principles-Molecular-Dynamics simulations, which show that the origin for the favored nucleation at the bound complexes is electron donation from the DNA bases to platinum [107]. The dependency of the DNA metallization on several control parameters, like activation time, reaction kinetics and concentrations, shows that a heterogeneous nucleation, resulting in the formation of cluster chains, takes only place within a small reaction window. The morphology of the obtained DNA metallization can be tuned by additives like citrate, and cluster chains with well separated clusters could be obtained.

Continuous gold wires can be synthesized by electroless metallization of the cluster chains. This way wires with a diameter of 50 nm could be prepared.

Will DNA-based nanoelectronics be a perspective for the future?

The different methods, which were developed in the framework of this thesis, can be seen as steps towards a future DNA-based assembly of electronic circuits. To go further in this direction, the introduced procedures have to be combined, i.e. to be put together into the assembly scheme proposed at the beginning. This means in particular, that DNA junctions have to be metallized, DNA junctions have to be attached to gold electrodes in a defined way, the metallization procedure has to be adopted to DNA, which is attached to the surface, a real device has to be built, larger DNA networks have to be assembled and so on. There is plenty of work, which can and also should be done in this field.

However, what are the perspectives? Will it one day be possible to assemble a whole computer chip only with the help of DNA? In short term, i.e. the next years, this will probably not be accomplished. The lithographical techniques applied in chip production are still much more powerful. A chance for the near future is maybe to replace single steps during the whole fabrication process of a chip with DNA-based techniques. For example, the wiring between certain functional elements, e.g. carbon nanotubes, could be done using DNA. Or DNA can be applied for the assembly of simpler nanostructures, like periodic arrays and single wires, as this technique does not require large technical effort and could be much cheaper than other technologies.

The problems in the application of DNA and other molecules for the fabrication of artificial nanostructures is the complexity of the systems, which one wants to fabricate. In comparison to modern computer chips, the structures, which were self-assembled using biomolecules, are up to now rather simple. Beside the formation of single tubes or wires, the structures with the highest complexity are periodic arrays of clusters [13,14,111] and DNA [6,34], which extend over a range of some hundreds lattice constants. However, advanced circuits will require a much higher degree of complexity than simple periodicity. In the recently developing field of DNA com-

putation several ways to increase the complexity of DNA structures were proposed. One idea is to construct periodic arrays of bits, where each bit represents a dual information [112]. This theoretical approach, where sticky-ended cohesion controls the assembly of structures of any complexity, has under experimental conditions to deal with the serious problem of errors. Although ways for an error reduction are suggested [113,114], the association of complementary DNA sequences will never be completely precise. Furthermore, the number of errors scales exponentially with the size of an array structure, which leads to a restriction of the self-assembled arrays or networks to a rather small size.

The inaccuracy of the *in-vitro* assembly of biomolecules is not surprising. In living nature errors are even desired. For example, mutations and recombinations of the genome are among the driving forces of evolution. Furthermore, errors are not avoidable because *in vivo* processes are highly dynamic and based on association and separation of biomolecular units at about room temperature. A reason, why such a complex system like a single cell can be assembled to possess a high specific functionality, is that in living nature exist well elaborated feedback and error correction mechanisms. Up to know, such feedback loops have not been considered for the *in vitro* assembly of artificial biomolecular nanostructures, which has been the main limitation for a successful assembly of much more complex structures. The development of appropriate feedback and error correction mechanisms will decide, if a biomolecule-, in particular DNA-based nanostructure assembly will be suitable to fabricate such complex structures, as they will be required for future nanoelectronics. The design, even of a simple feedback loop, is not trivial as the assembly units are biomolecules. The task is, however, a technical problem, e.g. to establish a certain DNA bridge or in a wider framework to achieve a certain electronic behavior between two points of a network. Maybe one day solutions for this kind of problems will be found. Maybe biomolecule-based electronics will revolutionize future nanotechnology. But, this will finally be shown by time.

Appendix

A.1 Calculations

A.1.1 Calculation of the chain line

The chain line is the curve $y(x)$ which under the influence of gravity assumes a homogeneous flexible non-elastic chain, which is anchored at its end points $(x1, y1)$ and $(x2, y2)$ (Fig. A.1a). At each point of the chain the gravity force of a segment of length dl can be written as $dF_G = C\,dl$. Due to the curvature of the chain, the force along the chain F_{chain} generates at each point a force dF acting against the dF_G, as the directions of the forces acting in the two different directions along the chain differ about an angle $d\alpha$. From Figure A.1b one obtains

$$\Delta F = F_{chain} 2 \sin(\Delta\alpha/2) \quad \Longrightarrow \quad dF = F_{chain} d\alpha, \quad with\ \Delta\alpha \longrightarrow d\alpha. \tag{A.1}$$

From $y'(x) = \tan\alpha$ follows $d\alpha = y''/(1 + y'^2)dx$. Furthermore, using $\tan\alpha = \sin\alpha/\cos\alpha$ and $1 = \cos^2\alpha + \sin^2\alpha$, one obtains $\cos^2\alpha = 1/(1 + y'^2)$ and $\sin^2\alpha = y'^2/(1 + y'^2)$. With $dl = \sqrt{dx^2 + dy^2}$ and $y'(x) = dy/dx$ one can write $dl = \sqrt{1 + y'^2}\,dx$. As can be seen in Figure A.1a, $dF = dF_G \cos\alpha = C\,\cos\alpha\,dl$. Thus, transforming Equation A.1 by using the last equation results to

$$\begin{aligned} dF = F_{chain}\frac{y''}{(1+y'^2)}dx &= C\sqrt{1+y'^2}dx\frac{1}{\sqrt{1+y'^2}} = dF_G\cos\alpha, \\ F_{chain}\frac{y''}{(1+y'^2)} &= C. \end{aligned} \tag{A.2}$$

At each point F_{chain} is changed by the part of the gravity force dF_G, which is acting along the chain. This leads to

$$dF_{chain} = dF_G \sin\alpha = Cdl\sin\alpha = C\sqrt{1+y'^2}dx\frac{y'}{\sqrt{1+y'^2}} = Cy'dx, \tag{A.3}$$

and after integration of the equation to

$$F_{chain} = C(y + A). \tag{A.4}$$

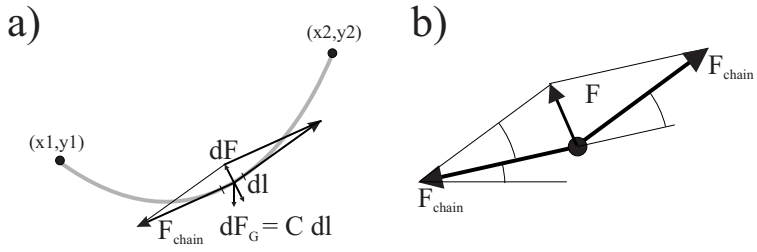

Figure A.1: Forces at the chain line problem.

Combining equations A.2 and A.4 one gets the following differential equation:

$$y'^2 + 1 = (y + A)y'' = (y + A)\frac{dy'}{dy}\frac{dy}{dx} = (y + A)y'\frac{dy'}{dy}. \tag{A.5}$$

After separation of y and y' and subsequent integration this expression can be transformed to $y' = [B(y + A)]^2 - 1$. From that $y(x)$ is finally obtained:

$$y = \frac{1}{B}\cosh[B(x + D)] - A = \frac{1}{B}\{\cosh[B(x - x_0)] - 1\} + y_0, \tag{A.6}$$

where (x_0, y_0) is the local minimum of the curve. The factor B depends on the total chain length L.

$$L = \int_{x_1}^{x_2} \sqrt{1 + y'^2}dx = \frac{1}{B}\{\sinh[B(x_2 - x_0)] - \sinh[B(x_1 - x_0)]\} \tag{A.7}$$

Combining Equations A.4 and A.6, the force along the chain F_{chain} results to

$$F_{chain} = \frac{C}{B}\cosh[B(x - x_0)]. \tag{A.8}$$

At each point of the chain it is split into a horizontal component of size $F_H = C/B$ and a vertical component $F_V = |C/B \sinh[B(x - x_0)]|$. Adding F_V for the two anchor points, equals, as expected, the total gravity force of the chain $F_G = C\,L$. From this the ratio between the total vertical force and the horizontal force can be obtained with F_G/F_H =L B.

A.1.2 Equilibrium concentrations and kinetics for the hydrolysis of $PtCl_4^{2-}$

The percentages of $PtCl_4^{2-}$, $[PtCl_3\,H_2O]^-$ and *cis*-$[PtCl_2\,(H_2O)_2]^0$ in Figure 4.4 (p. 74) after 20 h hydrolysis were calculated by assuming equilibrium. Then, the following equations are valid:

$$\begin{aligned} 1 &= x_4 + x_3 + x_{2c}, \\ K_{eq,4} &= \frac{c_3 \cdot c_{Cl}}{c_4} = \frac{x_3 \cdot (x_3 + 2x_{2c})}{x_4}\, c_0, \\ K_{eq,3c} &= \frac{c_{2c} \cdot c_{Cl}}{c_3} = \frac{x_{2c} \cdot (x_3 + 2x_{2c})}{x_3}\, c_0, \end{aligned}$$

with x_i, c_i denoting the fraction, concentration of the complex species with i chlorine ligands. c_0 is the total concentration of Pt complexes, c_{Cl} the concentration of Cl^- ions in solution. Solving the equation array for varying c_0 provides the concentration dependence of the complex distribution (Fig. 4.4, p. 74).

The kinetics of the hydrolysis can be calculated with the following equations:

$$\begin{aligned} 1 &= x_4 + x_3 + x_{2c}, \\ x_4'(t) &= k_{B,4} \cdot x_3(t)[x_3(t) + 2x_{2c}(t)]\, c_0 - k_{F,4} \cdot x_4(t), \\ x_{2c}'(t) &= -k_{B,3c} \cdot x_{2c}(t)[x_3(t) + 2x_{2c}(t)]\, c_0 + k_{F,3c} \cdot x_3(t), \end{aligned}$$

assuming that *trans*-$[PtCl_2(H_2O)_2]^0$ and $[PtCl(H_2O)_3]^+$ can be neglected, which is valid for reaction times below 100 h. Calculation is done numerically using commercial software[1]. For the hydrolysis of freshly dissolved $PtCl_4^{2-}$ the start conditions are $x_4 = 1$, $x_3 = x_{2c} = 0$. If an aged stock solution is diluted one has first to calculate the fractions of Pt complexes after aging for a certain time and then use them as new inputs for the equation array. Figure A.2 shows the kinetics of the hydrolysis of a freshly prepared 1 mM $PtCl_4^{2-}$ solution and a 1 mM $PtCl_4^{2-}$ solution obtained by diluting a one day old 10 mM stock.

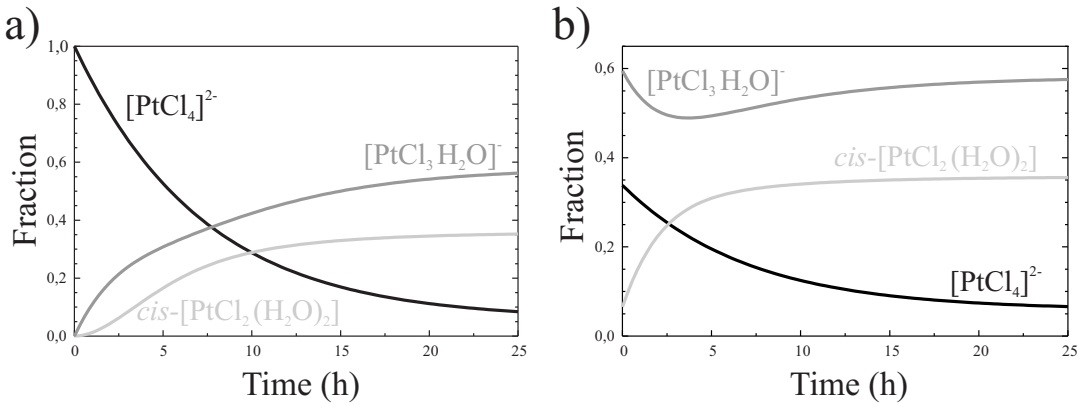

Figure A.2: Kinetics of the hydrolysis of $PtCl_4^{2-}$. Hydrolysis of a) a freshly prepared 1 mM $PtCl_4^{2-}$ solution, b) a 1 mM solution obtained by diluting a one day old 10 mM stock.

A.1.3 Mie theory applied to platinum clusters

According the Mie theory, the absorbance section σ for a spherical particle, which is much smaller than the wavelength of light can be written as [115]

$$\sigma = 18\pi \frac{V}{\lambda} n_0^3 \frac{\varepsilon_2}{(\varepsilon_1 + 2n_0^2)^2 + \varepsilon_2^2}, \tag{A.9}$$

[1] Mathematica 2.0, Wolfram Research, Inc.

where V denotes the particle volume, n_0 the index of refraction of the aqueous solvent, λ the wavelength of the light, ε_1 and ε_2 the real and imaginary parts of the dielectric constant of the particle material. ε_1 and ε_2 can be obtained from the index of refraction n and the extinction coefficient k by the relations $\varepsilon_1 = n^2 - k^2$ and $\varepsilon_2 = 2nk$. With the particle density N and the optical path length l the absorbance A in the UV/VIS spectrometer results to

$$A = \frac{\sigma N l}{\ln 10} \tag{A.10}$$

With these equations it is possible to calculate the absorbance spectrum for free platinum clusters in solution at the particular conditions applied in the metallization experiments. For this an average Pt cluster diameter of 3.6 nm with a volume of 25 nm^3 is assumed, which corresponds to 2057 Pt atoms, according to the "magic numbers" coming from the Jellium model[2] [116]. If all Pt complexes of the 1 mM solution are reduced a particle concentration of $3 \cdot 10^{14}$ cm^{-3} is obtained. Together with the refraction index for water $n_0 = 1.34$, an optical pathlength $l = 10$ mm for the used spectrometer and the wavelength dependent values of n and k for platinum, which are taken from Ref. [117], the curve depicted in Figure A.3 is obtained.

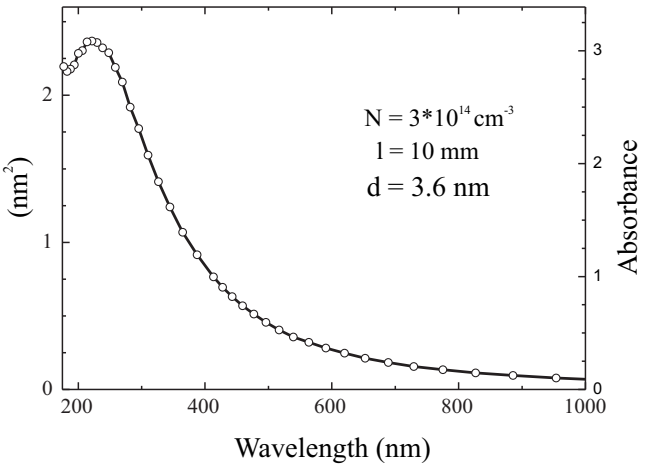

Figure A.3: Absorbance spectrum of a Pt cluster suspension obtained by the Mie theory. The concentration of platinum atoms is 1 mM.

One can see, that at 600 nm wavelength, where the kinetics of the cluster formation process is followed, an absorbance value of about 0.35 is obtained, which is valid for free, i.e. non-aggregated particles. For a given, fixed number of Pt atoms the absorbance is within the Mie theory independent from the particle diameter as $A \sim NV$ and the particle density N is proportional $1/V$ for the volume of a

[2] The magic numbers of the Jellium modell for closed shell clusters are:
13 55 147 309 561 923 1415 2057...
corresponding for platinum to cluster diameters of:
0.4 0.9 1.4 1.8 2.3 2.7 3.2 3.6 nm

single particle V. Therefore, for a 1 mM solution of $PtCl_4^{2-}$, which is completely reduced, an absorbance of 0.35 should be obtained at 600 nm, if the formed clusters are non-aggregated, spherical and small in comparison to the wavelength of the light.

A.2 Experimental methods

A.2.1 Formation of multi-branched DNA junctions

Linker hybridization

The 3-armed linkers were hybridized from three oligonucleotides, which sequence is given in section 2.1.1, by preparing the following mixture: 15 μl 100 mM Tris pH 8.0, 1.5 μl 1 M NaCl, 1.5 μl 100 mM $MgCl_2$, 6 μl H_2O, 2 μl of each oligomer at a concentration of 100 pM/μl. Hybridization was done by heating the solution to 95°C and subsequent cooling to 20°C at a rate of 0.1°C per min.

Phosphorylation of the linkers was done by preparing the following solution: 20 μl H_2O, 3 μl 10x reaction buffer (supplied with enzyme), 5 μl of hybridized linkers, 1 μl ATP 0.5 mM (SIGMA, A7699), 1 μl T4-polynucleotide kinase, 10 U/μl (NEB, M0201S) and subsequent incubation at 37°C . The phosphorylated linkers were cleaned up with Microcon enzyme spin filters (Millipore) at 14000 g and Microcon YM30 spin filters (Millipore) at 12000 g. The final DNA concentration was determined with an UV/VIS spectrometer.

Preparation of the elongations

A 1078 bp fragment is amplified from λ-DNA by PCR. The primer sequences are: forward primer 5'-CAATAAATTCTGACTGTAGCTG, backward primer 5'-AGTAGTACTGCAAGAGGTTCC. The following mixture was prepared: 25 μl 2x PCR-Mastermix (Promega, M7502), 22 μl nuclease free H_2O, 1 μl forward primer 100 pmol/μl, 1 μl backward primer 100pmol/μl, 1 μl λ-DNA (0.01 μg/μl) (NEB, N3011L). The PCR process was performed by heating the solution to 95°C for 4 min and repeating 30 cycles of denaturation at 95°C for 0:45 min, primer annealing at 55°C for 0:45 min and primer extension at 72°C for 1:00 min. The final primer extension was done at 72°C for 5:00 min. The PCR product was purified using a Qiaquick spin filter kit (Qiagen).

The 1078 bp fragment was digested with *Hin*dIII restriction enzyme by mixing 5 μl 10x reaction buffer (supplied with enzyme), max. 3 μg PCR product, 1 μl *Hin*dIII (NEB, R0104S), H_2O up to 50 μl. Digestion was done 1 h at 37°C , followed by 20 min enzyme deactivation at 65°C . Cleanup is done either with the QIAquick kit or with Microcon YM100 spin filters (Millipore).

The 5'-overhang of the elongation was filled with one adenine by preparing the following solution: 5 μl 10x reaction buffer (supplied with enzyme), about. 3 μg *Hin*dIII digested PCR fragments 1 μl dTTP and 1 μl dATP, both 10 mM stock solutions, 1 μl Klenow polymerase 5 U/μl (NEB, M0210S), water up to 50 μl. Cleanup is done either with the QIAquick kit or with Microcon YM100 spin filters (Millipore).

Ligation of the junctions

Ligation of linkers and elongations is done for 16 h or 32 h at 16°C by preparing the following solutions:

3-armed junction: 3 μl 10x reaction buffer (supplied with enzyme), 1μg elongations (3 pmol), 0.034μg 3-armed linker (1 pmol), 4 μl T4 DNA ligase (NEB, M0202S), 1:200 diluted with Diluent A (NEB, B8001S), H_2O up to 30 μl.

4-armed junction: 3 μl 10x reaction buffer (supplied with enzyme), 1μg elongations (3 pmol), 0.02μg 3-armed linker $\langle\sqsubset\circ\circ\rangle$, 0.02$\mu$g 3-armed linker $\langle\square\circ\circ\rangle$, 6 μl T4 DNA ligase (NEB, M0202S), 1:200 diluted with Diluent A (NEB, B8001S), H_2O up to 30 μl.

6-armed junction: 3 μl 10x reaction buffer (supplied with enzyme), 1μg elongations (3 pmol), 0.01μg 3-armed linker $\langle\sqsubset\sqsubset\sqsubset\rangle$, 0.034$\mu$g 3-armed linker $\langle\square\circ\circ\rangle$, 6 μl T4 DNA ligase (NEB, M0202S), 1:200 diluted with Diluent A (NEB, B8001S), H_2O up to 30 μl.

Subsequent to the ligation the DNA is separated with gel electrophoresis (1% low melting point agarose, 1x TAE). The desired product is sliced out of the gel and the DNA is extracted from the agarose using a QIAexII kit (Qiagen).

Attachment of gold colloids to 3-armed junctions

Biotin modified DNA junctions are prepared by using biotinylated elongations. They were functionalized by replacing 1 μl dATP with 5 μl biotin-14-dATP (Invitrogen, 19524-016) during the fill-in step of the *Hin*dIII digested PCR fragments. All the other preparation steps were done according to the synthesis procedure of unmodified junctions.

5 nm gold colloids (Sigma-Aldrich) were purified from free streptavidin by five centrifugations with Microcon YM100 spin filters (Millipore) at 10000 g in TE buffer. Subsequently they were incubated with the biotin modified DNA junctions at slight stoichiometric excess to biotin binding sites.

A.2.2 Integration of DNA into microstructures

Biotinylation of λ-DNA

Biotinylation of both ends of λ-DNA was done by incubating 20 µl λ-DNA (10 *mug*) in 15 µl H_2O and 5 µl 10x reaction buffer (supplied with enzyme) 5 min at 65°C followed by cooling on ice. Subsequently, 1 µl of a 10 mM stock of each dNTP (dTTP, dATP, dGTP), 5 µl Biotin-14-dCTP (Invitrogen) and 2 µl Klenow polymerase (NEB) were added. The fill-in reaction was done 25 min at 25°C followed by 10 min enzyme deactivation at 75°C . Clean up was done by three centrifugations steps with Microcon YM100 spin filters (Millipore) at 500 g in TE buffer.

Biotinylation of a single end of λ-DNA was done according to the biotinylation of both ends, but under absence of dATP in the reaction mix.

Preparation of BT-DNA

Dephosphorylation of λ-DNA was done by mixing 78 µl H_2O, 20 µl 10x reaction buffer (supplied with enzyme), 100 µl λ-DNA (50g, NEB) and 2 µl Shrimp alkaline phosphatase (Amersham Pharmacia). The reaction was done 30 min at 37°C followed by 15 min enzyme deactivation at 65°C and rapid cooling on ice.

Phosphorylation of 3'-thiol modified oligomers (5'-AGGTCGCCGCCC-SH) was done with 245 µl H_2O, 30 µl 10x reaction buffer (supplied with enzyme), 10 µl thiol modified oligomer (100 pmol/µl), 5 µl ATP (1mM) and 10 µl T4 Kinase (NEB, 10 U/µl) at 37°C for 30 min and 65°C for 20 min.

Dephosphorylated λ-DNA and phosphorylated oligomers were hybridized, by mixing both solutions and slow cooling down from 75°C to 10°C at a rate of 0.1°C per 20 s.

Ligation of the single stranded nick after hybridization was done by mixing 310 µl H_2O, 100 µl 10x reaction buffer (supplied with enzyme), 500 µl hybridized λ-DNA and 90 µl T4 Ligase (NEB) 1:200 diluted with Diluent A (NEB). The reaction was done 16 h at 16°C followed by 10 min enzyme deactivation at 65°C . The thiolated λ-DNA (T-DNA) was purified by four centrifugations with Microcon YM100 spin filters at 500 g in TE buffer.

T-DNA is biotinylated at its unmodified end using the above described biotinylation procedure of a single end of λ-DNA.

Stretching of DNA between electrodes using aminothiol

Gold electrodes are cleaned overnight in 3 volumes H_2SO_4 with 1 volume H_2O_2. Amine modification is done by 30 min incubation of the sample in a ethanol solution of 1 mM aminoethanethiol (cysteamine, Fluka). The sample is rinsed with water, put into the flow cell and a solution of 2.5 µg YOYO labelled λ-DNA in

100 mM Tris, pH 8.0 is applied. YOYO labelling is done by mixing 5 μl YOYO 1 (Molecular Probes, 1 mM stock diluted 1:100 in 1xTBE) with 90 μl TE buffer and adding 5 μl λ-DNA (NEB, 2.5 μg).

A.2.3 Preparation of cluster chains along DNA

If it was not otherwise stated, the reduction experiments were performed by mixing 1 ml of an at least 24 h aged 1 mM solution of K_2PtCl_4 or K_2PdCl_4 (Fluka) with 0 to 100 μg of λ-DNA (New England Biolabs NEB) or DNA from salmon testes (SIGMA). Then, the DNA was activated by incubating it a certain time with the salt solution at room temperature. The cluster growth was started by heating the solution to 37°C and adding 100 μl of a 10 mM solution of dimethylaminoborane (DMAB, Fluka). Optionally, sodium citrate was added to the DNA solution to 0.5 mM final concentration before the reduction step.

Kinetics of the cluster formation process was studied using a Cary 50 UV/VIS photospectrometer (Varian) and measuring the 600 nm absorbance. The distortion of the DNA base stacking was investigated with the same spectrometer recording time series of whole spectra.

Samples for scanning force microscopy (SFM) and transmission electron microscopy (TEM) were prepared 30 min after starting the reduction. Transmission electron microscopy (TEM) investigations were carried out using a Philips CM 200 with tungsten cathode at 160 kV while a Philips CM 200 equipped with field emission cathode was employed for high resolution work. Samples were prepared by placing a droplet of the cluster suspension onto a carbon-coated copper grid for 5 min. Afterwards the sample was rinsed with water and excess water was removed with filter paper.

DNA activation was investigated by diluting differently concentrated 24 h aged stock solutions of K_2PtCl_4 to 1mM and mixing them with 5 μg/ml λ-DNA. Optionally Na_2SO_4 was added to a final concentration of 10 or 100 mM. Samples were placed in the photospectrometer and absorbance spectra from 240 nm to 600 nm were recorded every 30 min. SFM samples from activated DNA were prepared following the instructions below.

The single- or double-stranded conformation of activated λ-DNA and λ-DNA *Hin*dIII digested (NEB) was tested by gel electrophoresis. For this 5 μg of λ-DNA and λ-DNA *Hin*dIII digested were activated in 1 ml of 1 mM 24 h aged K_2PtCl_4 solution for 20 h. The DNA used for the incubation with the Pt complexes was either double-stranded or single-stranded. The latter one was obtained by thermal denaturation at 95°C and subsequent cooling on ice. After activation 20 μl of each sample was mixed with 1 μl 1 mM DMAB to cover the DNA with nucleation sites for the in-gel gold stain. Electrophoresis was performed in a 0.5% agarose gel for 1.5 h in 1xTAE-Buffer at 4.2 V/cm. Subsequently the gel was covered with a gold

stain solution [17] until the DNA bands appeared. The reaction was stopped by rinsing the gel with excess water.

A.2.4 Preparation of SFM samples

SFM samples were prepared as described by Bezanilla *et al.* [118] by diluting the DNA-cluster suspension with HEPES/Mg buffer (40 mM HEPES, 5 mM $MgCl_2$, pH 7.6) to a final DNA concentration of 1 μg/ml and placing a droplet onto freshly cleaved mica for 2 min to allow adsorption. Subsequently the sample was rinsed with water and blown dry with nitrogen. Imaging was performed with a Nanoscope IIIa (Digital Instruments) in tapping mode at air.

A.2.5 Gold enhancement

The gold enhancement solution of Ref. 17 was used in different concentrations.

Gel staining: 1200 μl $KAuCl_4$ (23 mg/ml) mixed with 1200 μl KSCN (60 mg/ml) followed by centrifugation at 5000 g. The pellet is dissolved in 10 ml 1 M sodium phosphate buffer, pH 5.5 and 0.5 ml 5.5 mg/ml hydrochinone are added.

Cluster chain enhancement: 60 μl $KAuCl_4$, 60 μl KSCN, 480 μl phosphate buffer, 120 μl hydrochinone. The solution is placed about 1 min onto the sample containing the Pt cluster chains and subsequently rinsed with H_2O.

Publications

The following publications were done in the framework of the present thesis.

Published works:

[119] W. Pompe, M. Mertig, R. Kirsch, R. Wahl, L. Colombi-Ciacchi, J. Richter, R. Seidel, und H. Vinzelberg, *Formation of metallic nanostructures on biomolecular templates*, Zeitschrift für Metallkunde **90**, 1085-1091 (1999)

[18] J. Richter, R. Seidel, R. Kirsch, M. Mertig, W. Pompe, J. Plaschke, H.-K. Schackert, *Nanoscale Palladium Metallization of DNA*, Advanced Materials **12**, 507-510 (2000)

[19] R. Seidel, M. Mertig, W. Pompe, *Scanning force microscopy of DNA metallization*, Surface and Interface Analysis **33**, 151-154 (2002)

[20] M. Mertig, L. Colombi Ciacchi, R. Seidel, W. Pompe, A. De Vita, *DNA as a selective metallization template*, Nanoletters **2**, 841-844 (2002)

[73] M. Mertig, R. Seidel, L. Colombi Ciacchi, W. Pompe, *Nucleation and growth of metal clusters on a DNA template*, AIP Conference Proceedings **633**, 449-453 (2002)

[120] L. Colombi Ciacchi, A. De Vita, R. Seidel, M. Mertig, W. Pompe, *The formation of metal clusters in solution and on biopolymers investigated by first-principles molecular dynamics*, Proceedings in Applied Mathematics and Mechanics **2**, 5-8 (2003)

[107] L. Colombi Ciacchi, M. Mertig, R. Seidel, W. Pompe, A. De Vita, *Nucleation of platinum clusters on biopolymers: A first principles study of the molecular mechanisms*, Nanotechnology **14**, 840-848 (2003)

Submitted works:

[121] M. Mertig, L. Colombi Ciacchi, R. Seidel, W. Pompe, A. De Vita, *Verfahren zur Schaffung metallischer Nukleationszentren für das Clusterwachstum auf DNA*, German patent application **DE 101 31 551.1** (2001), US patent application **19/177.775** (2003)

[122] B. Voit, F. Braun, Ch. Loppacher, S. Trogisch, L.M. Eng, R. Seidel, A. Gorbunoff, W. Pompe, M. Mertig, *Photolabile Ultrathin Polymer Films for Spatially Defined Attachment of Nanoobjects*, subm. to ACS Proceedings (2002)

[123] W. Pompe, R. Seidel, M. Mertig, *Formation of metallic nanostructures on biomolecular templates: Basic strategies for the development of a DNA-based nanoelectronics*, subm. to VDI proceedings (2002)

[75] S. Diez, C. Reuther, R. Seidel, M. Mertig, W. Pompe, W and J. Howard, *Stretching and Transporting DNA Molecules using Motor Proteins*, subm. (2003)

Bibliography

[1] E. S. Lander et al., *Initial sequencing and analysis of the human genome*, Nature **409**(6822), 860–921 (2001) 1

[2] J. C. Venter et al., *The sequence of the human genome*, Science **291**(5507), 1304–1351 (2001) 1

[3] G. E. Moore, *Cramming more components onto integrated circuits*, Electronics magazine **38**(8), 114–117 (1965) 2

[4] J. Chen and N. C. Seeman, *The synthesis from DNA of a molecule with the connectivity of a cube*, Nature **350**, 631–633 (1991) 2, 3, 15

[5] Y. Zhang and N. C. Seeman, *The construction of a DNA truncated octahedron*, J. Am. Chem. Soc. **116**, 1661–1669 (1994) 2, 3, 15

[6] E. Winfree, F. Liu, L. A. Wenzler and N. C. Seeman, *Design and self-assembly of two-dimensional DNA crystals*, Nature **394**, 539–544 (1998) 2, 3, 15, 107

[7] A. P. Alivisatos, K. P. Johnsson, X. G. Peng, T. E. Wilson, C. J. Loweth, M. P. Bruchez and P. G. Schultz, *Organization of 'nanocrystal molecules' using DNA*, Nature **382**(6592), 609–611 (1996) 2, 25, 39, 41

[8] C. A. Mirkin, R. L. Letsinger, R. C. Mucic and J. J. Storhoff, *A DNA-based method for rationally assembling nanoparticles into macroscopic materials*, Nature **382**(6592), 607–609 (1996) 2, 39, 41

[9] R. Kirsch, M. Mertig, W. Pompe, R. Wahl, G. Sadowski, K. J. Bohm and E. Unger, *Three-dimensional metallization of microtubules*, Thin Sol. Films **305**(1-2), 248–253 (1997) 2, 70, 81, 101

[10] M. Mertig, R. Kirsch and W. Pompe, *Biomolecular approach to nanotube fabrication*, Appl. Phys. A **196**, S723–S727 (1998) 2, 70, 81, 101

[11] W. Shenton, T. Douglas, M. Young, G. Stubbs and S. Mann, *Inorganic-organic nanotube composites from template mineralization of tobacco mosaic virus*, Adv. Mat. **11**(3), 253–256 (1999) 2

[12] E. Dujardin, C. Peet, G. Stubbs, J. N. Culver and S. Mann, *Organization of metallic nanoparticles using tobacco mosaic virus templates*, Nanolett. **3**(3), 413–417 (2003) 2

[13] M. Mertig, R. Kirsch, W. Pompe and H. Engelhardt, *Fabrication of highly oriented nanocluster arrays by biomolecular templating*, Eur. Phys. J. D **9**, 45–48 (1999) 2, 70, 107

[14] R. Wahl, M. Mertig, J. Raff, S. Selenska-Pobell and W. Pompe, *Electron-beam induced formation of highly ordered palladium and platinum nanoparticle arrays on the S-layer of bacillus sphaericus NCTC 9602*, Adv. Mat. **13**(10), 736–740 (2001) 2, 70, 107

[15] E. Braun, Y. Eichen, U. Sivan and G. Ben-Yoseph, *DNA-templated assembly and electrode attachment of a conducting silver wire*, Nature **391**(6669), 775–778 (1998) 2, 24, 25, 26, 44, 47, 48, 51, 69

[16] J. L. Coffer, S. R. Bigham, L. X, R. F. Pinizzotto, Y. G. Rho, R. Pirtle and I. L. Pirtle, *Dictation of the shape of mesoscale semiconductor nanoparticle assemblies by plasmid DNA*, Appl. Phys. Lett **69**, 3851–3853 (1996) 2, 25, 26, 69

[17] K. Keren, M. Krueger, R. Gilad, G. Ben-Yoseph, U. Sivan and E. Braun, *Sequence-specific molecular lithography on single DNA molecules*, Science **297**(5578), 72–75 (2002) 2, 25, 26, 47, 101, 102, 117

[18] J. Richter, R. Seidel, R. Kirsch, M. Mertig, W. Pompe, J. Plaschke and H. K. Schackert, *Nanoscale palladium metallization of DNA*, Adv. Mat. **12**, 507–510 (2000) 2, 25, 69, 81, 119

[19] R. Seidel, M. Mertig and W. Pompe, *Scanning force microscopy of DNA metallization*, Surface and Interface Analysis **33**, 151–154 (2002) 2, 25, 119

[20] M. Mertig, L. Colombi Ciacchi, R. Seidel, W. Pompe and A. De Vita, *DNA as a selective metallization template*, Nanolett. **2**, 841–844 (2002) 2, 25, 93, 119

[21] W. E. Ford, O. Harnack, A. Yasuda and J. M. Wessels, *Platinated DNA as precursors to templated chains of metal nanoparticles*, Adv. Mater. **13**(23), 1793–1797 (2001) 2, 25, 26, 89

[22] C. F. Monson and A. T. Woolley, *DNA-templated construction of copper nanowires*, Nanolett. **3**(3), 359–363 (2003) 2, 25, 26, 89

[23] S. B. Smith, Y. Cui and C. Bustamante, *Overstretching B-DNA: The elastic response of individual double-stranded and single-stranded DNA molecules*, Science **271**(5250), 795–799 (1996) 2, 21

[24] W. Saenger, *Principles of Nucleic Acid Structure* (Springer Verlag Inc., 1984) 3

[25] H. F. Judson, *Der 8. Tag der Schöpfung. Sternstunden der neuen Biologie* (Meyster, 1980) 6

[26] J. D. Watson and F. H. C. Crick, *Molecular structure of nucleic acids: a structure for deoxyribose nucleic acid*, Nature **171**, 737–738 (1953) 6

[27] F. S. Sanger, S. Nicklen and A. R. Coulson, *DNA sequencing with chain-terminating inhibitors*, Proc. Natl. Acad. Sci. USA **74**(12), 5463–5467 (1977) 6

[28] K. B. Mullis and F. A. Faloona, *Specific synthesis of DNA in vitro via a polymerase-catalyzed chain reaction*, Methods Enzymol. **155**, 335–350 (1987) 6, 11

[29] J. Sambrook, E. F. Fritsch and T. Maniatis, *Molecular Cloning* (Cold Spring Harbor Laboratory Press, 1989) 8

[30] F. J. Baldino, M. F. Chesselet and M. E. Lewis, *High-resolution in situ hybridization histochemistry*, Methods Enzymol **168**, 761–777 (1989) 8

[31] K. J. Breslauer, R. Frank, H. Blöcker and L. A. Marky, *Predicting DNA duplex stability from the base sequence*, J. Am. Chem. Soc. **83**, 3746–3750 (1986) 9

[32] O. H. Willemsen, M. M. E. Snel, A. Cambi, J. Greve, B. G. De Grooth and C. G. Figdor, *Biomolecular interactions measured by atomic force microscopy*, Biophys. J. **79**, 3267–3281 (2000) 10, 24

[33] N. C. Seeman, *Nucleic acid junctions and lattices*, J. theor. Biol. **99**, 237–247 (1982) 15, 16, 17

[34] C. Mao, W. Sun and N. C. Seeman, *Designed two-dimensional DNA Holliday junction arrays visualized by atomic force microscopy*, J. Am. Chem. Soc. **121**, 5437–5443 (1999) 15, 107

[35] C. Mao, W. Sun, Z. Shen and N. C. Seeman, *A DNA nanomechanical device based on the B-Z transition*, Nature **397**, 144–146 (1999) 15

[36] C. Mao, T. LaBean, J. H. Reif and N. C. Seeman, *Logical computation using algorithmic self-assembly of DNA triple crossover molecules*, Nature **407**, 493–496 (2000) 15

[37] R. Holliday, *A mechanism for gene conversion in fungi*, Genet. Res. **5**, 282–304 (1964) 16

[38] N. R. Kallenbach, R. I. Ma and N. C. Seeman, *An immobile nucleic acid junction constructed from oligonucleotides*, Nature **305**, 829–831 (1983) 17

[39] Y. Wang, J. E. Mueller, B. Kemper and N. C. Seeman, *The assembly and characterization of 5-arm and 6-arm DNA junctions*, Biochem. **30**, 5667–5674 (1991) 17, 29

[40] M. Scheffler, A. Dorenbeck, S. Jordan, M. Wüstefeld and G. von Kiedrowski, *Selbstanordnung von Trisoligonucleotidylen: "Nano-Acetylen" und "Nano-Cyclobutadien"*, Angew. Chem. **111**(22), 3514–3518 (1999) 17

[41] L. H. Lars Henning Eckardt, K. Naumann, W. M. Pankau, M. Rein, M. Schweitzer, N. Windhab and G. von Kiedrowski, *DNA nanotechnology: Chemical copying of connectivity*, Nature **420**, 286 (2002) 17

[42] C. M. Niemeyer, M. Adler, B. Pignataro, S. Lenhert, S. Gao, L. Chi, H. Fuchs and D. Blohm, *Self-assembly of DNA-streptavidin nanostructures and their use in imuno-PCR*, Nucl. Acids. Res. **27**(23), 4553–4561 (1999) 17

[43] C. M. Niemeyer, M. Adler, S. Gao and L. Chi, *Supramoleculare Nanoringe aus Streptavidin und DNA*, Angew. Chem. **112**(17), 3184–3187 (2000) 17

[44] P. J. Flory, *Statistical mechanics of chain molecules* (Hanser Publishers, 1988) 18, 19

[45] O. Kratky and G. Porod, *Röntgenuntersuchung gelöster Fadenmoleküle*, Rec. Trav. Chim. **68**, 1106–1123 (1949) 20

[46] C. Baumann, S. B. Smith, V. A. Bloomfield and C. Bustamante, *Ionic effects on the elasticity of single DNA molecules*, Proc. Natl. Acad. Sci. **94**, 6185–6190 (1997) 20, 98

[47] T. R. Strick, J. F. Allemand, D. Bensimon and V. Croquette, *Behavior of supercoiled DNA*, Biophys. J. **74**, 2016–2028 (1998) 59, 65

[48] J. B. Mill, E. Vacano and J. Hagerman, *Flexibility of single-stranded DNA*, J. Mol. Biol. **285**, 245–257 (1999) 20

[49] P. Cluzel, A. Lebrun, C. Heller, R. Lavery, J. L. Viovy, D. Chatenay and F. Caron, *DNA: An extensible molecule*, Science **283**, 1689–1695 (1996) 21

[50] A. Bensimon, A. Simon, A. Chiffaudel, V. Croquette, F. Heslot and D. Bensimon, *Alignment and sensitive detection of DNA by a moving interface*, Science **265**, 2096–2098 (1994) 22

[51] J. F. Allemand, D. Bensimon, L. Jullien, A. Bensimon and V. Croquette, *pH-dependent specific binding and combing of DNA*, Biophys. J. **73**, 2064–2070 (1997) 22, 45, 54, 101

[52] H. Yokota, F. Johnson, H. Lu, R. M. Robinson, A. M. Belu, M. D. Garrison, B. D. Ratner, B. J. Trask and D. L. Miller, *A new method for straightening DNA molecules for optical restriction mapping*, Nucleic Acids Res. **25**(5), 1064–1070 (1997) 22

[53] Z. Gueroui, C. Place, E. Freyssingeas and B. Berge, *Observation by fluourescence microscopy of transcription on single combed DNA*, Proc. Nat. Acad. Sci. **99**(9), 6005–6010 (2002) 22

[54] M. Grandbois, M. Beyer, M. Rief, H. Clausen-Schaumann and H. E. Gaub, *How strong is a covalent bond?*, Science **283**, 1727–1730 (1999) 23

[55] M. K. Beyer, *The mechanical strength of a covalent bond calculated by density functional theory*, J. Chem. Phys. **112**(17), 7307–7312 (2000) 23

[56] L. H. Pope, M. C. Davies, C. A. Laughton, C. J. Roberts, S. J. B. Tendler and P. M. Williams, *Force-induced melting of a short DNA double helix*, Eur. Biophys. J. **30**, 53–62 (2001) 23

[57] R. M. Zimmermann and E. C. Cox, *DNA stretching on functionalized gold surfaces*, Nucleic Acids Res. **22**(3), 492–497 (1994) 24, 45, 46, 48

[58] R. Merkel, P. Nassoy, A. Leung, K. Ritchie and E. Evans, *Energy landscapes of receptor-ligand bonds explored with dynamic force spectroscopy*, Nature **397**, 50–53 (1999) 24

[59] A. J. Storm, J. van Noort, S. de Vries and C. Dekker, *Insulating behavior for DNA molecules between nanoelectrodes*, Appl. Phys. Lett. **79**, 3881–3883 (2001) 25

[60] P. J. De Pablo, F. Moreno-Herrero, J. Colchero, J. G. Herrero, P. Herrero, A. M. Baro, P. Ordejon, J. M. Soler and E. Artacho, *Absence of dc-conductivity in λ-dna*, Phys. Rev. Lett. **85**(23), 4992–4995 (2000) 25

[61] C. M. Niemeyer, W. Bürger and J. Peplies, *Kovalente DNA-Streptavidin-Konjugate als Bausteine für neuartige biometallische Nanostrukturen*, Angew. Chem. **110**(16), 2391–2395 (1998) 25, 39

[62] T. Torimoto, M. Yamashita, S. Kuwabata, T. Sakata, H. Mori and H. Yoneyama, *Fabrication of CdS nanoparticle chains along DNA double strands*, J. Phys. Chem. B **103**, 8799–8803 (1999) 25

[63] C. J. Loweth, W. B. Caldwell, X. Peng, A. P. Alivisatos and P. G. Schultz, *DNA-based assembly of gold nanocrystals*, Angew. Chem. Int. Ed. **38**(12), 1808–1812 (1999) 25, 39

[64] K. Keren, Y. Soen, G. Ben-Yoseph, R. Gilad, E. Braun, U. Sivan and Y. Talmon, *Microscopics of complexation between long DNA molecules and positively charged colloids*, Phys. Rev. Lett. **89**, 088103 (2002) 25, 88

[65] O. Harnack, W. E. Ford, A. Yasuda and J. M. Wessels, *Tris(hydroxymethyl)-phosphine-capped gold particles templated by DNA as nanowire precursors*, Nanolett. **2**(9), 919–923 (2002) 26

[66] J. Richter, M. Mertig, W. Pompe, I. Mönch and H. K. Schackert, *Construction of highly conductive nanowires on a DNA template*, Appl. Phys. Lett. **78**(4), 536–538 (2001) 26

[67] E. A. Oussatcheva, L. S. Shlyakhtenko, R. Glass, R. R. Sinden, Y. L. Lyubchenko and V. N. Potaman, *Structure of branched DNA molecules: gel retardation and atomic force microscopy studies*, J. Mol. Biol. **292**, 75–86 (1999) 37

[68] L. S. Shlyakhtenko, V. N. Potaman, R. R. Sinden, A. A. Gall and Y. L. Lyubchenko, *Structure and dynamics of three-way DNA junctions: atomic force microscopy studies*, Nucleic Acids Res. **28**, 3472–3477 (2000) 37

[69] K. A. Williams, P. T. M. Veenhuizen, B. G. de la Torre, R. Eritja and C. Dekker, *Carbon nanotubes with DNA recognition*, Nature **420**, 761 (2002) 38

[70] D. Zanchet, C. M. Micheel, W. J. Parak, D. Gerion and A. A. P, *Electrophoretic isolation of discrete Au nanocrystal/DNA conjugates*, Nanolett. **1**(1), 32–35 (2001) 39, 41, 100

[71] D. Zanchet, C. M. Micheel, W. J. Parak, D. Gerion, S. C. Williams and A. P. Alivisatos, *Electrophoretic and structural studies of DNA-directed Au nanoparticle groupings*, J. Phys. Chem. B **106**(45), 11758–11763 (2002) 39

[72] S. Xiao, F. Liu, A. E. Rosen, J. F. Hainfeld, N. C. Seeman, K. Musier-Forsyth and R. A. Kiehl, *Selfassembly of metallic nanoparticle arrays by DNA scaffolding*, J. Nanoparticle Res. **4**, 313–317 (2002) 39, 41

[73] M. Mertig, R. Seidel, L. Colombi Ciacchi and W. Pompe, *Nucleation and growth of metal clusters on a DNA template*, AIP Conf. Proc. **633**, 449–453 (2002) 45, 119

[74] M. J. van Stipdonk, R. D. English and E. A. Schweikert, *SIMS of organic anions adsorbed onto an aminoethanethiol self-assembled monolayer*, Anal. Chem. **72**(11), 2618–2626 (2000) 45

[75] S. Diez, C. Reuther, R. Seidel, M. Mertig, W. Pompe and J. Howard, *Stretching and transporting DNA molecules using motor proteins*, submitted (2003) 46, 48, 120

[76] R. G. Larson, T. T. Perkins, D. E. Smith and S. Chu, *Hydrodynamics of a DNA molecule in a flow field*, Phys. Rev. E **55**(2), 1794–1797 (1997) 48, 49, 51, 52, 59

[77] O. B. Bakajin, T. A. J. Duke, C. F. Chou, S. S. Chan, R. H. Austin and E. C. Cox, *Electrohydrodynamic stretching of DNA in confined environments*, Phys. Rev. Let. **80**(12), 2737–2740 (1998) 48

[78] W. Kuhn, *Über die Gestalt fadenförmiger Moleküle in Lösungen*, Kolloid Z. **68**(1), 2 (1934) 49

[79] D. E. Smith, T. T. Perkins and S. Chu, *Dynamical scaling of DNA diffusion coefficients*, Macromolecules **29**(4), 1372–1373 (1996) 49, 64

[80] M. Doi and S. F. Edwards, *The theory of polymer dynamics* (Oxford University Press, 1986) 49, 50

[81] W. Greiner and H. Stock, *Hydrodynamik* (Verlag Harri Deutsch, 1991) 50

[82] B. Åkerman and E. Tuite, *Single- and double-strand photocleavage of DNA by YO, YOYO and TOTO*, Nucleic Acids Res. **24**(6), 1080–1090 (1996) 51, 52

[83] A. Larsson, C. Carlsson, M. Jonsson and B. Albinssont, *Characterization of the binding of the fluorescent dyes YO and YOYO to DNA by polarized light spectroscopy*, J. Am. Chem. Soc. **116**(19), 8459–8465 (1994) 51

[84] F. Reif, *Grundlagen der physikalischen Statistik und der Physik der Wärme* (Walter de Gruyter, 1976) 65

[85] B. Lippert, *Cisplatin* (Wiley-VHC, 1999) 69, 70

[86] A. Henglein, B. G. Ershov and M. Malow, *Absorption spectrum and some chemical reactions of colloidal platinum in aqueous solution*, J. Phys. Chem. **99**, 14129–14136 (1995) 69, 85, 93

[87] L. Colombi Ciacchi, W. Pompe and A. De Vita, *Initial nucleation of platinum clusters after reduction of K_2PtCl_4 in aqueous solution : A first principles study*, J. Am. Chem. Soc. **123**, 7371–7380 (2001) 69, 92, 93

[88] L. Colombi Ciacchi, W. Pompe and A. De Vita, *Growth of platinum clusters via addition of Pt(II) complexes: A first principles investigation*, J. Phys. Chem. B **107**, 1755–1764 (2003) 69, 92, 93

[89] E. T. Sacharenko and Y. S. Moschkowski, Кинетическое изучение реакции хлороплатината калия с ДНК, Биофизика **7**, 373–378 (1972) 70, 71

[90] J. P. Macquet and T. Theophanides, *Spécificité de l'interaction DNA-platine. Dosage du platine, pH-métrie*, Biopolymers **14**, 781–799 (1975) 70, 71, 73, 81, 91, 95

[91] D. P. Bancroft, C. A. Lepre and S. J. Lippard, *^{195}Pt NMR kinetic and mechanistic studies of cis- and trans-diamminedichloroplatinum(II) binding to DNA*, J. Am. Chem. Soc. **112**, 6860–6871 (1990) 70, 74

[92] S. J. Lippard and M. Berg, *Principles of bioinorganic chemistry* (University Science Books, 1994) 70

[93] P. M. Takahara, A. C. Rosenzweig and S. J. Lippard, *Crystal structure of double-stranded DNA containing the major adduct of the anticancer drug cisplatin*, Nature **377**, 649–652 (1995) 71

[94] P. M. Takahara, C. A. Frederick and S. J. Lippard, *Crystal structure of the anticancer drug cisplatin bound to duplex DNA*, J. Am. Chem. Soc. **118**, 12309–12321 (1996) 71

[95] G. B. Onoa, G. Cervantes, V. Moreno and M. J. Prieto, *Study of the interaction of DNA with cisplatin and other Pd(II) and Pt(II) complexes by atomic force microscopy*, Nucleic Acids Res. **26**, 1473– (1998) 71, 80

[96] J. P. Macquet and T. Theophanides, *DNA-platinum interactions. Characterization of solid DNA-$K_2[PtCl_4]$ complexes*, Inorg. Chim. Acta **18**, 189–194 (1976) 71, 91

[97] J. P. Macquet and J. L. Butour, *A circular dichroism study of DNA·platinum complexes*, Eur. J. Biochem **83**, 375–387 (1978) 71, 91

[98] R. Žaludova, V. Kleinächter and V. Brabec, *The effect of ionic strength on melting of DNA modified by platinum(II) complexes*, Biophys. Chem. **60**, 135–142 (1996) 71

[99] L. I. Elding, *The stepwise dissociation of the tetrachloroplatinate(II) ion in aqueous solution: VI. Rates of formation and equilibria of the chloro aqua complexes of platinum(II)*, Acta Chem. Scand. **24**(5), 1527–1540 (1970) 74, 95

[100] P. R. van Rheenen, M. J. McKelvy and W. S. Glaunsinger, *Synthesis and characterization of small platinum particles formed by the chemical reduction of chloroplatinic acid*, J. Sol. State Chem. **67**, 151–167 (1987) 81

[101] A. Henglein and M. Giersig, *Reduction of Pt(II) by H_2: Effects of citrate and NaOH and reaction mechanism*, J. Phys. Chem. B **104**(29), 6767–6772 (2000) 82, 92

[102] S. R. Bigham and J. L. Coffer, *The influence of adenine content on the properties of Q-CdS clusters stabilized by polynucleotides*, Coll. Surf. **95**, 211–219 (1995) 84

[103] R. Gans, *Über die Form ultramikroskopischer Goldteilchen*, Ann. Phys. **37**, 881–900 (1912) 88

[104] R. Kirsch, *Metallische Nanostrukturen auf biomolekularen Templaten*, Ph.D. thesis, Technische Universität Dresden (1998) 88

[105] S. S. Wong, A. T. Woolley, T. W. Odom, J. L. Huang, P. Kim, D. V. Vezenov and C. M. Lieber, *Single-walled carbon nanotube probes for high-resolution nanostructure imaging*, Appl. Phys. Lett. **73**(23), 3465–3467 (1998) 90

[106] L. Colombi Ciacchi, *Growth of platinum clusters in solution and on biopolymers: The microscopic mechanisms*, Ph.D. thesis, Technische Universität Dresden (2002) 92

[107] L. Colombi Ciacchi, M. Mertig, R. Seidel, W. Pompe and A. De Vita, *Nucleation of platinum clusters on biopolymers: A first principles study of the molecular mechanisms*, Nanotechnology **14**(8), 840–848 (2003) 92, 93, 94, 107, 119

[108] T. E. Müller, F. Ingold, S. Menzer, D. M. P. Mingos and D. J. Williams, *Platinum(I) dimers and platinum(0) triangles with polyaromatic phosphine ligands*, J. organomet. Chem. **528**(1-2), 163–178 (1997) 92

[109] M. A. Watzky and R. G. Finke, *Transition metal nanocluster formation kinetic and mechanistic studies. A new mechanism when hydrogen is the reductant: Slow, continuous nucleation and fast autocatalytic surface growth*, J. Am. Chem. Soc. **119**(43), 10382–10400 (1997) 93

[110] J. Richter, *Erzeugung und Charakterisierung von Nanostrukturen auf DNA*, Ph.D. thesis, Technische Universität Dresden (2001) 96

[111] W. Shenton, D. Pum, U. B. Sleytr and S. Mann, *Synthesis of CdS superlattices using self-assembled bacterial S-layers*, Nature **389**, 585–587 (1997) 107

[112] S. Roweis, E. Winfree, R. Burgoyne, N. V. Chelyapov, M. F. Goodman, P. W. Rothemund and L. M. Adleman, *A sticker-based model for DNA computation*, J. Comput. Biol. **5**(4), 615–629 (1998) 108

[113] S. Roweis and E. Winfree, *On the reduction of errors in DNA computation*, J. Comput. Biol. **6**(1), 65–75 (1999) 108

[114] E. Winfree, *Algorithmic self-assembly of DNA: Theoretical motivations and 2D assembly experiments*, J. Biomol. Struct. Dyn. **Conv. 11**(2), 263–270 (2000) 108

[115] G. Mie, *Beiträge zur Optik trüber Medien, speziell kolloidaler Metallösungen*, Ann. Phys. **25**(3), 377 (1908) 111

[116] G. Schmid, *Clusters and Colloids: From theory to applications* (VCH, 1994) 112

[117] D. R. Lide and H. P. R. Frederikse, *CRC Handbook of chemistry and physics* (CRC press, 1996) 112

[118] M. Bezanilla, S. Manne, D. E. Laney, Y. L. Lyubchenko and H. G. Hansma, *Adsorption of DNA to mica, silylated mica, and minerals: Characterization by atomic force microscopy*, Langmuir **11**(2), 655–659 (1995) 117

[119] W. Pompe, M. Mertig, R. Kirsch, R. Wahl, L. Colombi-Ciacchi, J. Richter, R. Seidel and H. Vinzelberg, *Formation of metallic nanostructures on biomolecular templates*, Z. Metallkd. **90**(12), 1085–1091 (1999) 119

[120] L. Colombi Ciacchi, A. De Vita, R. Seidel, M. Mertig and W. Pompe, *The formation of metal clusters in solution and on biopolymers investigated by first-principles molecular dynamics*, Proc. in Appl. Math. and Mech. **2**, 5–8 (2003) 119

[121] M. Mertig, L. Colombi Ciacchi, R. Seidel, W. Pompe and A. De Vita, *Verfahren zur Schaffung metallischer Nukleationszentren für das Clusterwachstum auf DNA*, German patent application **DE 101 31 551.1** (2001), US patent application **19/177.775** (2003) 119

[122] B. Voit, F. Braun, C. Loppacher, S. Trogisch, L. M. Eng, R. Seidel, A. Gorbunoff, W. Pompe and M. Mertig, *Photolabile ultrathin polymer films for spatially defined attachment of nanoobjects*, subm. to ACS Proc. (2002) 120

[123] W. Pompe, R. Seidel and M. Mertig, *Formation of metallic nanostructures on biomolecular templates: Basic strategies for the development of a DNA-based nanoelectronics*, VDI Proceedings (2002) 120

Danksagung

Vier Jahre, in denen diese Dissertation angefertigt wurde, sind vergangen. Und obwohl es mir in der tagtäglichen Arbeit gar nicht so aufgefallen ist, rückblickend war diese Zeit für mich ein gewaltiger Entwicklungssprung sowohl, in privater als auch wissenschaftlicher Hinsicht. Ich möchte mich nun bei all denen bedanken, die mich dabei unterstützt haben.

An erster Stelle sei Prof. Wolfgang Pompe genannt, nicht zuletzt dafür, dass er mir die Arbeit am Institut ermöglichte. Was ich besonders an ihm schätze, sind seine ,,visionären“ Weitblicke, über dessen Kühnheit ich manchmal erst erschrak, aber bei deren Verwirklichung in der Arbeit ich lernte, dass auch Visionen stückweise realisierbar sind.

Ein herzlicher Dank gilt meinem Betreuer Dr. Michael Mertig für die zahlreichen Diskussionen über die Arbeit als auch über die Welt an sich. Er war es, der mir half, den täglichen Forschungsaufgaben Struktur zu geben. Dabei sind wir manchmal aneinander geraten, aber das hat unser freundschafliches Verhältnis nicht getrübt.

Bedanken möchte ich mich auch bei Prof. Jonathon Howard, der mir, ohne zu zögern, die wissenschaftliche Betreuung seitens der Physik zusagte. Ich bin auch dankbar für die Ratschläge und Kommentare im Rahmen des Forschergruppenprojektes. Sein Buch ,,Mechanics of motor proteins and the cytoskeleton“, das ich von ihm geschenkt bekam, schätze ich sehr.

Reiner, Dir möchte ich für das schöne und harmonische Miteinander in den vielen Arbeitsräumen, die wir seit dem Studium teilten, danken. Ich schätze Deine ruhige und aufrechte Art. Es ist fast unglaublich, dass wir so viele Jahre miteinander verbracht haben. Schade, dass wir jetzt getrennte berufliche Wege gehen, aber ich hoffe dafür auf noch zahlreiche private Begegnungen.

Lucio, capo, danke für Deine ungestühme Art. Du hast damit vieles in den Experimenten zur Metallisierung vorangetrieben, auch wenn Dir einiges zu langsam ging. Es hat Spaß gemacht, sich mit Dir zu unterhalten. Gedankt sei auch den

anderen Mitgliedern der Arbeitgruppe für die meist nette und freundliche Arbeitsatmosphäre. Ein besonderer Dank gilt den ,,HIWIs“ Elias Mohn und Michael Weigel, die zu zahlreichen Ergebnissen beitrugen. Außerdem sei Alexander Huhle sowie Sascha Heinemann für ihre fleißige Arbeit im Labor gedankt. Im Rahmen ihrer Belegarbeiten stellten sie die DNA-Verzweigungen bzw. die Verzweigungen mit immobilisierten Kolloiden her.

Gedankt sei an dieser Stelle für die technische Hilfe, die ich bei den Experimenten erhielt. Dr. Ingolf Mönch stellte den größten Teil der Gold-Mikrostrukturen her. Prof. Goldberg danke ich für die großzügige Unterstützung bei der Nutzung des Elektronenmikroskopes. Vielen Dank auch an Prof. Lichte, der mit seinem Speziallabor die hochauflösenden Elektronenmikroskopieaufnahmen ermöglichte. Dabei sei auch seinen Mitarbeitern Dr. Paul Simon sowie Dr. Michael Lehmann für die technische Durchführung gedankt. Prof. Hans K. Schackert danke ich für die vielen Diskussionen zu den DNA-Experimenten.

Vielen Dank an Kinneret Keren, Prof. Uri Sivan, Prof. Erez Braun, Michael Krüger, Gidi Ben-Yoseph und Rachel Gilad von Technion Haifa in Israel. Der Aufenthalt in der Arbeitsgruppe war eine bewegende Zeit für mich. Ich erfuhr dort einen ,,technologischen Entwicklungssprung“. Außerdem habe ich die freundschaftliche und warme Atmosphäre sehr genossen. Kinneret, das Arbeiten mit Dir war Klasse!

Vielen Dank ,,meinen Männern“ Matthias, Frank, Olaf und Andreas. Ihr wart mir mit Eurem Rat zu den tagtäglichen Problemen eine große Hilfe. Ohne Euch hätte ich den Kopf nicht so freigehabt. Damit habt Ihr wesentlich zum Gelingen dieser Arbeit beigetragen. Danke!

Manuela, nun stehst Du hier am Schluß. Dabei bist Du mit dieser Arbeit auf besondere Weise verbunden. Zu Beginn der Promotionszeit bin ich in die Osterbergstraße gezogen. Dort haben wir uns kurz darauf kennengelernt und sind seitdem zusammen. Du hast mir keinen wissenschaftlichen Rat gegeben, natürlich nicht. Aber Du warst in dieser Zeit meine engste Weggefährtin und hast mein Leben bereichert. Ich denke, wir sind in den letzten Jahren ein Stück aneinander gewachsen. Ich danke Dir dafür, dass Du auf unserem Lebensweg mitziehst. Ich danke Dir auch dafür, dass Du meine berufliche Weiterentwicklung mit tragen willst und mit mir und unserer Tochter Elena nach Delft ziehst.

Erklärung

Die vorliegende Arbeit wurde unter der wissenschaftlichen Betreuung von Herrn Prof. Dr. Jonathon Howard vom Institut für Biophysik an der Technischen Universität Dresden, unter der Leitung von Prof. Dr. Wolfgang Pompe vom Institut für Werkstoffwissenschaft, Lehrstuhl für Materialwissenschaft und Nanotechnik an der Technischen Universität Dresden, angefertigt.
Die Promotionsordnung der Fakultät Mathematik und Naturwissenschaften der Technischen Universität Dresden vom 20. März 2000 erkenne ich an.
Hiermit versichere ich, daß ich die vorliegende Arbeit ohne unzulässige Hilfe Dritter und ohne Benutzung anderer als der angegebenen Hilfsmittel angefertigt habe; die aus fremden Quellen direkt oder indirekt übernommenen Gedanken sind als solche kenntlich gemacht. Die Arbeit wurde bisher weder im Inland noch im Ausland in gleicher oder ähnlicher Form einer anderen Prüfungsbehörde vorgelegt.

Dresden, den 13.06.2003

Ralf Seidel